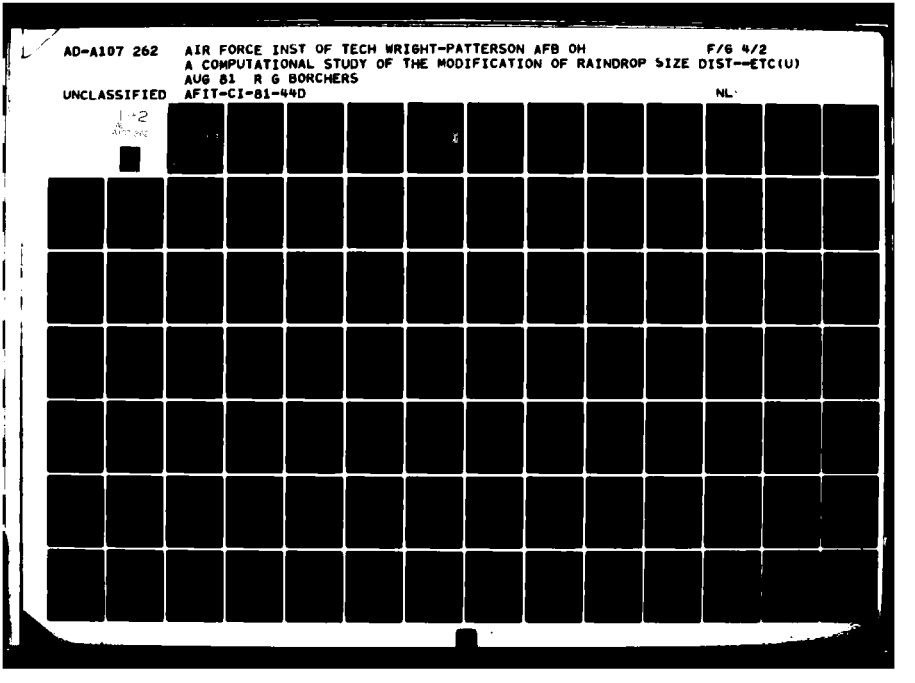
AD-A107 262
AIR FORCE INST OF TECH WRIGHT-PATTERSON AFB OH
F/G 4/2
A COMPUTATIONAL STUDY OF THE MODIFICATION OF RAINDROP SIZE DIST--ETC(U)
AUG 81 R G BORCHERS
UNCLASSIFIED
AFIT-CI-81-44D
NL

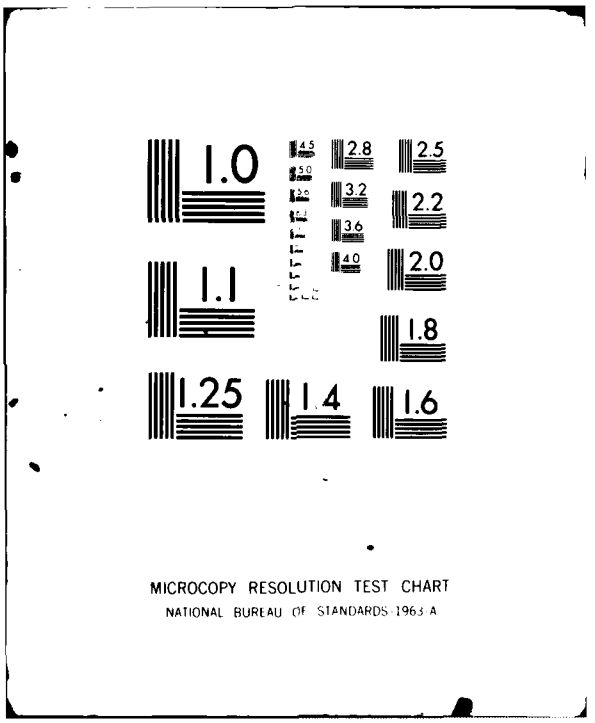
1.0
1.1
1.25
1.4
1.6
1.8
2.0
2.2
2.5
2.8
3.2
3.6
4.0
4.5
5.0
MICROCOPY RESOLUTION TEST CHART
NATIONAL BUREAU OF STANDARDS-1963-A

UNCLASS

SECURITY CLASSIFICATION OF THIS PAGE (When Data Entered)

REPORT DOCUMENTATION PAGE	READ INSTRUCTIONS BEFORE COMPLETING FORM
1. REPORT NUMBER: 81-44D (6)	2. GOVT ACCESSION NO.: AD-A107 262	3. RECIPIENT'S CATALOG NUMBER:
4. TITLE (and Subtitle): A Computational Study of the Modification of Raindrop Size Distributions in Subcloud Downdrafts,	5. TYPE OF REPORT & PERIOD COVERED: ~~THESIS~~/DISSERTATION (DISSERTATION)
	6. PERFORMING ORG. REPORT NUMBER:
7. AUTHOR(s): (10) Robert George Borchers (1)	8. CONTRACT OR GRANT NUMBER(s):
9. PERFORMING ORGANIZATION NAME AND ADDRESS: AFIT STUDENT AT: Texas A&M Univ	10. PROGRAM ELEMENT, PROJECT, TASK AREA & WORK UNIT NUMBERS: (9 Doctoral thesis,)
11. CONTROLLING OFFICE NAME AND ADDRESS: AFIT/NR WPAFB OH 45433	12. REPORT DATE: (11) August 1981
	13. NUMBER OF PAGES: ~~143~~ (12) 161
14. MONITORING AGENCY NAME & ADDRESS (if different from Controlling Office): LEVEL II	15. SECURITY CLASS. (of this report): UNCLASS
	15a. DECLASSIFICATION/DOWNGRADING SCHEDULE:

16. DISTRIBUTION STATEMENT (of this Report)

APPROVED FOR PUBLIC RELEASE; DISTRIBUTION UNLIMITED

(14) AFIT-CI-81-44D

DTIC ELECTE NOV 6 1981 S D H

17. DISTRIBUTION STATEMENT (of the abstract entered in Block 20, if different from Report)

APPROVED FOR PUBLIC RELEASE AFR 190-17.

16 OCT 1981

Fredric C. Lynch

FREDRIC C. LYNCH, Major, USAF
Director of Public Affairs
Air Force Institute of Technology (ATC)
Wright-Patterson AFB, OH 45433

18. SUPPLEMENTARY NOTES

APPROVED FOR PUBLIC RELEASE: IAW AFR 190-17

19. KEY WORDS (Continue on reverse side if necessary and identify by block number)

20. ABSTRACT (Continue on reverse side if necessary and identify by block number)

ATTACHED

81 10 27 248

DD FORM 1 JAN 73 1473 EDITION OF 1 NOV 65 IS OBSOLETE

UNCLASS

SECURITY CLASSIFICATION OF THIS PAGE (When Data Entered)

012200

AD A107262

DTIC FILE COPY

ABSTRACT

A Computational Study of the Modification of Raindrop Size Distributions in Subcloud Downdrafts. (August 1981)

Robert George Borchers, B.S., Texas A&M University;
M.S., University of Michigan

Co-Chairmen of Advisory Committee: Dr. Phanindramohan Das
Dr. James R. Scoggins

A computational study is made of the variation of steady-state raindrop-size distributions (0.004 cm ≤ radius ≤ 0.40 cm) in adiabatic subcloud downdrafts of constant magnitude. The cloud base drop-size distribution is assumed to be Marshall-Palmer. The microphysical processes progressively introduced are evaporation, collision-coalescence, aerodynamic and collisional breakup of drops. Collision-coalescence and breakup are treated through a stochastic model. Thermodynamic and hydrometeoric variables of temperature, relative humidity, total liquid water, rainfall rate and radar reflectivity are computed as functions of height below cloud base along with the drop-size distributions.

It is found that evaporation tends to deplete, as expected, the smaller members of the droplet population. The slope of the Marshall-Palmer distribution as determined by the distribution of larger size drops remains virtually unaffected by evaporation. When collision-coalescence is included, the depletion of the smaller drops is enhanced by the larger drops sweeping out the smaller ones. Aerodynamic breakup when added to evaporation and collision-coalescence has little effect on the resulting drop-size distribution except for very high

initial precipitation rates. When collisional breakup is added to the previously mentioned microphysical processes, the effect of aerodynamic breakup is virtually eliminated because collisional breakup quickly depletes the concentration of drops with radii greater than 0.15 cm. Computed raindrop-size distributions agree quite well with measured maritime raindrop spectra reported in the literature, the agreement being better for the higher precipitation rates measured.

Other results of the study, as anticipated, are (i) that the downdraft remains unsaturated in the presence of precipitation, the degree of subsaturation increasing with the strength of the downdraft, and (ii) that the temperature in the downdraft lies between the moist-adiabatic and the dry-adiabatic lapse rates of temperature.

81-44D

AFIT RESEARCH ASSESSMENT

The purpose of this questionnaire is to ascertain the value and/or contribution of research accomplished by students or faculty of the Air Force Institute of Technology (ATC). It would be greatly appreciated if you would complete the following questionnaire and return it to:

AFIT/NR
Wright-Patterson AFB OH 45433

RESEARCH TITLE: A Computational Study of the Modification of Raindrop Size Distributions in Subcloud Downdrafts

AUTHOR: Robert George Borchers

RESEARCH ASSESSMENT QUESTIONS:

1. Did this research contribute to a current Air Force project?

( ) a. YES ( ) b. NO

2. Do you believe this research topic is significant enough that it would have been researched (or contracted) by your organization or another agency if AFIT had not?

( ) a. YES ( ) b. NO

3. The benefits of AFIT research can often be expressed by the equivalent value that your agency achieved/received by virtue of AFIT performing the research. Can you estimate what this research would have cost if it had been accomplished under contract or if it had been done in-house in terms of manpower and/or dollars?

( ) a. MAN-YEARS _____ ( ) b. $_____

4. Often it is not possible to attach equivalent dollar values to research, although the results of the research may, in fact, be important. Whether or not you were able to establish an equivalent value for this research (3. above), what is your estimate of its significance?

( ) a. HIGHLY SIGNIFICANT ( ) b. SIGNIFICANT ( ) c. SLIGHTLY SIGNIFICANT ( ) d. OF NO SIGNIFICANCE

5. AFIT welcomes any further comments you may have on the above questions, or any additional details concerning the current application, future potential, or other value of this research. Please use the bottom part of this questionnaire for your statement(s).

NAME GRADE POSITION

ORGANIZATION LOCATION

STATEMENT(s):

FOLD DOWN ON OUTSIDE - SEAL WITH TAPE

AFIT/NR
WRIGHT-PATTERSON AFB OH 45433

OFFICIAL BUSINESS
PENALTY FOR PRIVATE USE, $300

NO POSTAGE
NECESSARY
IF MAILED
IN THE
UNITED STATES

BUSINESS REPLY MAIL
FIRST CLASS PERMIT NO. 73236 WASHINGTON D.C.

POSTAGE WILL BE PAID BY ADDRESSEE

AFIT/ DAA
Wright-Patterson AFB OH 45433

FOLD IN

81-44D

A COMPUTATIONAL STUDY OF THE MODIFICATION OF RAINDROP SIZE DISTRIBUTIONS IN SUBCLOUD DOWNDRAFTS

A Dissertation

by

ROBERT GEORGE BORCHERS

Submitted to the Graduate College of
Texas A&M University
in partial fulfillment of the requirements for the degree of

DOCTOR OF PHILOSOPHY

August 1981

Major Subject: Meteorology

A COMPUTATIONAL STUDY OF THE MODIFICATION OF RAINDROP SIZE DISTRIBUTIONS IN SUBCLOUD DOWNDRAFTS

A Dissertation

by

ROBERT GEORGE BORCHERS

Approved as to style and content by:

Phanindramohan Das
Dr. Phanindramohan Das
(Co-Chairman of Committee)

James R. Scoggins
Dr. James R. Scoggins
(Co-Chairman of Committee)

Vance Mayer
Dr. Vance E. Mayer
(Member)

Dusan Djuric
Dr. Dusan Djuric
(Member)

Glen Williams
Dr. Glen N. Williams
(Member)

Roger R. Smith
Dr. Roger R. Smith
(Member)

James R. Scoggins
Dr. James R. Scoggins
(Head of Department)

August 1981

ABSTRACT

A Computational Study of the Modification of Raindrop Size Distributions in Subcloud Downdrafts. (August 1981)

Robert George Borchers, B.S., Texas A&M University;

M.S., University of Michigan

Co-Chairmen of Advisory Committee: Dr. Phanindramohan Das
Dr. James R. Scoggins

A computational study is made of the variation of steady-state raindrop-size distributions (0.004 cm $\leq$ radius $\leq$ 0.40 cm) in adiabatic subcloud downdrafts of constant magnitude. The cloud base drop-size distribution is assumed to be Marshall-Palmer. The microphysical processes progressively introduced are evaporation, collision-coalescence, aerodynamic and collisional breakup of drops. Collision-coalescence and breakup are treated through a stochastic model. Thermodynamic and hydrometeoric variables of temperature, relative humidity, total liquid water, rainfall rate and radar reflectivity are computed as functions of height below cloud base along with the drop-size distributions.

It is found that evaporation tends to deplete, as expected, the smaller members of the droplet population. The slope of the Marshall-Palmer distribution as determined by the distribution of larger size drops remains virtually unaffected by evaporation. When collision-coalescence is included, the depletion of the smaller drops is enhanced by the larger drops sweeping out the smaller ones. Aerodynamic break-up when added to evaporation and collision-coalescence has little effect on the resulting drop-size distribution except for very high

initial precipitation rates. When collisional breakup is added to the previously mentioned microphysical processes, the effect of aerodynamic breakup is virtually eliminated because collisional breakup quickly depletes the concentration of drops with radii greater than 0.15 cm.

Computed raindrop-size distributions agree quite well with measured maritime raindrop spectra reported in the literature, the agreement being better for the higher precipitation rates measured.

Other results of the study, as anticipated, are (i) that the downdraft remains unsaturated in the presence of precipitation, the degree of subsaturation increasing with the strength of the downdraft, and (ii) that the temperature in the downdraft lies between the moist-adiabatic and the dry-adiabatic lapse rates of temperature.

ACKNOWLEDGMENTS

The author's doctoral program was sponsored by the Air Force Institute of Technology. Additional support was provided by the National Oceanographic and Atmospheric Administration (NOAA) Grant #NA 79 RAD 00019, and the Department of Meteorology.

I am indebted to several individuals without whose assistance this research would not have been completed. Dr. Phanindramohan Das is singled out for his astute direction and judgment which stimulated me to persevere with the research program. I will always value his wise counsel. I am indebted to Dr. James R. Scoggins who provided valuable guidance throughout my doctoral program. My thanks go to Dr. Vance Moyer, Dr. Glen Williams, and Dr. Roger Smith for their advice and assistance. My warmest regards go to Dr. Dusan Djuric whose friendship and valuable suggestions greatly aided me, especially during preparation of the final manuscript. Special thanks go to Lt. Col. John Madura who urged me to finish this work and granted me the time to do so, and Capt. Daniel McMorrow who provided room, board, and moral support during the final days of work.

Last but not the least, I wish to thank my wife, Lynn, who provided valuable typing skills, and along with my daughter, Kelly, and son, Scott, never doubted my ability to finish this work. Their affection and understanding sustained me through the five years it took to complete my doctoral program.

TABLE OF CONTENTS

	Page
ABSTRACT	iii
ACKNOWLEDGMENTS	v
LIST OF TABLES	viii
LIST OF FIGURES	x
I. INTRODUCTION	1
a. Background	1
b. Objectives	4
II. BASIC EQUATIONS	6
a. Thermodynamic Equation	6
b. Equation for Water Vapor	7
c. Equation for Drop Concentration	8
d. Equation for Drop Growth	9
III. MODIFYING PROCESSES FOR RAINDROP-SIZE DISTRIBUTION	10
a. Evaporation	10
b. Collision-coalescence	14
c. Aerodynamic Breakup of Drops	18
d. Collisional Breakup of Drops	19
IV. PROCEDURE	24
a. Cloud-Base Conditions	25
b. Grid System and Numerical Procedures	28
c. Numerical Formulation for Raindrop Size	28
d. Numerical Formulation of the Thermodynamic and Moisture Equations	31
e. Numerical Formulation of the Evaporation Effects	32

TABLE OF CONTENTS (Continued)

Page

f. Numerical Formulation for Collision-coalescence . . . 34

g. Numerical Formulation for Aerodynamic Breakup 36

h. Numerical Formulation for Collisional Breakup 36

i. Numerical Formulation for Rainfall Rate and Radar Reflectivity. 39

V. RESULTS 40

a. Case A: Evaporation. 40

b. Case B: Evaporation and Collision-Coalescence. . . . 54

c. Case C: Evaporation, Collision-Coalescence, and Aerodynamic Breakup 63

d. Case D: Evaporation, Collision-Coalescence, and Collisional Breakup 70

e. Case E: Evaporation, Collision-Coalescence, Collisional and Aerodynamic Breakup 94

VI. COMPARISON WITH OBSERVED RAINDROP SPECTRA 103

a. Warm Raindrop Measurements. 103

b. Thunderstorm Raindrop Measurements. 110

VII. SUMMARY AND CONCLUSIONS 114

VIII. RECOMMENDATIONS 119

REFERENCES 121

APPENDIX A 127

APPENDIX B 131

APPENDIX C 133

APPENDIX D 139

VITA 143

LIST OF TABLES

Table		Page
1	Marshall-Palmer drop-size distribution for a precipitation rate of 50 mm/hr	27
2	Summary of collisional processes.	38
3	Vertical distributions of thermodynamic and hydrometeoric quantities for Case A in a constant subcloud downdraft of 5 mm/sec, where z = height above the surface (1500 m = cloud base), T_D = dry-adiabatic temperature, T = rain-shaft temperature, S = relative humidity, M = liquid water content, R = rainfall rate, and Z = radar reflectivity. .	41
4	Vertical distributions of thermodynamic and hydrometeoric quantities for Case A in a subcloud downdraft of 10 m/sec	42
5	Vertical distributions of thermodynamic and hydrometeoric quantities for Case A in a subcloud downdraft of 15 m/sec	43
6	Drop-size distributions at cloud base (Marshall-Palmer distribution for a precipitation rate of 25 mm/hr) and 1500 m below cloud base for constant downdrafts of 5, 10, and 15 m/sec for Case A	52
7	Drop-size distributions at cloud base (Marshall-Palmer distribution for a precipitation rate of 100 mm/hr) and 1500 m below cloud base for constant downdrafts of 5, 10, and 15 m/sec for Case A	53
8	Vertical distributions of thermodynamic and hydrometeoric quantities for Case B in a subcloud downdraft of 5 m/sec.	55
9	Vertical distributions of thermodynamic and hydrometeoric quantities for Case B in a subcloud downdraft of 10 m/sec	56
10	Vertical distributions of thermodynamic and hydrometeoric quantities for Case B in a subcloud downdraft of 15 m/sec	57
11	Vertical distributions of thermodynamic and hydrometeoric quantities for Case C in a subcloud downdraft of 5 m/sec.	66
12	Vertical distributions of thermodynamic and hydrometeoric quantities for Case C in a subcloud downdraft of 10 m/sec	67
13	Vertical distributions of thermodynamic and hydrometeoric quantities for Case C in a subcloud downdraft of 15 m/sec	68

Table		Page
14	Probability of aerodynamic drop breakup.	69
15	Drop-size distributions at cloud base (Marshall-Palmer) and 1500 m below cloud base for Case B and Case C. The constant downdraft is 5 m/sec and the initial precipitation rate is 25 mm/hr.	75
16	Drop-size distributions at cloud base (Marshall-Palmer) and 1500 m below cloud base for Case B and Case C. The constant downdraft is 5 m/sec and the initial precipitation rate is 100 mm/hr	76
17	Vertical distributions of thermodynamic and hydrometeoric quantities for Case D in a subcloud downdraft of 5 m/sec	78
18	Vertical distribution of thermodynamic and hydrometeoric quantities for Case D in a subcloud downdraft of 10 m/sec.	79
19	Vertical distribution of thermodynamic and hydrometeoric quantities for Case D in a subcloud downdraft of 15 m/sec.	80
20	Vertical distribution of thermodynamic and hydrometeoric quantities in a subcloud downdraft of 5 m/sec .	95
21	Vertical distributions of thermodynamic and hydrometeoric quantities for Case E in a subcloud downdraft of 10 m/sec.	96
22	Vertical distributions of thermodynamic and hydrometeoric quantities for Case E in a subcloud downdraft of 15 m/sec.	97
C.1	Evaporation of freely falling water drops (after Kinzer and Gunn, 1951).	134
C.2	Computed evaporation of freely falling water drops . . .	136

LIST OF FIGURES

Figure		Page
1	The continuous and stochastic models.	
	A. The continuous model assumes that small droplets are swept out as if their water were distributed uniformly in space, and that 100 large drops grow at the same rate, becoming 100 similar larger drops.	16
	B. The stochastic model assumes that, say 1 in 10 of 100 large droplets will collect a small droplet during a given time, and then 1 in 10 of each larger size will collect a smaller droplet. Large droplets then grow at different rates (after Berry, 1967).	16
2	Marshall-Palmer drop-size distributions for precipitation rates of 25, 50, 75, and 100 mm/hr.	26
3	Percent of total liquid water as a function of drop radius in the Marshall-Palmer raindrop distribution for a precipitation rate of 50 mm/hr.	29
4	Subcloud relative humidity profiles in Case A for different downdrafts. The initial precipitation rate is 25 mm/hr.	45
5	Same as in Fig. 4 except for an initial precipitation rate of 100 mm/hr	46
6	Evaporation time constants for several values of relative humidity.	48
7	Drop-size distributions 1500 m below cloud base for various constant downdrafts. The cloud base drop-size distribution is Marshall-Palmer for R = 25 mm/hr.	50
8	Same as in Fig. 7 except that the cloud base drop-size distribution is Marshall-Palmer for R = 100 mm/hr. . . .	51
9	Relative humidity profiles for Case A and Case B for a constant downdraft of 15 m/sec and initial precipitation rate of 25 mm/hr.	59
10	Same as Fig. 9 except for a constant downdraft of 5 m/sec and initial precipitation rate of 100 mm/hr	60
11	Same as Fig. 7 except for Case B	61

Figure		Page
12	Same as Fig. 8 except for Case B.	62
13	Drop-size distributions 1500 m below cloud base for Case A and Case B, a constant downdraft of 5 m/sec and an initial precipitation rate of 25 mm/hr.	64
14	Same as Fig. 13 except for an initial precipitation rate of 100 mm/hr.	65
15	Same as Fig. 7 except for Case C.	71
16	Same as Fig. 8 except for Case C.	72
17	Drop-size distributions 1500 m below cloud base for Case B and Case C, a constant downdraft of 5 m/sec and an initial precipitation rate of 25 mm/hr.	73
18	Same as Fig. 17 except for an initial precipitation rate of 100 mm/hr.	74
19	Same as Fig. 7 except for Case D.	82
20	Same as Fig. 8 except for Case D.	83
21	Drop-size distributions 1500 m below cloud base for Case C and Case D, a constant downdraft of 5 m/sec and an initial precipitation rate of 25 mm/hr.	84
22	Same as Fig. 21 except for an initial precipitation rate of 100 mm/hr.	85
23	Evolution of drop-size distribution in Case D for an initial precipitation rate of 25 mm/hr and a constant downdraft of 5 m/sec.	87
24	Same as Fig. 23 except for an initial precipitation rate of 100 mm/hr.	88
25	Evolution with altitude of drop-size distribution through collision-coalescence and collisional breakup from an initial Marshall-Palmer distribution for rainfall rate of 25 mm/hr (after Gillespie and List, 1978/79).	89
26	Drop-size distributions in Case D compared with analogous computation of Gillespie and List (1978/79) . .	90
27	Time evolution through coalescence and breakup of a raindrop spectrum from an initial Marshall-Palmer distribution for the rainfall rate of 100 mm/hr (after List and Gillespie, 1976)	91

Figure		Page
28	Comparison of drop-size distributions at 1500 m below cloud base, for Case D computed with incorrect and correct fragment distribution of List and Gillespie (1976). The initial precipitation rate is 100 mm/hr and the subcloud downdraft is 5 m/sec	93
29	Same as Fig. 7 except for Case E.	98
30	Same as Fig. 29 except for initial R = 50 mm/hr	99
31	Same as Fig. 29 except for initial R = 75 mm/hr	100
32	Same as Fig. 8 except for Case E.	101
33	Comparison of drop-size distributions computed in Case E with those observed by Austin and Geotis (1979) in convective rain. Computed distributions refer to 1500 m below cloud base, and are for initial precipitation rates of 25 and 50 mm/hr and a downdraft velocity of 5 m/sec. Observed distributions are for a precipitation rate of 34.4 mm/hr at the surface	104
34	Same as Fig. 33 except that computed distributions are for precipitation rates of 75 and 100 mm/hr and observed distributions are for a precipitation rate of 82 mm/hr. .	106
35	Computed drop-size distributions in Case E, 1500 m below cloud base, for constant downdrafts of 5 and 15 m/sec, and a precipitation rate of 100 mm/hr. Also plotted is the drop-size distribution for Austin and Geotis (1979) for R = 83 mm/hr.	107
36	Averaged observed drop-size distributions from Mueller and Sims (1967), Geotis (1968), and Austin and Geotis (1979) together with a computed distribution for Case E. The initial precipitation rate is 25 mm/hr.	108
37	Averaged observed drop-size distributions from Mueller and Sims (1967), Geotis (1968), and Austin and Geotis (1979) together with a computed distribution for Case E. The initial precipitation rate is 50 mm/hr.	109
38	Drop-size distributions computed in Case E for an initial precipitation rate of 25 mm/hr compared with an averaged drop-size distribution observed by Dingle and Hardy (1962) in thunderstorm rain of 24.2 mm/hr intensity	111
39	Same as Fig. 38 except that the computed distribution is for an intensity of 75 mm/hr and the observed distribution is for a precipitation rate of 65.5 mm/hr.	113

Figure | Page

D.1 Bimodal type distribution resulting from the evaporation process. 139

CHAPTER I

INTRODUCTION

Raindrop size distribution and its variation in the vertical is of interest because, as Srivastava (1978) pointed out, (i) it is important in understanding processes affecting the growth and evaporation of raindrops, (ii) a knowledge of the distribution of raindrop sizes is essential for remote measurements of rainfall by radar, and (iii) the size distribution of raindrops has important bearing on precipitation loading and its effect on the dynamics of clouds. More specifically, most raindrop measurements are made at the ground while the precipitation development occurs in the cloud. Besides, radar observations, in general, relate to conditions near the cloud base. It is of obvious theoretical and practical importance, therefore, to relate the drop-size distribution at the cloud base to that at the ground.

a. Background

The modification of the size distribution of raindrops during their fall has been investigated by several researchers. Early investigators such as Mason and Ramanadham (1954), Rigby et al. (1954), Sivaraman and Sivaramakrishnan (1962), and Hardy (1963) calculated the raindrop-size distributions resulting from mutual coalescence, accretion with cloud droplets, and evaporation below cloud base.

The citations on this and the following pages follow the style of the Journal of the Atmospheric Sciences.

They assumed an exponential, Marshall-Palmer type distribution at the melting level, no downdraft, and a constant lapse rate of temperature and relative humidity below cloud base. Their results indicated that small drops were depleted by each modification process considered. The concentration of large drops, on the other hand, increased due to collision-coalescence and accretion but decreased by evaporation.

Hitschfeld (1955) and Srivastava (1967), working with coalescence only, concluded that an initial exponential drop-size distribution underwent comparatively little change between cloud base and ground. In a later computation, Srivastava (1971) added aerodynamic breakup of water drops as a modification process. Using the data of Komabayasi et al. (1964) on the probability of aerodynamic breakup and the size distribution of the fragments resulting from such breakup, he found that the equilibrium drop-size distribution was similar to, but flatter than, observed raindrop-size distributions. Srivastava suggested that the effects of evaporation and collisional breakup may help produce better agreement between theory and observation.

Experiments on collisional breakup and the resulting fragment-size distributions were reported by Brazier-Smith et al. (1972), McTaggart-Cowan and List (1975) and Bradley and Stow (1979). Brazier-Smith et al. (1973a, b), Young (1975), List and Gillespie (1976), Srivastava (1978) and Gillespie and List (1978/79) computed the evolution of drop-size spectra by collisional breakup as well as other processes. Brazier-Smith et al. used collision-coalescence and collisional breakup to compute changes in drop-size spectra. They found that the drop-size distribution after several minutes was

insensitive to the choice of an initial spectrum and became markedly bimodal. On the other hand, Gillespie and List (1976) considered the same two modification processes and found that the initial exponential drop-size spectra remained essentially exponential as the drops fell to the surface. Gillespie and List (1978/79) extended their 1976 work to apply to a vertical rainshaft in a steady state with no interactions with the surroundings.

Young (1975) and more recently Srivastava (1978) considered both collisional and aerodynamic breakup together with collision-coalescence and condensation processes. They found that collisional breakup dominated over aerodynamic breakup. The resulting equilibrium raindrop distribution was in good agreement with the empirical Marshall-Palmer distribution. Bradley and Stow (1977) developed a raindrop-size distribution model by using evaporation and drop interaction which incorporated collisional breakup. They found that an initial exponential distribution remained essentially exponential between cloud base and ground.

Research by Kamburova and Ludlam (1966) showed how a downdraft remained unsaturated in spite of evaporation of the rain carried with it. Analogous research into the evaporation of raindrops in the unsaturated downdraft below the cloud was reported by Das and Subbarao (1968, 1972), and Caplan (1969). They assumed the precipitation water to be divided into drops of uniform size falling in a downdraft of constant magnitude and found the subsaturation to be greater with smaller water content, larger drop sizes, and stronger downdrafts. The temperature in the

downdraft was found to lie between the values obtained by either a dry-adiabatic or moist-adiabatic process. Kintigh and Das (1970) investigated the modifications of a drop-size distribution as it descended from cloud base to ground in an unsaturated downdraft by both evaporation and collision-coalescence. Comparing their evaporation results to the earlier studies of monodisperse precipitation, they found that the presence of smaller drops in the population leads to a higher relative humidity in the downdrafts.

b. Objectives

Except for the incomplete study of Kintigh and Das (1970) no effort has been made toward incorporating the primary physical processes in a comprehensive study on the modification of drop-size distribution in a downdraft. The objective of this research is to fill this gap by constructing a raindrop-size distribution model incorporating evaporation, collision-coalescence, aerodynamic breakup, and collisional breakup of drops in a rainshaft accompanying a steady-state, nonentraining downdraft. Calculations will be made for five different situations in order to isolate the modification processes which most affect the raindrop-size distribution. These situations will be characterized by:

a) evaporation only;

b) evaporation and collision-coalescence;

c) evaporation, collision-coalescence, and aerodynamic breakup;

d) evaporation, collision-coalescence, and collisional breakup; and

e) evaporation, collision-coalescence, collisional breakup, and aerodynamic breakup.

The problem as posed will result in variable lapse rates of temperature and relative humidity in the downdraft based on the amount of raindrop evaporation in the subcloud region. Drop-size distributions for several downdraft velocities and precipitation rates will be calculated so that comparisons with observed raindrop spectra can be made. Additionally, the change in rainfall rate and radar reflectivity will be computed in the subcloud region. An effort will be made to compare the computational results of this research to measurements of raindrop-size distributions.

CHAPTER II

BASIC EQUATIONS

The basic equations in this research consist of a thermodynamic equation, a moisture equation and a set of equations for drop concentration including the effects of evaporation, collision-coalescence and aerodynamic and collisional breakup of drops. These equations are applied to the subcloud region under the assumption of a one-dimensional, steady-state downdraft.

a. Thermodynamic Equation

The thermodynamic equation is used to calculate temperature in the downdraft and to account for compressional heating as well as the cooling due to the amount of liquid water evaporated in the subcloud layer. We start with the simplified equation derived by Das (1969):

$$\frac{d\phi}{dt} = \frac{-L_v}{T} \frac{d\xi}{dt} \quad . \quad * \tag{1}$$

Writing $\phi = C_p \ln \theta +$ constant, we have

$$\frac{d\phi}{dt} = \frac{C_p}{\theta} \frac{d\theta}{dt} \quad . \tag{2}$$

By assuming conditions of one-dimensionality and steady-state, and employing the Poisson relationship for potential temperature, the hydrostatic equation, and the equation of state, we can write the vertical temperature gradient as

---

*The symbols used in this paper are listed and defined in Appendix A.

$$\frac{dT}{dz} = - \gamma_d + \frac{L_v}{wC_p} \frac{d\xi}{dt} \quad , \tag{3}$$

where γ_d ($= g/C_p$) is the dry-adiabatic lapse rate of temperature.

b. Equation for Water Vapor

The second term on the right-hand side in (3) requires the substantial rate-of-change of water vapor mixing ratio with time. The equation for $d\xi/dt$ as derived by Das (1969) is

$$\frac{d\xi}{dt} = N' \frac{DM}{Dt} \quad , \tag{4}$$

where N' is the total number of drops per unit mass of air, and DM/Dt is the substantial change of drop mass with time as observed by an observer moving with the drop. Note that (4) assumes a monodisperse population. This substantial change is explained in more detail later. For a polydisperse population, we write $N_r dr$ for the number of drops per unit mass of air lying in the radius interval between radius r and r + dr. With this notation Das (1969) has generalized (4) to

$$\frac{d\xi}{dt} = - \frac{DM_r}{Dt} \int_o^\infty [N_r \, dr] \tag{5}$$

for a polydisperse raindrop population. In this research (5) forms the basis for computing the temporal change in water vapor mixing ratio needed in (3).

c. Equation for Drop Concentration

The equation for drop concentration can be written formally as

$$\frac{\partial n_r}{\partial t} + \nabla \cdot n_r(\vec{V}+\vec{V}_r) = (Q_r)_{EV} + (Q_r)_{CC} + (Q_r)_{AB} + (Q_r)_{CB} \quad , \qquad (6)$$

where n_r is the number of drops per cubic meter per radius interval, $\vec{V}$ is the velocity of the gaseous phase (dry air plus water vapor), $\vec{V}_r$ is the velocity of the liquid phase with respect to the gaseous phase, and Q_r's represent the source and sink effects caused by the respective microphysical processes. The subscripts EV, CC, AB, and CB respectively represent the processes of evaporation, collision-coalescence, aerodynamic breakup and collisional breakup. On the left-hand side (LHS) of (6), the first term represents the local change with time of raindrop concentration and the second term is the divergence of the flux of raindrops.

Using the continuity equation, $d\rho/dt + \rho\nabla\cdot\vec{V} = 0$, and noting that $N_r = n_r/\rho$, we can show that

$$\text{LHS of (6)} = \rho \frac{dN_r}{dt} + \nabla\cdot(n_r\vec{V}_r) \qquad (7)$$

and,

$$\frac{dN_r}{dt} = -\frac{1}{\rho}\nabla\cdot(n_r\vec{V}_r) + \frac{1}{\rho}[(Q_r)_{EV} + (Q_r)_{CC} + (Q_r)_{AB} + (Q_r)_{CB}]. \qquad (8)$$

Applying the assumption of one-dimensional, steady-state motion, we arrive at

$$\frac{dN_r}{dz} = \frac{1}{\rho w_D} \nabla\cdot(n_r \vec{V}_r) - \frac{1}{\rho w_D} [(Q_r)_{EV} + (Q_r)_{CC} + (Q_r)_{AB} + (Q_r)_{CB}], \tag{9}$$

where w_D is the steady-state downdraft velocity. A complete explanation of each of the source terms on the right-hand side of (9) is given in Chapter 3.

d. Equation for Drop Growth

According to Das (1969), the equation for the substantial change in drop growth by condensation or evaporation can be written as

$$\frac{DM_r}{Dt} = \frac{dM_r}{dt} + \vec{V}_r \cdot \nabla M_r \tag{10}$$

where $\frac{dM_r}{dt}$ represents the mass change as seen by an observer moving with the gaseous parcel, and $\vec{V}_r$ is the velocity of the liquid relative to the mixture of dry air and water vapor. Assuming that the water drops share the horizontal motion of the gaseous phase - a possibility which is intuitively accepted and is strongly indicated by the analysis of Das (1962) - we can approximate $\vec{V}_r = -\hat{k}\, V_{T,r}$ where $V_{T,r}$ is the terminal velocity of the raindrops of radius r. Consequently (10) becomes

$$\frac{dM_r}{dt} = \frac{DM_r}{Dt} + V_{T,r} \frac{dM_r}{dz} \quad . \tag{11}$$

CHAPTER III

MODIFYING PROCESSES FOR RAINDROP-SIZE DISTRIBUTION

The physical processes modifying a subcloud drop-size distribution, considered in this research, are (a) evaporation, (b) collision-coalescence, (c) aerodynamic breakup, and (d) collisional breakup of the drops. The continuity equation for raindrop concentration in (8) symbolically incorporates these processes. An equation formulated by Das (1969) forms the basis of the algorithm used in this research to account for evaporation. The procedure used for collision-coalescence is similar to that used by Ogura and Takahashi (1973). The treatment of aerodynamic breakup follows the development of Srivastava (1971), and that of collisional breakup uses the formulation of List and Gillespie (1976). The details of these treatments are described below.

a. Evaporation

Considering evaporation to be the only modifying process in a rainshaft accompanying a steady, one-dimensional downdraft of magnitude w_D, one can rewrite (9) as:

$$\frac{dN_r}{dz_{EV}} = \frac{-1}{w_D \rho} \frac{d\,(\rho N_r V_{T,r})}{dz} + \frac{1}{W_D} \frac{\partial}{\partial r} \left(N \frac{dr}{rdt} \right). \qquad (12)$$

In this expression, the first term on the right-hand side represents vertical sorting of raindrops, and $\frac{dr}{dt}$ is the growth rate of the drop due to evaporation so that the explicit form $(\partial/\partial r)\ (N_r\ dr/dt)$ stands

for the symbolic quantity $(Q_r)_{EV}/\rho$ in (9). In other words, the second term represents the decrease in drop concentration due to diffusion of vapor away from the drops of a particular radius class.

If both sides of (12) are multiplied by the class interval, Δr, the resulting equation can be expressed as

$$\left(\frac{dN}{dz}\right)_{EV} = -\frac{V_{T,r}}{W_D}\frac{dN}{dz} + \frac{1}{W_D}\frac{\partial}{\partial r}\left(N\frac{dr}{dt}\right) - \frac{Nr}{W_D}\frac{dr}{dt}\frac{\partial}{\partial r}(\Delta r), \qquad (13)$$

where $N = N_r \Delta r$ and ρ and V_T are assumed to be constant. Appendix B provides an analysis of the error committed in assuming constant ρ and V_T. The error incurred does not significantly affect the results since we look at the relative effects of each microphysical process on the drop-size distribution. Solving for the change of drop concentration with height, we have

$$\left(\frac{dN}{dz}\right)_{EV} = \left(\frac{1}{W_D + V_{T,r}}\right)\left[\frac{\partial}{\partial r}\left(N\frac{dr}{dt}\right) - N_r\frac{dr}{dt}\frac{\partial}{\partial r}(\Delta r)\right] . \qquad (14)$$

The first term on the right represents the shifting of the drop categories because of drop-size changes due to evaporation. The second term represents an adjustment due to change in the radius intervals for the categories.

In order to obtain an expression for the rate of change of drop radius given in (14), a spherical raindrop is assumed. The mass of a given drop is then

$$M_r = \frac{4}{3}\pi r^3 \delta_\ell \quad , \qquad (15)$$

where δ_ℓ is the density of liquid water. Taking the time derivative of both sides and solving for the rate-of-change of drop radius we have

$$\frac{dr}{dt} = \frac{1}{4\pi r^2 \delta_\ell} \frac{dM_r}{dt} \quad . \tag{16}$$

As pointed out by Das (1969), $\frac{dM_r}{dt}$ does not represent all the mass change of a drop due to evaporation, but only the part of the change moving with the gaseous parcel. The actual change of mass due to evaporation is really the "substantial change" and can be denoted by the "substantial change" and can be denoted by

$$\frac{DM_r}{Dt} = \frac{dM_r}{dt} + \vec{V}_r \cdot \nabla M_r \quad . \tag{17}$$

Combining (16) and (17), we have

$$\frac{dr}{dt} = \frac{1}{4\pi r^2 \delta_\ell} \left[\frac{DM_r}{Dt} + V_{T,r} \frac{dM_r}{dz} \right] \quad . \tag{18}$$

Now, we must obtain an expression for $\frac{dM}{dz}$ so that (18) can be used to calculate the rate-of-change of drop radius. Imposing the condition of a one-dimensional, steady-state downdraft on (17) one can obtain

$$\frac{dM_r}{dz} = \frac{-1}{w_D + V_{T,r}} \frac{DM_r}{Dt} \quad , \tag{19}$$

which, when combined with (18), yields

$$\frac{dr}{dt} = \frac{1}{4\pi r^2 \delta_\ell}\left[\left(\frac{w_D}{w_D+V_{T,r}}\right)\frac{DM_r}{Dt}\right] \quad . \tag{20}$$

This is the expression used to compute the rate of change of drop radius in (14).

The mass evaporation rate, $\frac{DM_r}{Dt}$, given in (20) was tabulated by Kinzer and Gunn (1951). Their experimental results appear in the Smithsonian Meteorological Tables (List, 1949) for raindrop radii from 0.005 cm to 0.21 cm. In this research, the raindrop spectrum ranges from 0.004 cm to 0.4 cm, which requires an extension of the Kinzer and Gunn results. The method used to extend the Kinzer and Gunn raindrop evaporation data is shown in Appendix C.

According to Byers (1965), the rate of change of mass for a spherical drop can be written as

$$\frac{DM_r}{Dt} = \frac{4\pi r(S-1)}{a' + b'} \tag{21}$$

where

$$a' = \frac{L_v^2}{KR_vT^2} \quad , \quad b' = \frac{R_vT}{e_sD} \quad ,$$

and S is the saturation ratio:

$$S = e_a/e_s \quad . \tag{22}$$

Here the saturation vapor pressure, e_s, is computed from an equation

given by Murray (1967):

$$e_s = 6.1078 \exp [17.2694(T-273.16)/(T-35.86)] \qquad (23)$$

It can be seen from (21) that $\frac{DM_r}{Dt}$ is negative for unsaturated conditions and that the mass evaporation rate increases as the air becomes more unsaturated.

b. Collision-coalescence

The collision-coalescence mechanism is commonly named the collection process (Berry, 1967). In this process raindrops grow by gravitational collection: larger drops which fall faster collide and coalesce with smaller drops in their path. The importance of the collection process in warm rain is well established. Houghton (1968) stated that even under conditions in which the ice phase is responsible for the initiation of precipitation, collection is the dominant growth mechanism in the nonfreezing regions of the cloud and is, therefore, important in shaping the drop-size distribution.

There are two collection models used in precipitation physics; they are commonly referred to as the continuous and stochastic models. The continuous collection model is a straightforward concept and can be credited to such early workers as Schumann (1939) and Findeisen (1939). It is characterized by a raindrop distribution consisting of many small droplets and a few large drops; all large drops grow at a continuous rate as they sweep out the small droplets. The basic notion underlying the stochastic model, on the other hand, is that of a "fortunate drop," and was ushered in by Telford (1955). Berry

(1967) described the essential differences between the continuous and the stochastic models and his interpretation is given in Fig. 1. According to the stochastic collection model, depending on an associated probability of collection, a fraction of the large drops of a given class will collect smaller droplets contained in the swept-out volume and grow into a larger drop class. This probabilistic condition arises from the random locations of the smaller droplets with respect to the volume swept out by the larger drop. During any particular time interval, only a fraction of the drops in any particular size class will grow into larger size classes.

The stochastic collection model is the one employed in this research. Following the notation of Ogura and Takahashi (1973), the stochastic collection process can be represented by the symbolic integro-differential equation

$$\left(\frac{dN_i}{dz}\right) = \frac{-\rho}{\rho_d(w_D+V_T)} \frac{1}{2}\int_o^i N_\ell N_{i-\ell}\Phi(\ell,\ i-\ell)d\ell - N_i \int_o^\infty N\Phi(i,\ell)\,d\ell \qquad (24)$$

where i and ℓ, etc., refer to the size categories of the droplets. The first term on the RHS of (24) represents the gain in N_i due to drops of radius r_ℓ coalescing with drops of radius $r_{i-\ell}$ to form drops of radius r_i, while the second term represents the loss of N_i due to drops of radius r_i coalescing with all other drops.

In (24), $\Phi(i,\ \ell)$ is the collection kernel defined in terms of the sweep-out rate of a geometric volume relative to the two drops of radius r_i and r_ℓ and the collection efficiency; it represents the probability that two drops will coalesce per unit time. For

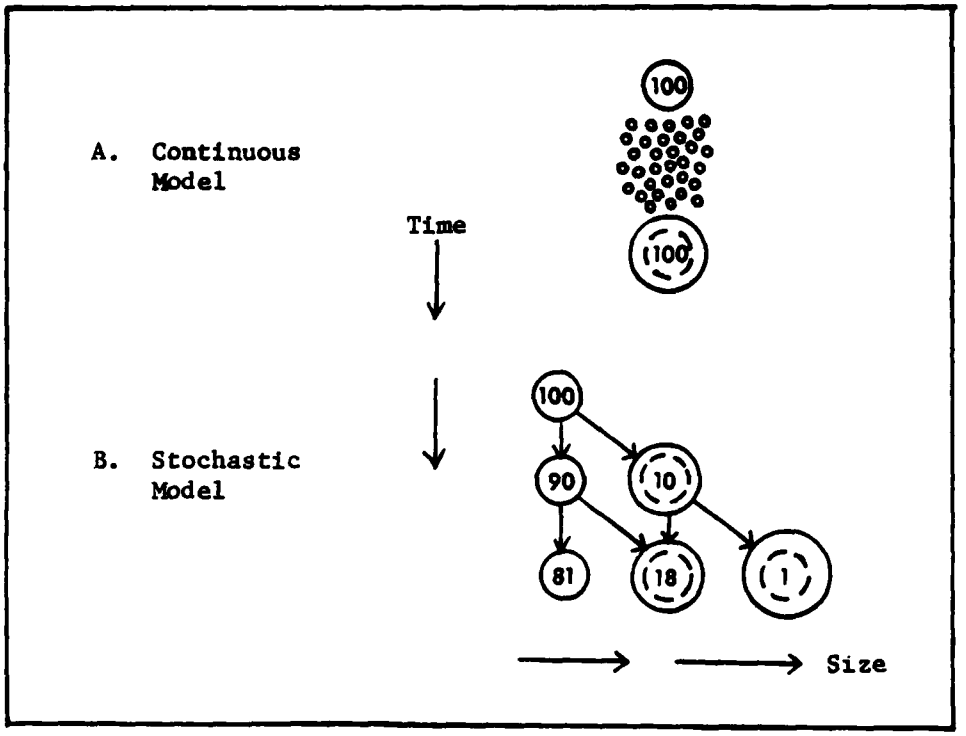

Fig. 1. The continuous and stochastic models.

A. The continuous model assumes that small droplets are swept out as if their water were distributed uniformly in space, and that 100 large drops grow at the same rate, becoming 100 similar larger drops.

B. The stochastic model assumes that, say 1 in 10 of 100 large droplets will collect a small droplet during a given time, and then 1 in 10 of each larger size will collect a smaller droplet. Large droplets then grow at different rates (after Berry, 1967).

this research, the collection kernel given by Srivastava (1967) is used, viz.,

$$\Phi(i,\ell) = \pi(r_i+r_\ell)^2 \, E(i,\ell)|v_i - v_\ell| \tag{25}$$

where r_i and r_ℓ are the radii of the drops with mass i and ℓ, respectively, and $E(i,\ell)$ is the collection efficiency. The collection efficiency, $E(i,\ell)$, is a product of the collision efficiency $E_1(i,\ell)$ and the coalescence efficiency $E_2(i,\ell)$.

In this study, the collision efficiency is taken as equal to one representing geometric sweep-out. In the experiments revised by List and Gillespie (1976), it appears that for raindrops the inertial effects are large enough to prevent the incoming small drop from being deflected noticeably by the flow around the larger one. Thus, raindrop trajectories are essentially straight lines. In addition, in the portion of the present research in which consideration was given to collision-coalescence in conjunction with evaporation and aerodynamic breakup, the coalescence efficiency was set equal to one. This was done so results could be compared with those of Srivastava (1971). When collisional breakup was included with collision-coalescence, the coalescence efficiency as formulated by Whelpdale and List (1971) was used. This will be discussed in greater detail later in this section.

An important constraint on the stochastic collection process is that the total mass under distribution N_i should remain constant. This serves as a check on the numerical accuracy of the finite difference scheme. This mass represents the liquid water content of the

rainshaft, and can be written as

$$\rho_\ell = \int_0^\infty n_r M_r \, dr \tag{26}$$

c. Aerodynamic Breakup of Drops

Langmuir (1948) proposed a chain process as a possible mechanism for producing the drop-size distributions observed in warm clouds. According to Langmuir, there was a critical drop radius beyond which all drops would immediately become unstable and breakup. He adopted the radius of 0.3 cm to be the critical value. However, the experimental work of Komabayasi et al. (1964) indicates that the critical size is not very sharp; instead, a gradual growth of aerodynamic instability appears to be the case. Srivastava (1971) has analyzed the experimental data of Komabayasi et al. (1964) on the probability of aerodynamic breakup of water drops and the size distribution of the fragments resulting from the breakup. When the aerodynamic breakup is the only process modifying the drop-size distribution, the rate of change of N_i with time can be represented by

$$\left(\frac{dN_i}{dz}\right)_{AB} = \frac{1}{(w_D+V_T)}\left[-N_i P_i + \int_i^\infty N_\ell Q(i,\ell) P_\ell \, d\ell\right], \tag{27}$$

where P_i represents the probability with which a drop of radius r_i breaks up per unit time, and $Q(i,\ell)$ represents the number of fragments of radius r_i given by the breakup of one drop of radius r_ℓ. Expressions for P_i and $Q(i,\ell)$ are

$$P_i = 2.94 \times 10^{-7} \exp (34 r_i) \tag{28}$$

and

$$Q(i,\ell) = 436.1 \frac{r_i}{r_\ell} \exp \left(-7 \frac{r_i}{r_\ell}\right) , \tag{29}$$

where r_i is expressed in centimeters. The expressions for P_i and $Q(i, \ell)$ as given above insure the requirement for total mass conservation.

d. Collisional Breakup of Drops

On reviewing the experimental studies on aerodynamic breakup including those of Komabayasi et al. (1964), List et al. (1970) implied that aerodynamic breakup did not appear to explain the observed size distributions of raindrops. Computations of Srivastava (1971), who regarded aerodynamic breakup to be the only drop-disintegration process, produced a raindrop size distribution having relatively more large drops than observed in rain formed in all-liquid processes. Consequently, in the Langmuir chain model of warm rain development a more effective drop-disruption process appears to be needed and, according to List et al. (1970), the process of temporary collision, between drops of sizes too small to be aerodynamically unstable, appears to be the answer. This process, commonly referred to as collisional breakup, has been studied experimentally by List et al. (1970), Brazier-Smith et al. (1972), McTaggart-Cowan and List (1975), and Bradley and Stow (1979). List et al. (1970) investigated the fragment size spectra developing

after collisions of drops with radii 0.10 to 0.23 cm, but did not consider drops falling at terminal velocity. They concluded that, in order to study the growth of warm rain by chain process and to make definite statements about drop-size limitations, more collision and breakup experiments would be needed in a larger range of smaller and larger drop combinations, preferably with drops falling at terminal velocity. Experimental studies by Brazier-Smith et al. (1972) involving drops of radii 0.015 to 0.075 cm and later studies by Bradley and Stow (1979) involving drops in the radius range 0.06-0.17 cm failed to use drops falling at terminal velocity. McTaggart-Cowan and List (1975) updated the studies of List et al. (1970) by conducting experiments with drops of radii 0.05 to 0.23 cm, all falling at terminal velocity. They used a high-speed photographic method to observe several hundred collisions of five different drop pairs. The radii (r_s) of the smaller drops were 0.05 or 0.09 cm while those of the large ones (r_L) were 0.15, 0.18, or 0.23 cm. Their work showed that the coalescence of large drops with smaller ones was a rare event, the most likely outcome of the collisions being the production of numerous fragments with loss of mass from the large participating drop. Thus the coalescence efficiency was much less than unity.

Since McTaggart-Cowan and List (1975) experimented with drops at their terminal velocities, it is their fragment size distributions that have been chosen for this research. Using their experimental observations, List and Gillespie (1976) developed formal expressions for the statistical rates of production of small and

large fragments resulting from collisional breakup of a pair of drops. The contribution of these fragments to a drop-size category is expressed through a function $W_i(L,s)$ which is the rate of formation of drops of radius r_i by collision-induced breakup of a larger drop of radius r_L interacting with smaller drops of radius r_s:

$$W_i(L,s) = \rho\pi \int_o^L N_s (r_L + r_s)^2 \, E_1(L,s)(V_L - V_s) P_i(L,s) ds \quad . \tag{30}$$

Here $P_i(L,s)$ denotes the probability of obtaining a drop of radius r_i by collision between and subsequent breakup of a larger drop of radius r_L and a smaller drop of radius r_s. Thus the rate of increase of drop concentration in i-th category can be written

$$\frac{dN_i}{dz} = \frac{1}{(w_D + V_T)} \left[\int_{r_i}^{\infty} N_L W_i dr_L - N_i \int_o^{r_i} W_i dr_L \right] \quad , \tag{31}$$

where N_i is the drop concentration per unit mass of air. The first term on the R.H.S. of (31) represents a gain in the i-th category due to collision between drops of radii larger than r_i, whereas the second team gives the loss in the category due to their collison with smaller drops.

In the experiments of McTaggart-Cowan and List, a typical overall distribution of fragments shows two peaks, one toward the small and the other toward the large drop end. List and Gillespie conclude that the observed fragment distributions are fairly well represented by the following expressions:

$$\bar{f} = 1.44 \times 10^3 \, (r_L^3 r_s)^{1/2} \, (0.41 - 0.30 \, \frac{r_s}{r_L}) \quad , \qquad (32)$$

$$\bar{D} = -1.0 - \frac{0.0196}{r_s} \quad , \qquad (33)$$

with

$$P(s) = \left(0.3 \, \frac{\bar{f}}{r_s}\right) \, (1.529 \times 10^5 M_i)^{\bar{D}} \quad , \text{ if } M_i \leq 1 \times 10^{-6} \text{Kg}, \qquad (34)$$

or

$$P(s) = \left(0.3 \, \frac{\bar{f}}{r_s}\right) \, \frac{(M_i \times 10^6)}{(0.0654)^{\bar{D}}} \quad , \text{ if } M_i > 1 \times 10^{-6} \text{ Kg}, \qquad (35)$$

where $\bar{f}$ is the total number of small fragments, and $\bar{D}$ is the power law constant used to fit the small-fragment distribution. In these expressions the radius, r, and mass, M, are expressed in units of centimeters and kilograms, respectively.

A Gaussian function fitted by List and Gillespie to the large fragment distribution is written*

$$P(L) = \begin{cases} H \exp\left[-(M_i - M_L)^2 H^2/2\right] & \text{for } M_i \leq (M_L + M_s) \\ 0 & \text{for } M_i > (M_L + M_s) \end{cases} \qquad (36)$$

with

---

*There is a sign error in the expression as printed and it is possible that the computation of List and Gillespie (1976) failed to correct the expression; further comments on this possibility are made later in this dissertation.

$$H = \frac{0.37}{r_s^4 r_L (0.41-0.3r_s/r_L)} \quad . \tag{37}$$

The distribution is cut off for $M_i > M_L + M_s$ because no fragment larger than the sum of the incoming masses can be produced. Finally, the overall fragment probability, P_i (L,s) is written

$$P_i(L,s) = P(L) + P(s) \quad . \tag{38}$$

As mentioned earlier, the experiments of McTaggart-Cowan and List (1975) indicated the coalescence efficiency of interacting drops to be much less than unity. For the purpose of this research, the coalescence efficiency according to Whelpdale and List (1971) is used, modified to agree with the absence of coalescence once the small drop exceeds 0.05 cm radius. The resulting form of the coalescence efficiency, E_2, is

$$E_2 (L,s) = \begin{cases} (1 + r_s/r_L)^{-2} & \text{for } r_s \leq 0.05 \text{ cm} \\ 0 & \text{for } r_s > 0.05 \text{ cm} \quad . \end{cases} \tag{39}$$

It is understood that such clearly defined limits as those in (39) probably do not occur in nature. These coalescence efficiencies are used so our results can be compared with those of List and Gillespie (1976) and Gillespie and List (1978/1979).

CHAPTER IV

PROCEDURE

The change in raindrop concentration in a subcloud downdraft results from the microphysical processes incorporated in (14), (24), (27), and (31). This study consists of a numerical integration of these four equations as an initial value problem. Conditions at the cloud base consist of saturated air at an assumed temperature, a Marshall-Palmer drop-size distribution corresponding to an assigned rainfall rate, and a constant subcloud downdraft. As for the choice of the Marshall-Palmer distribution at the cloud base, we may recall that this expression provided a good average fit to the experimental data of Laws and Parsons (1943) except for a tendency to overestimate the numbers of small droplets ($r < 0.001$ cm). Although the measurements of Laws and Parsons were made at the surface, the work of several researchers suggests that an exponential drop-size distribution may be valid aloft. Srivastava (1967), who summarized previous drop-size distribution studies, suggests that the exponential distribution may be quasi-stable with respect to modification during fall, and while the exponential distribution itself changes slowly, other distributions might tend toward an exponential shape. In addition, we want to compare our computed drop-size distributions with those obtained in other studies that used the Marshall-Palmer distribution at cloud base.

In the computational setup, the subcloud region is divided into a finite number of layers and the thermodynamic and hydrometeoric

quantities are calculated at the base of eacy layer for a given subcloud downdraft and a set of subcloud conditions. The computation is continued down to 1500 m below the cloud, which is referred to as the "surface." Once the temperature, relative humidity, total liquid water, rainfall rate, radar reflectivity, and drop-size distribution at the surface are calculated for a given set of conditions, the procedure is repeated for other constant downdraft velocities and cloud base precipitation rates in order to gauge the sensitivity of the resulting steady-state distributions to these parameters. Our study uses constant downdraft velocities of 5, 10, and 15 m/sec with cloud-base precipitation rates of 25, 50, 75, and 100 mm/hr.

a. Cloud-Base Conditions

The Marshall-Palmer distribution of raindrops at the cloud base is written

$$n_r = 0.16 \exp(-\Lambda r), \quad \Lambda = 82\, R^{-0.21} \tag{40}$$

where n_r has units of cm^{-4}, r is in cm, and R is in mm/hr. Fig. 2 shows the Marshall-Palmer drop-size distributions for several rainfall rates.

For numerical purposes the drop-size distributions are discretized into 40 categories with mean radii (r_i, i = 1,40) ranging from 0.004 to 0.4 cm on a logarithmic scale. Table 1 gives n_r according to (40) for each radius category along with the mass of each drop in that category as well as the radius interval (Δr_i) for each category. The

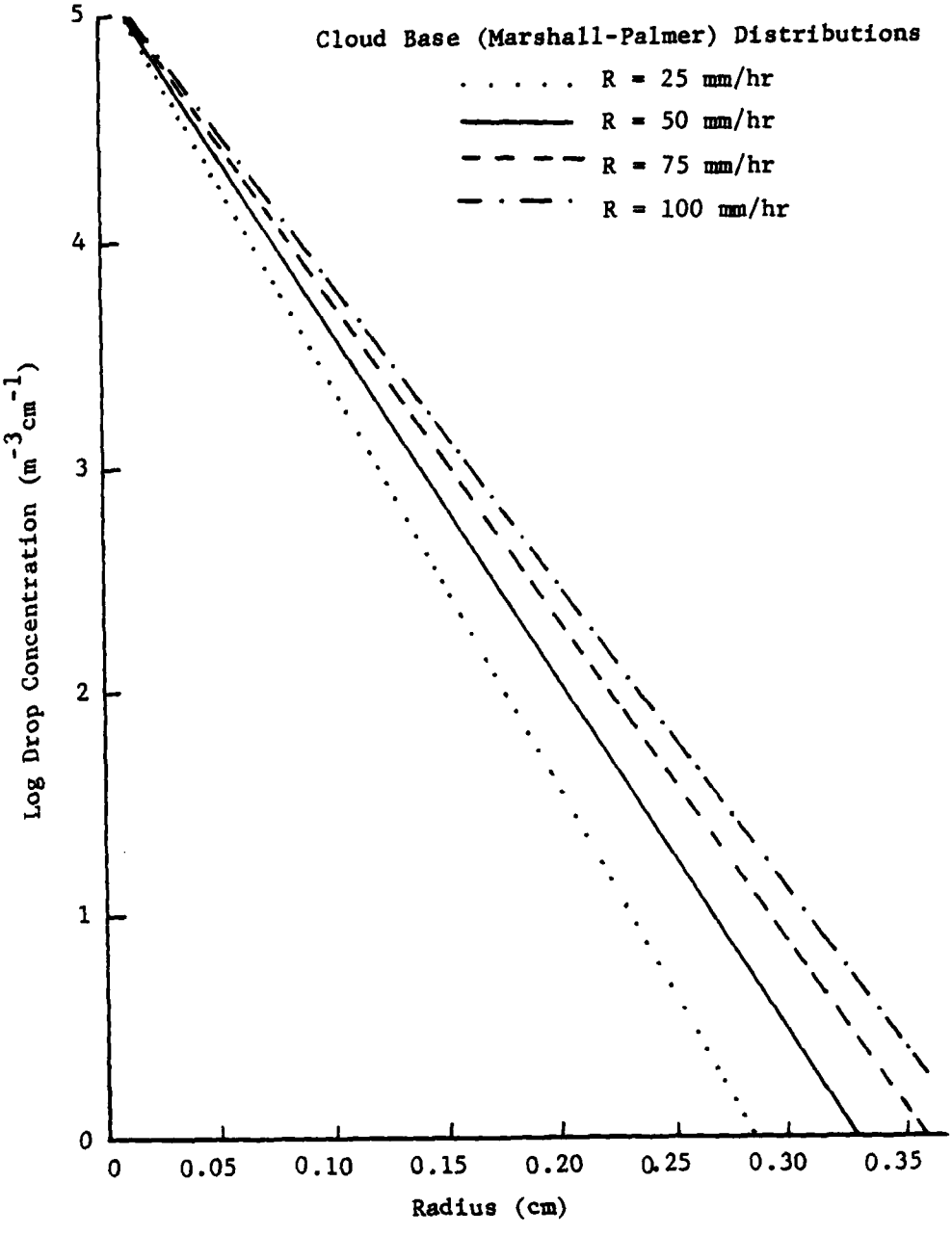

Fig. 2. Marshall-Palmer drop-size distributions for precipitation rates of 25, 50, 75, and 100 mm/hr.

Table 1. Marshall-Palmer drop-size distribution for a precipitation rate of 50 mm/hr.

r_i (cm)	(cm)	V_i (m/sec)	N_i ($\#/m^3$cm)	M_i (kg)
.0042	.0005	0.24	1.373×10^{5}	3.187×10^{-10}
.0048	.0006	0.26	1.348×10^{5}	4.507×10^{-10}
.0053	.0006	0.29	1.320×10^{5}	6.374×10^{-10}
.0060	.0007	0.33	1.289×10^{5}	9.014×10^{-10}
.0067	.0008	0.38	1.255×10^{5}	1.275×10^{-9}
.0076	.0009	0.44	1.218×10^{5}	1.803×10^{-9}
.0085	.0010	0.52	1.178×10^{5}	2.549×10^{-9}
.0095	.0011	0.63	1.135×10^{5}	3.605×10^{-9}
.0109	.0012	0.73	1.088×10^{5}	5.099×10^{-9}
.0120	.0014	0.84	1.038×10^{5}	7.211×10^{-9}
.0135	.0016	0.97	9.847×10^{4}	1.020×10^{-8}
.0151	.0018	1.10	9.279×10^{4}	1.422×10^{-8}
.0170	.0020	1.21	8.680×10^{4}	2.039×10^{-8}
.0190	.0022	1.43	8.054×10^{4}	2.884×10^{-8}
.0214	.0025	1.62	7.404×10^{4}	4.079×10^{-8}
.0240	.0028	1.84	6.738×10^{4}	5.768×10^{-8}
.0269	.0031	2.08	6.060×10^{4}	8.157×10^{-8}
.0302	.0035	2.33	5.381×10^{4}	1.154×10^{-7}
.0339	.0039	2.63	4.709×10^{4}	1.631×10^{-7}
.0381	.0044	2.93	4.054×10^{4}	2.307×10^{-7}
.0427	.0049	3.29	3.427×10^{4}	3.263×10^{-7}
.0479	.0055	3.66	2.837×10^{4}	4.614×10^{-7}
.0538	.0062	4.04	2.296×10^{4}	6.525×10^{-7}
.0604	.0070	4.43	1.810×10^{4}	9.228×10^{-7}
.0678	.0078	4.82	1.386×10^{4}	1.305×10^{-6}
.0761	.0088	5.22	1.027×10^{4}	1.846×10^{-6}
.0854	.0099	5.66	7.339×10^{3}	2.610×10^{-6}
.0959	.0111	6.07	5.032×10^{3}	3.691×10^{-6}
.1076	.0124	6.53	3.294×10^{3}	5.220×10^{-6}
.1208	.0140	7.00	2.048×10^{3}	7.382×10^{-6}
.1356	.0157	7.43	1.201×10^{3}	1.044×10^{-5}
.1522	.0176	7.87	6.596×10^{2}	1.476×10^{-5}
.1708	.0198	8.23	3.367×10^{2}	2.088×10^{-5}
.1918	.0222	8.58	1.583×10^{2}	2.953×10^{-5}
.2152	.0249	8.79	6.784×10^{1}	4.176×10^{-5}
.2416	.0279	9.00	2.621×10^{1}	5.905×10^{-5}
.2712	.0314	9.08	9.013×10^{0}	8.351×10^{-5}
.3044	.0352	9.16	2.720×10^{0}	1.181×10^{-4}
.3417	.0395	9.20	7.087×10^{-1}	1.670×10^{-4}
.3835	.0443	9.25	1.566×10^{-1}	2.362×10^{-4}
.4305	.0498	9.27	2.877×10^{-2}	3.340×10^{-4}

method used to determine the radius intervals of the categories is given later. Fig. 3 shows the percent of total liquid water contained in each drop radius category for the Marshall-Palmer distribution at a rainfall rate of 50 mm/hr. It is easily seen that the bulk of liquid water is contained in the drop radii ranging from 0.004 to 0.4 cm.

A temperature of 5°C is assumed at cloud base. As already mentioned, constant downdrafts of 5, 10, and 15 m/sec are specified at the cloud base and kept constant in the subcloud layer.

b. Grid System and Numerical Procedures

The subcloud region is assumed to be 1500 m deep and is divided into layers of 25-m thickness. Consequently

$$z = j\Delta z, \tag{41}$$

where $j = 0, 1, 2, \ldots, 61$ and $\Delta z = 25$ m, with $j = 0$ at the surface and $j = 61$ at the cloud base.

c. Numerical Formulation for Raindrop Size

The size spectrum of raindrops is divided into 40 logarithmic categories covering the radius range 0.004-0.4 cm in a manner similar to Jorgensen (1974) with droplets of $r < 0.004$ cm lumped into one group. The conversion to the logarithmic scale is made so that the number of data points would be computationally manageable and, as will be seen later, the calculation of raindrop mass would be simplified. In order to facilitate the use of the forward difference scheme for the 40th drop category, one extra category is added at the larger

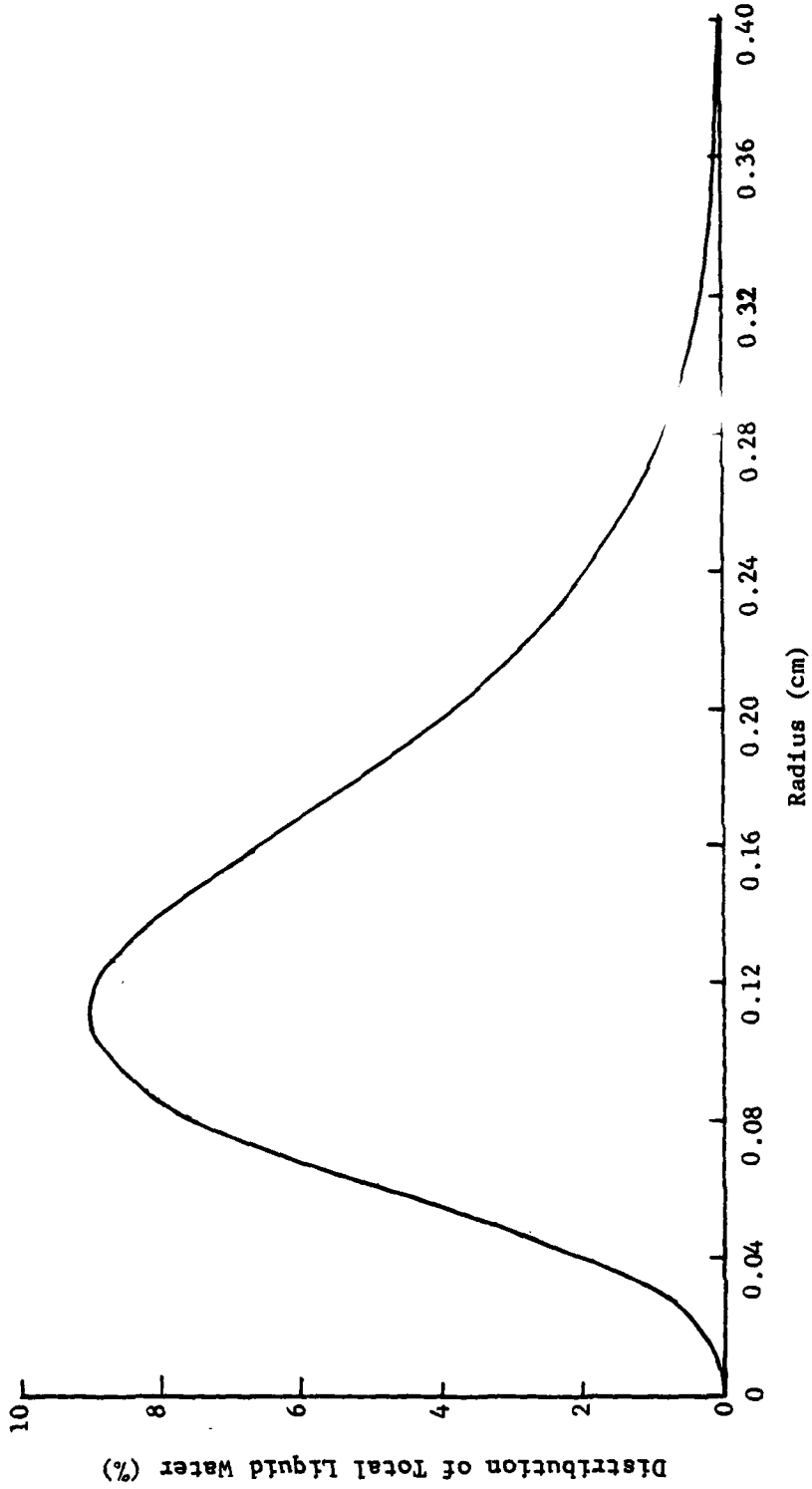

Fig. 3. Percent of total liquid water as a function of drop radius in the Marshall-Palmer raindrop distribution for a precipitation rate of 50 mm/hr.

drop-size end of the distribution. Starting with the smallest value of 0.004 cm, the drops fall into size classes that are obtained from the relation

$$r_{k+1} = 10^{(\log_{10} r_k + \text{DLOGR})}, \quad k = 1, 2, \ldots, 40 \tag{42}$$

where DLOGR is defined as the difference between the logarithms of radii of any two adjacent size classes and is written

$$\text{DLOGR} = (\log_{10} 2)/6 \ .$$

Berry (1967) introduced the logarithmic radius intervals as used in this study in order to emphasize the resolution in the smaller size classes which can be shown as follows. The mass of a drop in the k-th class is

$$M_k = \frac{4}{3} \pi r_k^3 \delta_\ell \ . \tag{43}$$

The mass of the (k+1)-th class can be shown to be

$$M_{k+1} = M_k \, 10^{3 \text{ DLOGR}} = 2M_{k-1} \ , \tag{44}$$

which means that the mass of the raindrops doubles every two radius classes. The high resolution at the smaller size end of the spectrum is especially suitable for this research since the small particles change size rapidly under the effect of evaporation.

The drop radius calculated from (42) represents the midpoint radius of a particular drop category. Table 1 gives the midpoint radii r_i, and the radius intervals, Δr_i (in cm), over which these midpoint

radii are valid. The mass, in kilograms, of a spherical raindrop with the midpoint radius of each category also is given in Table 1.

d. Numerical Formulation of the Thermodynamic and Moisture Equations

The finite-difference form of the thermodynamic equation is given by

$$T_{j+1} = T_j - \gamma_d \Delta z + \frac{L_v}{C_p} \frac{d\xi}{dz} \quad . \tag{45}$$

In order to calculate the temperature at each level, an initial guess for the change in mixing ratio is used. This permits the computation of the temperature change. Once the temperature is computed, the actual mixing ratio change is calculated using

$$\frac{d\xi}{dz} = \frac{1}{w_D} \sum_{i=1}^{40} N_i \frac{DM_i}{Dt} \quad , \tag{46}$$

where the negative sign which accompanies $\frac{DM_i}{Dt}$ has already been included. The values in Table C-2 (Appendix C), properly interpolated, are the mass evaporation rates, $\frac{DM_i}{Dt}$. The result of (46) is used in calculating the new mixing ratio is from

$$\xi_{j+1} = \xi_j + \frac{d\xi}{dz} \Delta z \quad . \tag{47}$$

The relative humidity is computed using (22). As previously mentioned, the saturation vapor pressure, e_s, is computed from (23) and the vapor pressure, e_a, is calculated with the help of

$$e_{a,j+1} = \frac{\xi_{j+1} \; P_{j+1}}{0.622 + \xi_{j+1}} \quad , \tag{48}$$

where P_{j+1} is the pressure at the new level. The pressure is computed from the hydrostatic relationship

$$P_{j+1} = P_j \exp\left[\frac{g\Delta z}{R_d \overline{T}}\right] \tag{49}$$

where $\overline{T}$ is the mean temperature in the layer.

e. Numerical Formulation of the Evaporation Effects

In formulating the finite-difference approximation to (14) we proceed as follows. Writing $N_k = (N_r \Delta r)_k$ where N_k represents the concentration of drops in the category k, we can rewrite (14) as

$$\left(\frac{dN_k}{dz}\right)_{EV} = \left(\frac{1}{W_D + V_T}\right)\left[\frac{\partial}{\partial r}\left(N_r \frac{dr}{dt} \Delta r\right) - N_r \frac{dr}{dt} \frac{\partial}{\partial r} (\Delta r)\right]_k \quad , \tag{50}$$

in which the last term arises from the fact that the categories have variable width Δr_k. The finite-difference form of (50) with respect to r can be written

$$\frac{dN_k}{dz}_{EV} = \left(\frac{1}{w_D + V_T}\right)\left[\frac{(\Delta r N_r dr/dt)_{k+1} - (\Delta r N_r dr/dt)_k}{r_{k+1} - r_k} - \left(N_r \frac{dr}{dt}\right)_k \right.$$

$$\left. \times \frac{\Delta r_{k+1} - \Delta r_k}{r_{k+1} - r_k}\right] \quad . \tag{51}$$

We observe the following:

$$\Delta r_k = r_{k+1} - r_k = r_k(\gamma - 1),$$

and

$$\Delta r_{k+1} = r_{k+2} - r_{k+1} = r_{k+1}(\gamma - 1),$$

where

$$r_{k+2}/r_{k+1} = r_{k+1}/r_k = \cdots = \gamma,$$

which, because of constant logarithmic intervals in our categorization, is a constant. Using these results we can reduce (51) to

$$\left(\frac{dN_k}{dz}\right)_{EV} = \left(\frac{\gamma}{w_d + V_{T,k}}\right)\left[\left(N_r \frac{dr}{dt}\right)_{k+1} - \left(N_r \frac{dr}{dt}\right)_k\right] . \tag{52}$$

Rewriting (52) in terms of finite-differences in z, we have

$$(\Delta N_k)_{EV} = \left(\frac{\gamma \Delta z}{w_D + V_{T,k}}\right)\left[\left(N_r \frac{dr}{dt}\right)_{k+1} - N_r\left(\frac{dr}{dt}\right)_k\right]_j , \tag{53}$$

or

$$\left(N_{k,j+1}\right)_{EV} = N_{k,j} + (\Delta N_k)_{EV} . \tag{54}$$

Eqs. (53) and (54) are used to compute the drop-size distribution which reflect the change due to evaporation only. Once the number concentration in each radius category is computed at the new level j+1, the liquid-water content at that level may be computed from

$$A_{j+1} = \sum_{k=1}^{40} M_k N_{k,j+1} \rho , \tag{55}$$

where M_k is mass of one spherical drop in the radius category k.

f. Numerical Formulation for Collision-Coalescence

A formulation similar to that given by Ogura and Takahashi (1973), is used to change the collision-coalescence equation given in (24) to a summation suitable for programming:

$$(\Delta N_k)_{CC} = \left(\frac{\rho_a \Delta z}{w_D + V_T}\right)\left[\sum_{k'=1}^{kh} N_{k'} N_{kc} \left(\frac{r_k}{r_{kc}}\right)^3 \Phi(kc,k') - N_k \sum_{k'=1}^{kmax} N_{k'} \Phi(k,k')\right] \quad (56)$$

or

$$\equiv (\Delta N_k)_{CC-G} - (\Delta N_k)_{CC-L} \quad .$$

Here the subscripts CC-G and CC-L stand for gain and loss respectively, in the concentration of drops in the k category due to collision-coalescence. In addition,

$$kh = k - \frac{k_o}{3} \ln 2 = k - 2\, k_o \,\text{DLOGR}\, \ln 10 \quad , \quad (57)$$

where k_o is an adjustable scale factor that fixes the desired data points at integer values of k. Since $k_o = 1/(\text{DLOGR}\ \ln 10)$, kh = k-2, which is the class index of drops whose mass is half that of class k. Further

$$k_c = k + \frac{k_o}{3} \ln\left[1 - \exp 3(k'-k)/k_o\right] \quad . \quad (58)$$

To calculate N_{kc}, the following four-point Lagrangian interpolation scheme is used:

$$N_{kc} = -\frac{1}{6}(1-\alpha)(\alpha)(1+\alpha)N_{k-2} + \frac{1}{2}(2-\alpha)(\alpha)(1+\alpha)N_{k-1}$$

$$+ \frac{1}{2}(2-\alpha)(1-\alpha)(1+\alpha)N_{k} - \frac{1}{6}(2-\alpha)(1-\alpha)(\alpha)N_{k+1} \quad , \tag{59}$$

where

$$\alpha \equiv k-k_c = \frac{k_o}{3} \ln\left[1-\exp\frac{3k'-k}{k_o}\right] . \tag{60}$$

Once $(\Delta N_k)_{CC}$ is calculated, the number concentration in the k-category is obtained by combining the effect of evaporation and collision-coalescence, that is,

$$(N_{k,j+1})_{EV+CC} = N_{k,j} + (\Delta N_k)_{EV} + (\Delta N_k)_{CC} \quad . \tag{61}$$

The collision-coalescence process operates under the constraint of conservation of total liquid water. No drops are allowed to enter the drop-size distribution at the small radius end (< 0.004 cm) due to collision-coalescence, but drops are allowed to move out the larger radius end (> 0.4 cm) of the spectrum. The first term in brackets in (56) is allowed to operate for the 41st radius category. This allows drops to collect in this category due to collection in the smaller radius categories, but does not allow any drop to leave due to collection between category 41 drops and all other drops in the distribution. Although this does not conserve total liquid mass between drops of radii 0.004 cm to 0.40 cm, it does conserve mass when the aerodynamic breakup process is considered.

g. Numerical Formulation for Aerodynamic Breakup

The finite difference formulation of Jorgensen (1974) is used to evaluate the aerodynamic breakup term given in (27), i.e.,

$$(\Delta N_k)_{AB} = \left(\frac{\Delta z}{w_D + V_{T,k}}\right)\left[-N_k P_k + \sum_{k=k+1}^{40} N_k \, Q(k,k') P_{k'}\right] , \qquad (62)$$

where the functions P and Q are given by (28) and (29), respectively. On combining the effects of evaporation, collision-coalescence, and aerodynamic breakup, we have

$$(N_{k,j+1})_{EV+CC+AB} = N_{k,j} + (\Delta N_k)_{EV} + (\Delta N_k)_{CC} + (\Delta N_k)_{AB} . \qquad (63)$$

h. Numerical Formulation for Collisional Breakup

The numerical procedure of List and Gillespie (1976) and Takahashi (1977) was reviewed in formulating the collisional breakup procedure. The collisional breakup computation is divided into two parts; one for the gain term (subscripted CB-G) and the other for the loss term (subscripted CB-L). The gain term is computed from

$$(\Delta N_k)_{CB-G} = \frac{\rho_a \Delta z}{(w_D + V_{T,k})} \sum_{l=32}^{41} \sum_{s=23}^{L-1} N_L N_s \phi(r_L, r_s) P_k(L,s) . \qquad (64)$$

Eq. (64) represents the gain in the concentration of drops in the radius category k due to breakup following collision between drops in the radius category r_L (large) and r_s (small). As mentioned previously, the smallest r_L used by McTaggart-Cowan and List (1975)

was 0.15 cm while the smallest r_s was 0.05 cm. The minimum r_L and r_s correspond to approximately categories 32 and 23, respectively. Although their experimental results did not cover the entire drop size distribution of our research, the P(L) and P(s) functions were considered continuous since they approached zero at $r = r_{max}$ and $r = r_{min}$. The one exception for P(s) was when the mass, M_k, was less than 1×10^{-6} kg. Rather than let P(s) increase exponentially at the small radius end of the spectrum, it was considered constant at $r_k = 0.025$ cm (radius category 16). This was done because McTaggart-Cowan and List (1975) could not resolve drop fragment information below this radius. Their results, however, appear to be reaching a fragment maximum near this radius value.

The loss of drops in the radius category k is considered in three different ways depending on whether (i) $k < 23$, (ii) $23 \leq k < 32$, or (iii) $k \geq 32$. No collisional breakup is allowed when $k < 23$ ($r_k < 0.05$ cm). This is consistent with the experimental data of McTaggart-Cowan and List. When $23 \leq k < 32$ (0.05 cm $< r_k <$ 0.15 cm), the loss term for the drops in category k is expressed as

$$(\Delta N_k)_{CB-L} = \left(\frac{\rho_a \Delta z}{w_D + V_{T,k}}\right) \sum_{L=32}^{41} \frac{N_L}{M_k + M_L} \sum_{fr=1}^{40} M_{fr} N_k \, \Phi(r_L, r_k) P_{fr}(L,k) \, , \tag{65}$$

where fr refers to a fragment drop resulting from the collisional breakup of drops of radius r_L and r_k. In order to determine the number of drops in category k lost by collision with category L drops, the total mass of fragments produced is multiplied

by the ratio, $\frac{M_k}{M_k+M_L}$. This product, when divided by M_k, yields the proportional number of category k drops lost.

For k greater than 32 the loss term is expressed as

$$(\Delta N_k)_{CB-L} = \left(\frac{\rho_a \Delta z}{w_D+V_{T,k}}\right) \sum_{s=23}^{31} \frac{N_s}{M_k+M_s} \sum_{fr=1}^{40} M_{fr} N_k \Phi(r_k,r_s) P_{fr}(k,s) \quad . \quad (66)$$

Again, the number of category k drops lost due to collisional breakup with category s drops is calculated by using the total mass concept explained earlier.

Table 2 reviews the collisional processes allowed in various radius category intervals when coalescence and breakup are considered together.

Table 2. Summary of collisional processes.

Radius Category Interval	Collisional Processes Allowed
$1 \leq k < 23$	CC-L, CC -G, CB-G
$23 \leq k < 41$	CC-G, CB-L, CB-G

When the collisional breakup gain and loss terms are combined with the microphysical processes in (63), the number of k drops at a given level is obtained from

$$(\Delta N_{k,j+1})_{EV,CC,AB,CB} = (\Delta N_{k_{EV}} + \Delta N_{k_{CC}} + \Delta N_{k_{AB}} + \Delta N_{k_{CB}})_{j+1} ,$$

or

$$N_{k,j+1} = N_{k,j} + (\Delta N_{k,j+1})_{EV,CC,AB,CB} \quad . \quad (67)$$

i. Numerical Formulation for Rainfall Rate and Radar Reflectivity

Rainfall rate is formulated in units of mm/hr numerically according to the following expression

$$R_j = \frac{3.6X10^6}{\delta_\ell} \sum_{k=1}^{40} n_{k,j} M_k V_{T,k} \quad . \tag{68}$$

Radar reflectivity is computed numerically in units of mm^6/m^3 by the following expression

$$Z_j = 6.4 \text{ X } 10^6 \sum_{k=1}^{40} n_{k,j} r_k^6 \quad . \tag{69}$$

The numerical factors in the above expressions appear because of conversion to the conventional units from the units used in the computation, namely, $V_{T,k}$ in m/sec, and r_k in cm. Also note that the conventional Z is computed with diameters rather than radii of drops.

CHAPTER V

RESULTS

In presenting the results we recall our objective which is to isolate the effects of the microphysical modification processes of evaporation, collision-coalescence, aerodynamic breakup, and collisional breakup on the drop-size distribution in a rainshaft accompanying a steady-state, non-entraining downdraft. To that end computations were made for five cases as follows:

Case A: Evaporation;

Case B: Evaporation and collision-coalescence;

Case C: Evaporation, collision-coalescence, and aerodynamic breakup;

Case D: Evaporation, collisional-coalescence, and collisional breakup; and

Case E: Combination of all the processes mentioned in Case A through Case D.

The variations of drop-size distribution resulting in each case are presented along with variations in temperature, relative humidity, rainfall rate, and radar reflectivity in the subcloud region. Computations were made by using steady state downdrafts of 5, 10, and 15 m/sec, and for still air precipitation rates of 25, 50, 75 and 100 mm/hr.

a. Case A: Evaporation

The vertical distributions of selected thermodynamic and moisture variables resulting from evaporation are listed in Tables 3, 4, and 5

Table 3. Vertical distributions of thermodynamic and hydrometeoric quantities for Case A in a constant subcloud downdraft of 5 m/sec, where z = height above the surface (1500 m = cloud base), T_D = dry-adiabatic temperature, T = rainshaft temperature, S = relative humidity, M = liquid water content, R = rainfall rate, and Z = radar reflectivity.

z (m)	T_D (K)	T (K)	S (%)	M($\times 10^{3}$) (kg/m^3)	R (mm/hr)	Z($\times 10^{-5}$) (mm^6/m^3)
			R = 25 mm/hr			
1500	278.0	278.0	100.0	1.24	25.0	0.33
1000	282.9	282.8	77.4	1.22	24.7	0.33
500	287.8	287.3	62.4	1.17	24.0	0.32
0	292.7	291.6	51.8	1.10	22.8	0.31
			R = 50 mm/hr			
1500	278.0	278.0	100.0	2.24	50.0	0.92
1000	282.9	282.7	78.1	2.21	49.7	0.91
500	287.8	287.0	64.3	2.15	48.6	0.90
0	292.7	291.1	54.9	2.06	46.9	0.89
			R = 75 mm/hr			
1500	278.0	278.0	100.0	3.28	75.0	1.77
1000	282.9	282.6	78.6	3.25	74.5	1.76
500	287.8	290.7	65.9	3.17	73.1	1.74
0	292.7	290.7	57.6	3.06	71.1	1.71
			R = 100 mm/hr			
1500	278.0	278.0	100.0	4.03	100.0	2.51
1000	282.9	282.6	79.0	3.99	99.4	2.50
500	287.8	286.7	66.9	3.90	97.9	2.47
0	292.7	290.5	59.3	3.79	95.6	2.44

Table 4. Vertical distributions of thermodynamic and hydrometeoric quantities for Case A in a subcloud downdraft of 10 m/sec.

z (m)	T_D (K)	T (K)	S (%)	M($\times 10^3$) (kg/m^3)	R (mm/hr)	Z($\times 10^{-5}$) (mm^6/m^3)
		R = 25 mm/hr				
1500	278.0	278.0	100.0	1.24	25.0	0.33
1000	282.9	282.8	76.7	1.23	24.8	0.33
500	287.8	287.5	60.5	1.18	24.1	0.32
0	292.7	292.1	48.8	1.12	23.0	0.31
		R = 50 mm/hr				
1500	278.0	278.0	100.0	2.24	50.0	0.92
1000	282.9	282.8	77.0	2.22	49.6	0.91
500	287.8	287.4	61.5	2.16	48.6	0.90
0	292.7	291.8	50.5	2.07	46.9	0.88
		R = 75 mm/hr				
1500	278.0	278.0	100.0	3.28	75.0	1.77
1000	282.9	282.8	77.4	3.25	74.5	1.76
500	287.8	287.3	62.4	3.18	73.1	1.74
0	292.7	291.6	52.0	3.07	71.0	1.71
		R = 100 mm/hr				
1500	278.0	278.0	100.0	4.03	100.0	2.51
1000	282.9	282.7	77.6	3.99	99.4	2.50
500	287.8	287.2	63.0	3.91	97.8	2.47
0	292.7	291.4	52.9	3.79	95.4	2.43

Table 5. Vertical distributions of thermodynamic and hydrometeoric quantities for Case A in a subcloud downdraft of 15 m/sec.

z (m)	T_D (K)	T (K)	S (%)	M($\times 10^3$) (kg/m^3)	R (mm/hr)	Z($\times 10^{-5}$) (mm^6/m^3)
			R = 25 mm/hr			
1500	278.0	278.0	100.0	1.24	25.0	0.33
1000	282.9	282.9	76.5	1.23	24.8	0.33
500	287.8	287.6	59.8	1.19	24.2	0.32
0	292.7	292.3	47.8	1.14	23.3	0.31
			R = 50 mm/hr			
1500	278.0	278.0	100.0	2.24	50.0	0.92
1000	282.9	282.8	76.6	2.22	49.7	0.92
500	287.8	287.5	60.5	2.17	48.7	0.90
0	292.7	292.1	48.9	2.09	47.3	0.88
			R = 75 mm/hr			
1500	278.0	278.0	100.0	3.28	75.0	1.77
1000	282.9	282.8	76.9	3.25	74.6	1.76
500	287.8	287.4	61.1	3.19	73.3	1.74
0	292.7	291.9	49.9	3.09	71.4	1.71
			R = 100 mm/hr			
1500	278.0	278.0	100.0	4.03	100.0	2.51
1000	282.9	282.8	77.0	4.00	99.5	2.50
500	287.8	287.4	61.5	3.92	98.1	2.47
0	292.7	291.8	50.6	3.82	95.9	2.43

for constant subcloud downdrafts of 5, 10, and 15 m/sec, respectively. The subcloud temperatures resulting from a dry-adiabatic lapse rate (T_D) are included in the tables for comparison with the computed rain-shaft temperature (T).

The details of the vertical variation of relative humidity are shown in Figs. 4 and 5 for different values of downdraft and for precipitation rates of 25 and 100 mm/hr, respectively. Clearly the lowest subcloud relative humidity is found in the downdraft with the smallest precipitation rate and highest downdraft velocity. The relative humidity throughout the subcloud layer should approach a value of 100% as the speed of the downdraft approaches zero, and a dry-adiabatic profile as the speed of the downdraft becomes very large. The relative humidity distributions are determined by the evaporation of precipitation, which is affected by two factors: first, the smaller, slower-moving drops have a longer time available to evaporate and thus help attain a higher relative humidity; and, second, at higher precipitation rates the larger concentration of small drops results in more evaporation and higher relative humidity.

Changes in drop radius due to evaporation are relatively large for smaller drops (see Appendix C). One way to see this more closely is through the evaporation time constant which is the time required for a drop to be reduced by evaporation to 1/e of its initial mass. Time constants were calculated for several values of relative humidities by using the definition

$$\tau_r \equiv \frac{1}{e}\left(\frac{1}{M_r}\frac{dM_r}{dt}\right)^{-1} , \qquad (70)$$

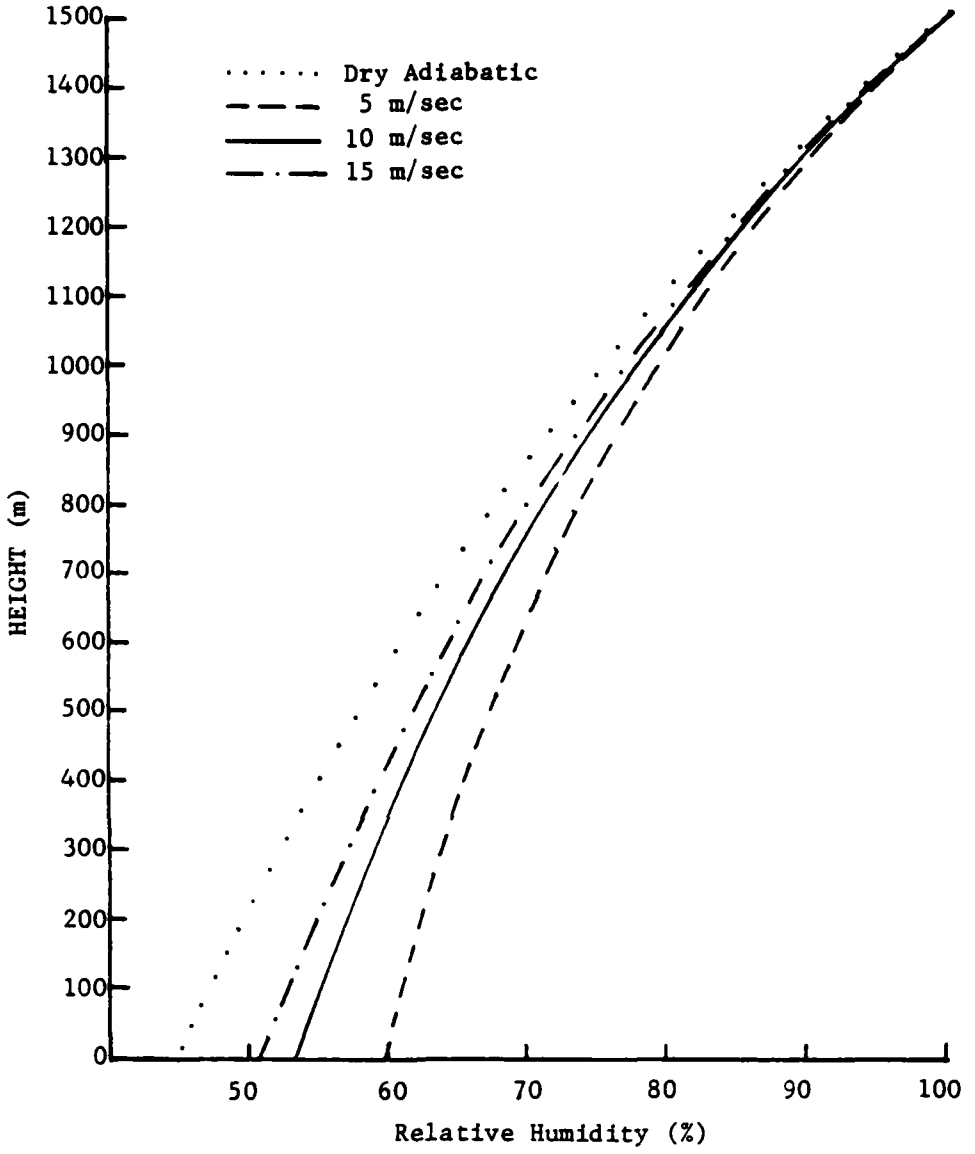

Fig. 4. Subcloud relative humidity profiles in Case A for different downdrafts. The initial precipitation rate is 25 mm/hr.

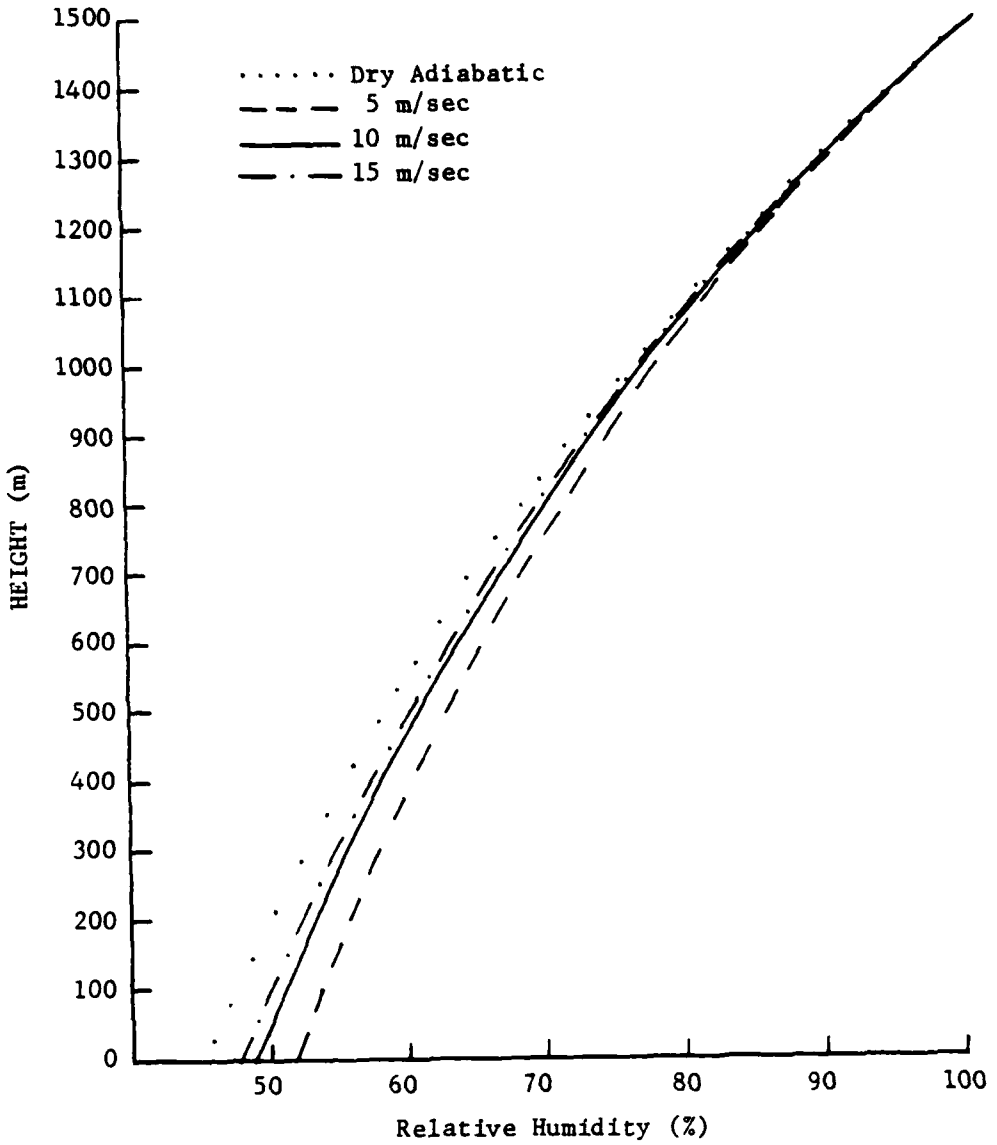

Fig. 5. Same as in Fig. 4 except for an initial precipitation rate of 100 mm/hr.

where e is the base of Naperian logarithms and τ_r is the time constant In addition, dM_r/dt is computed from (C.2). Fig. 6 illustrates the results of the time constant calculations. As the environmental relative humidity decreases, the time constant for the small raindrops decreases to the point where very few of these drops would survive falling through one height interval of $\Delta z = 25$ m. For this reason, drop-size distributions with a large number of smaller drops falling at a slower rate give relative humidity values nearer to saturation than with distributions dominated by larger, faster-falling raindrops. These conclusions are consistent with the results of Kamburova and Ludlam (1966), who concluded that raindrop size had an appreciable influence on evaporation, which proceeds more efficiently with smaller drop sizes. These conclusions also are consistent with those of Das and Subbarao (1972) who show that the rainshaft subsaturation is maximum with smaller water content, larger drop sizes, and stronger downdrafts.

The above results may be an explanation of the "humidity dip" observed by the U.S. Thunderstorm Project (Byers and Braham, 1949) in strong rain shafts accompanying thunderstorms.
Byers and Braham suggested that one reason for downdraft subsaturation was an evaporation rate too slow to provide for the increase in saturation mixing ratio as the air descended. In this case, the air of the downdraft would be heated at a rate between the moist and the dry-adiabatic lapse rates.

Rainfall rate and radar reflectivity are not significantly affected by evaporation alone, as can be seen from Tables 3-5.

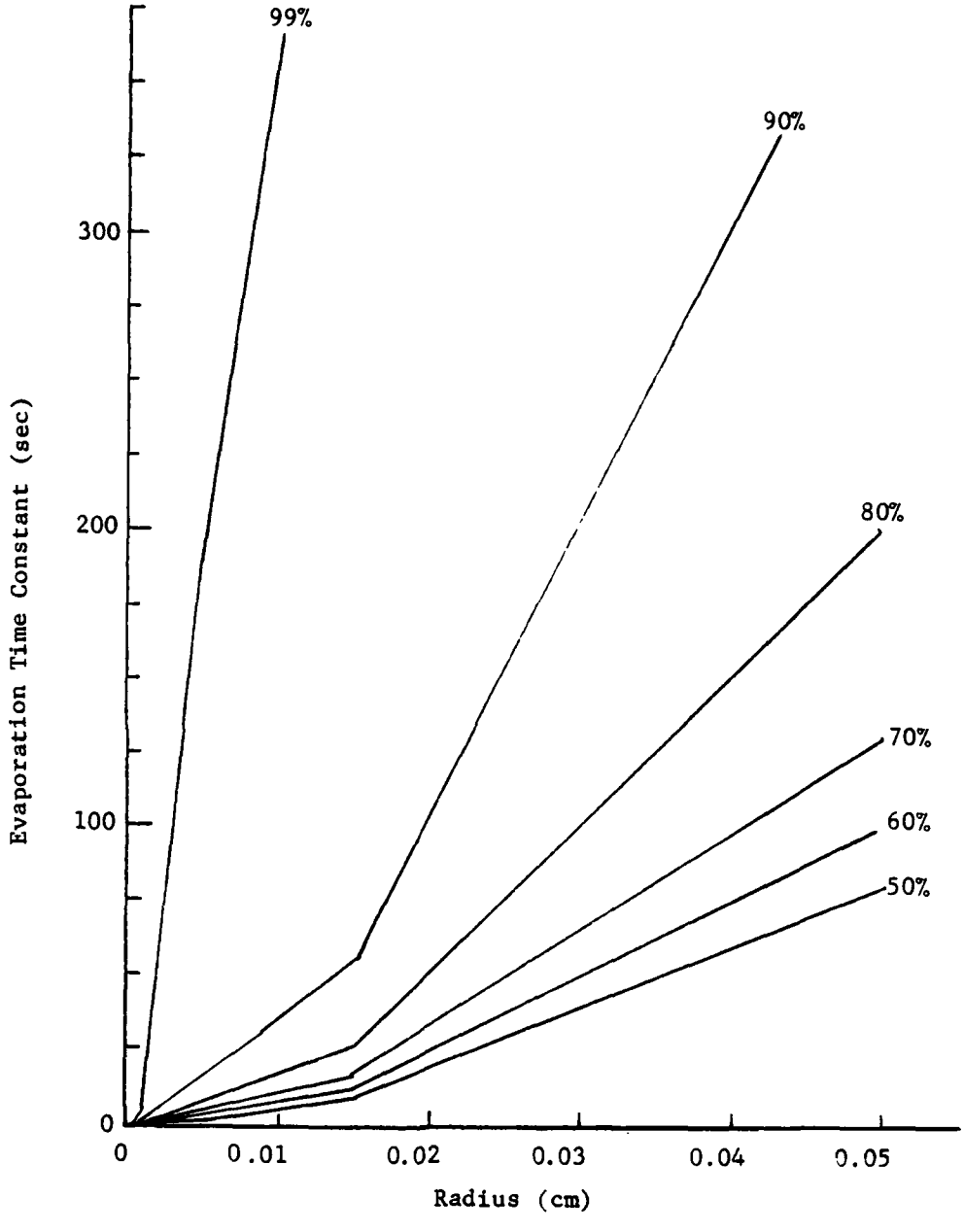

Fig. 6. Evaporation time constants for several values of relative humidity.

Figs. 7 and 8 depict the drop-size distribution 1500 m below cloud base for the conditions presented in Figs. 4 and 5, respectively. The increased loss of drops at the small radius end is quite obvious in these figures. On the other hand, the number concentrations of drops larger than 0.15 cm in radius are seen to change very little thereby implying that the number of drops leaving each drop category due to evaporation is nearly equal to the number of drops entering from the next larger category.

An intuitively apparent result is seen in Figs. 7 and 8 in which the peaks in number concentration are shifted to smaller radii for stronger downdraft velocities and higher initial precipitation rates. It is easy to visualize from these figures that in the limit as the downdraft approaches very high values, the peak in the drop-size distribution will continue to increase and shift toward small radii until it mirrors the cloud-base distribution. The data used to plot Figs. 7 and 8 are contained in Tables 6 and 7, respectively. The number concentrations of drops at the surface are maximum for large initial rainfall rates and strong downdraft velocities.

The drop-size distributions obtained by Kintigh and Das (1970) for pure evaporation showed the peak near a radius of 0.01 cm; however, their results were characterized by several empty drop-size classes. Brazier-Smith et al. (1973) found that the number concentrations of all drop sizes were reduced by evaporation with a preferential reduction at the small-radius end of the spectrum. Their results did not show a peak in the number concentration at 0.015-0.020 cm radius because they assumed a constant relative humidity gradient, which only

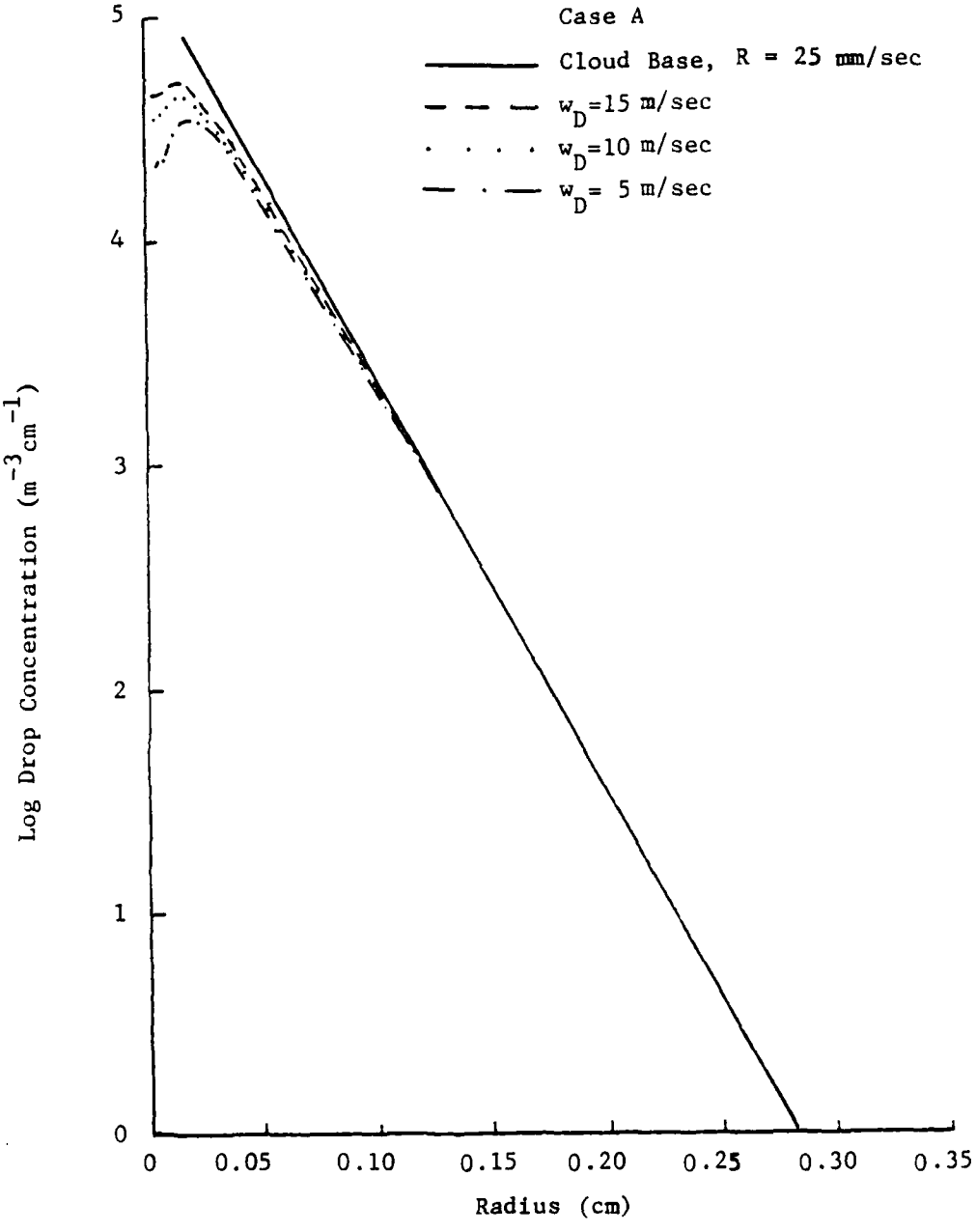

Fig. 7. Drop-size distributions 1500 m below cloud base for various constant downdrafts. The cloud base drop-size distribution is Marshall-Palmer for R = 25 mm/hr.

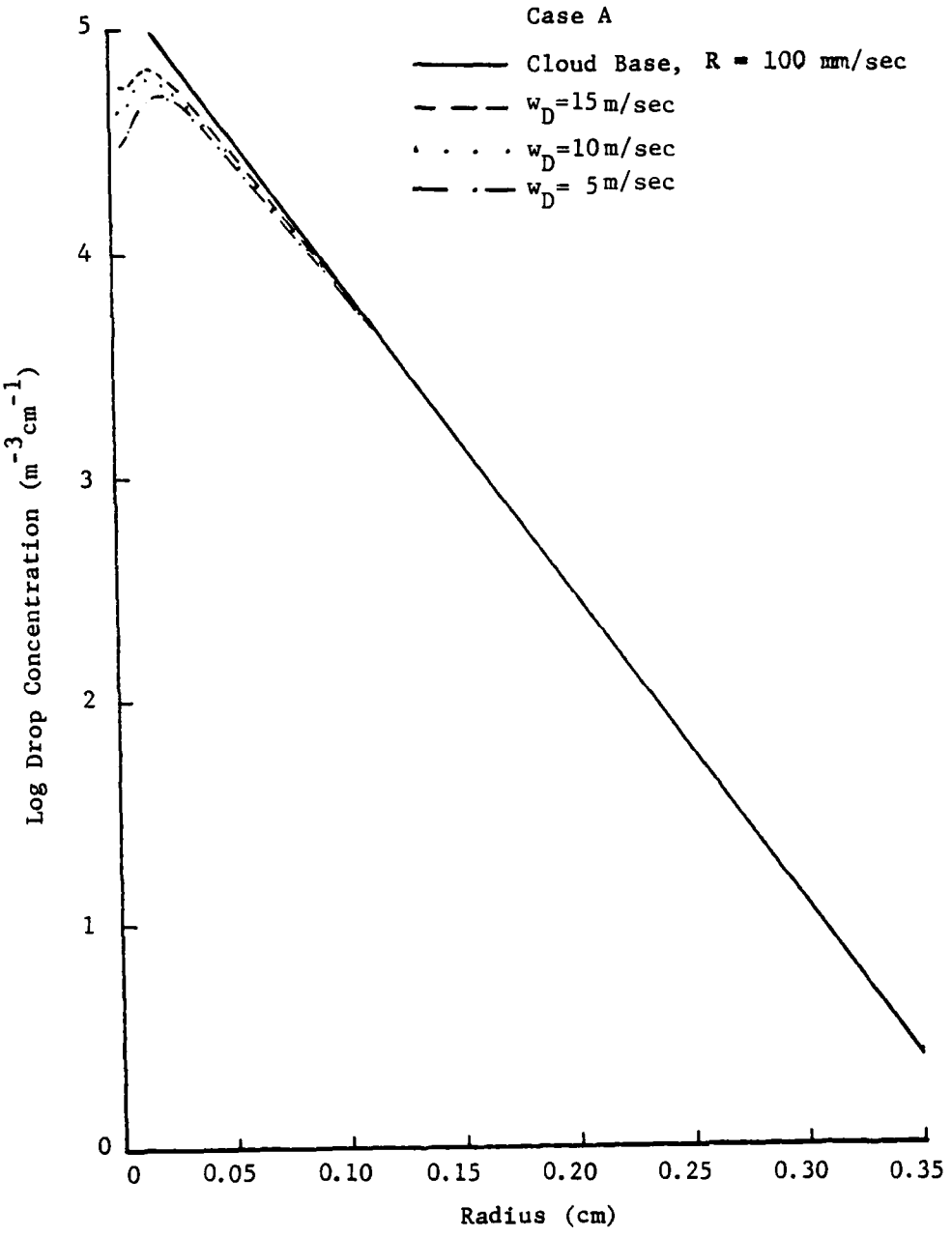

Fig. 8. Same as in Fig. 7 except that the cloud base drop-size distribution is Marshall-Palmer for R = 100 mm/hr.

Table 6. Drop-size distributions at cloud base (Marshall-Palmer distribution for a precipitation rate of 25 mm/hr) and 1500 m below cloud base for constant downdrafts of 5, 10, and 15 m/sec for Case A.

Radius (cm)	Drop Concentration ($m^{-3}cm^{-1}$)			
	Cloud Base	1500 m Below Cloud Base		
		5 m/sec	10 m/sec	15 m/sec
0.0042	1.340×10^{5}	1.890×10^{4}	3.015×10^{4}	3.999×10^{4}
0.0048	1.311×10^{5}	2.189×10^{4}	3.527×10^{4}	4.648×10^{4}
0.0053	1.280×10^{5}	2.243×10^{4}	3.567×10^{4}	4.657×10^{4}
0.0060	1.245×10^{5}	2.242×10^{4}	3.523×10^{4}	4.557×10^{4}
0.0067	1.208×10^{5}	2.292×10^{4}	3.555×10^{4}	4.553×10^{4}
0.0076	1.167×10^{5}	2.376×10^{4}	3.630×10^{4}	4.601×10^{4}
0.0085	1.123×10^{5}	2.494×10^{4}	3.743×10^{4}	4.689×10^{4}
0.0095	1.075×10^{5}	2.644×10^{4}	3.882×10^{4}	4.802×10^{4}
0.0107	1.024×10^{5}	2.812×10^{4}	4.040×10^{4}	4.932×10^{4}
0.0120	9.692×10^{4}	2.998×10^{4}	4.202×10^{4}	5.062×10^{4}
0.0135	9.115×10^{4}	3.189×10^{4}	4.350×10^{4}	5.163×10^{4}
0.0151	8.508×10^{4}	3.362×10^{4}	4.445×10^{4}	5.209×10^{4}
0.0170	7.875×10^{4}	3.400×10^{4}	4.383×10^{4}	5.048×10^{4}
0.0190	7.220×10^{4}	3.479×10^{4}	4.331×10^{4}	4.901×10^{4}
0.0214	6.550×10^{4}	3.463×10^{4}	4.179×10^{4}	4.657×10^{4}
0.0240	5.871×10^{4}	3.394×10^{4}	3.974×10^{4}	4.362×10^{4}
0.0269	5.193×10^{4}	3.246×10^{4}	3.698×10^{4}	4.003×10^{4}
0.0302	4.525×10^{4}	3.038×10^{4}	3.379×10^{4}	3.615×10^{4}
0.0339	3.876×10^{4}	2.757×10^{4}	2.999×10^{4}	3.175×10^{4}
0.0381	3.259×10^{4}	2.438×10^{4}	2.605×10^{4}	2.733×10^{4}
0.0427	2.682×10^{4}	2.099×10^{4}	2.205×10^{4}	2.294×10^{4}
0.0479	2.155×10^{4}	1.757×10^{4}	1.821×10^{4}	1.881×10^{4}
0.0538	1.686×10^{4}	1.420×10^{4}	1.456×10^{4}	1.495×10^{4}
0.0604	1.280×10^{4}	1.106×10^{4}	1.126×10^{4}	1.150×10^{4}
0.0678	9.392×10^{3}	8.311×10^{3}	8.407×10^{3}	8.552×10^{3}
0.0761	6.637×10^{3}	5.991×10^{3}	6.033×10^{3}	6.116×10^{3}
0.0854	4.495×10^{3}	4.126×10^{3}	4.140×10^{3}	4.184×10^{3}
0.0959	2.902×10^{3}	2.700×10^{3}	2.703×10^{3}	2.726×10^{3}
0.1076	1.776×10^{3}	1.672×10^{3}	1.671×10^{3}	1.682×10^{3}
0.1208	1.024×10^{3}	9.721×10^{2}	9.701×10^{2}	9.750×10^{2}
0.1356	5.513×10^{2}	5.263×10^{2}	5.247×10^{2}	5.269×10^{2}
0.1522	2.753×10^{2}	2.643×10^{2}	2.634×10^{2}	2.642×10^{2}
0.1708	1.263×10^{2}	1.215×10^{2}	1.210×10^{2}	1.213×10^{2}
0.1918	5.265×10^{1}	5.077×10^{1}	5.054×10^{1}	5.065×10^{1}
0.2152	1.972×10^{1}	1.904×10^{1}	1.895×10^{1}	1.899×10^{1}
0.2416	6.549×10^{0}	6.318×10^{0}	6.285×10^{0}	6.296×10^{0}
0.2712	1.900×10^{0}	1.842×10^{0}	1.833×10^{0}	1.836×10^{0}
0.3044	4.739×10^{-1}	4.605×10^{-1}	4.584×10^{-1}	4.590×10^{-1}
0.3417	9.970×10^{-2}	9.721×10^{-2}	9.682×10^{-2}	9.693×10^{-2}
0.3835	1.733×10^{-2}	1.695×10^{-2}	1.689×10^{-2}	1.691×10^{-2}

Table 7. Drop-size distributions at cloud base (Marshall-Palmer distribution for a precipitation rate of 100 mm/hr) and 1500 m below cloud base for constant downdrafts of 5, 10, and 15 m/sec for Case A.

Radius (cm)	Drop Concentration ($m^{-3}cm^{-1}$)			
	Cloud Base	1500 m Below Cloud Base		
		5 m/sec	10 m/sec	15 m/sec
0.0042	1.402×10^{5}	2.607×10^{4}	3.813×10^{4}	4.826×10^{4}
0.0048	1.380×10^{5}	3.074×10^{4}	4.465×10^{4}	5.617×10^{4}
0.0053	1.355×10^{5}	3.167×10^{4}	4.537×10^{4}	5.653×10^{4}
0.0060	1.327×10^{5}	3.159×10^{4}	4.483×10^{4}	5.540×10^{4}
0.0067	1.297×10^{5}	3.225×10^{4}	4.526×10^{4}	5.544×10^{4}
0.0076	1.265×10^{5}	3.340×10^{4}	4.629×10^{4}	5.617×10^{4}
0.0085	1.229×10^{5}	3.504×10^{4}	4.782×10^{4}	5.743×10^{4}
0.0095	1.190×10^{5}	3.715×10^{4}	4.976×10^{4}	5.907×10^{4}
0.0107	1.147×10^{5}	3.956×10^{4}	5.199×10^{4}	6.103×10^{4}
0.0120	1.101×10^{5}	4.226×10^{4}	5.439×10^{4}	6.309×10^{4}
0.0135	1.052×10^{5}	4.508×10^{4}	5.670×10^{4}	6.494×10^{4}
0.0151	9.994×10^{4}	4.770×10^{4}	5.859×10^{4}	6.626×10^{4}
0.0170	9.435×10^{4}	4.845×10^{4}	5.824×10^{4}	6.506×10^{4}
0.0190	8.844×10^{4}	4.989×10^{4}	5.829×10^{4}	6.416×10^{4}
0.0214	8.225×10^{4}	5.010×10^{4}	5.715×10^{4}	6.211×10^{4}
0.0240	7.581×10^{4}	4.971×10^{4}	5.540×10^{4}	5.948×10^{4}
0.0269	6.918×10^{4}	4.835×10^{4}	5.276×10^{4}	5.603×10^{4}
0.0302	6.243×10^{4}	4.625×10^{4}	4.958×10^{4}	5.215×10^{4}
0.0339	5.564×10^{4}	4.311×10^{4}	4.547×10^{4}	4.744×10^{4}
0.0381	4.889×10^{4}	3.938×10^{4}	4.103×10^{4}	4.251×10^{4}
0.0427	4.228×10^{4}	3.526×10^{4}	3.630×10^{4}	3.736×10^{4}
0.0479	3.592×10^{4}	3.095×10^{4}	3.154×10^{4}	3.228×10^{4}
0.0538	2.992×10^{4}	2.640×10^{4}	2.673×10^{4}	2.723×10^{4}
0.0604	2.436×10^{4}	2.191×10^{4}	2.207×10^{4}	2.240×10^{4}
0.0678	1.935×10^{4}	1.770×10^{4}	1.776×10^{4}	1.798×10^{4}
0.0761	1.494×10^{4}	1.387×10^{4}	1.388×10^{4}	1.401×10^{4}
0.0854	1.117×10^{3}	1.050×10^{3}	1.049×10^{3}	1.057×10^{3}
0.0959	8.065×10^{3}	7.657×10^{3}	7.639×10^{3}	7.682×10^{3}
0.1076	5.594×10^{3}	5.358×10^{3}	5.341×10^{3}	5.363×10^{3}
0.1208	3.710×10^{3}	3.577×10^{3}	3.563×10^{3}	3.574×10^{3}
0.1356	2.340×10^{3}	2.263×10^{3}	2.254×10^{3}	2.259×10^{3}
0.1522	1.395×10^{2}	1.355×10^{2}	1.349×10^{2}	1.351×10^{2}
0.1708	7.803×10^{2}	7.589×10^{2}	7.552×10^{2}	7.563×10^{2}
0.1918	4.066×10^{2}	3.960×10^{2}	3.941×10^{2}	3.945×10^{2}
0.2152	1.956×10^{1}	1.907×10^{1}	1.897×10^{1}	1.899×10^{1}
0.2416	8.604×10^{1}	8.376×10^{1}	8.325×10^{1}	8.330×10^{1}
0.2712	3.422×10^{1}	3.343×10^{1}	3.324×10^{1}	3.326×10^{1}
0.3044	1.216×10^{1}	1.190×10^{1}	1.183×10^{1}	1.184×10^{1}
0.3417	3.806×10^{0}	3.732×10^{0}	3.715×10^{0}	3.716×10^{0}
0.3835	1.033×10^{0}	1.016×10^{0}	1.012×10^{0}	1.012×10^{0}

allowed a 70% relative humidity 1500 m below cloud base. As indicated in Fig. 3, the subsaturation in a downdraft attains much greater magnitudes, thereby substantially reducing the evaporation time constant for the small drops.

An unexpected feature of the present computations is an oscillation in the drop concentration between the radii of 0.005 and 0.009 cm, that can be seen in Tables 6 and 7. An investigation (see Appendix D) into this anomaly showed its origin to be in the evaporation data of Kinzer and Gunn (1951). At any rate, this anomaly has little significance to the main thrust of the present study.

b. Case B: Evaporation and Collision-Coalescence

Collision-coalescence was added to Case A using (56) and (61). The combined effects of evaporation and collision-coalescence are presented in Tables 8, 9, and 10, which show many interesting changes from Case A. On comparing Tables 8-10 with Tables 3-5, the following differences become apparent:

1. The precipitation rates for Case B increase with depth below the cloud base because as the larger drops sweep out the smaller ones, the liquid water represented by the sum of their masses has increased their average terminal velocity and their contribution to the precipitation rate. This is generally true except for small deviations in the case of 25- and 50-mm/hr (initial) precipitation rates. The number of larger drops initially available for these smaller precipitation rates is much less than for precipitation rates of 75 and 100 mm/hr,

Table 8. Vertical distributions of thermodynamic and hydrometeoric quantities for Case B in a sub-cloud downdraft of 5 m/sec.

z (m)	T_D (K)	T (K)	S (%)	M($\times 10^3$) (kg/m^3)	R (mm/hr)	Z($\times 10^{-5}$) (mm^6/m^3)
			R = 25 mm/hr			
1500	278.0	278.0	100.0	1.24	25.0	0.33
1000	282.9	282.8	77.3	1.22	25.6	0.36
500	287.8	287.3	61.9	1.19	25.7	0.38
0	292.7	291.8	50.9	1.14	25.4	0.40
			R = 50			
1500	278.0	278.0	100.0	2.24	50.0	0.92
1000	282.9	282.7	77.8	2.22	52.1	1.05
500	287.8	287.2	63.3	2.17	53.2	1.16
0	292.7	291.4	53.0	2.12	53.5	1.26
			R = 75 mm/hr			
1500	287.0	287.0	100.0	3.28	75.0	1.77
1000	282.9	282.7	78.3	3.25	79.1	2.09
500	287.8	287.0	64.4	3.21	81.5	2.38
0	292.7	291.2	54.7	3.15	82.7	2.64
			R = 100 mm/hr			
1500	287.0	287.0	100.0	4.03	100.0	2.51
1000	282.9	282.6	78.6	4.00	105.9	3.02
500	287.8	286.9	65.1	3.95	109.2	3.49
0	292.7	291.0	55.7	3.89	111.1	3.91

Table 9. Vertical distributions of thermodynamic and hydrometeoric quantities for Case B in a sub-cloud downdraft of 10 m/sec.

z (m)	T_D (K)	T (K)	S (%)	M($\times 10^3$) (kg/m^3)	R (mm/hr)	Z($\times 10^{-5}$) (mm^6/m^3)
			R = 25 mm/hr			
1500	278.0	278.0	100.0	1.24	25.0	0.33
1000	282.9	282.8	76.7	1.23	25.3	0.35
500	287.8	287.5	60.4	1.19	25.2	0.36
0	292.7	292.2	48.5	1.14	24.7	0.37
			R = 50 mm/hr			
1500	278.0	278.0	100.0	2.24	50.0	0.92
1000	282.9	282.8	77.0	2.22	51.2	1.00
500	287.8	287.4	61.2	2.17	51.7	1.07
0	292.7	292.0	49.7	2.11	51.5	1.13
			R = 75 mm/hr			
1500	278.0	278.0	100.0	3.28	75.0	1.77
1000	282.9	282.8	77.2	3.25	77.6	1.98
500	287.8	287.4	61.8	3.22	79.0	2.17
0	292.7	291.8	50.7	3.13	79.4	2.33
			R = 100 mm/hr			
1500	278.0	278.0	100.0	4.03	100.0	2.51
1000	282.9	282.8	77.4	4.00	103.8	2.85
500	287.8	287.3	62.2	3.94	105.9	3.16
0	292.7	291.7	51.4	3.86	106.9	3.44

Table 10. Vertical distributions of thermodynamic and hydrometeoric quantities for Case B in a sub-cloud downdraft of 15 m/sec.

z (m)	T_D (K)	T (K)	S (%)	M($\times 10^3$) (kg/m^3)	R (mm/hr)	Z($\times 10^{-5}$) (mm^6/m^3)
			R = 25 mm/hr			
1500	278.0	278.0	100.0	1.24	25.0	0.33
1000	282.9	282.9	76.4	1.23	25.2	0.34
500	287.8	287.6	59.8	1.20	25.0	0.35
0	292.7	292.3	47.6	1.15	24.5	0.36
			R = 50 mm/hr			
1500	278.0	278.0	100.0	2.24	50.0	0.92
1000	282.9	282.8	76.7	2.22	50.9	0.98
500	287.8	287.5	60.3	2.18	51.1	1.03
0	292.7	292.2	48.5	2.12	50.8	1.07
			R = 75 mm/hr			
1500	278.0	278.0	100.0	3.28	75.0	1.77
1000	282.9	282.8	76.8	3.26	76.9	1.92
500	287.8	287.5	60.8	3.20	77.8	2.06
0	292.7	292.0	49.2	3.13	77.9	2.18
			R = 100 mm/hr			
1500	278.0	278.0	100.0	4.03	100.0	2.51
1000	282.9	282.8	77.0	4.00	102.7	2.76
500	287.8	287.4	61.1	3.94	104.3	2.99
0	292.7	292.0	49.7	3.86	104.9	3.20

so the shift of liquid water from the smaller to the larger drop radii is not as great. As a result, the precipitation rate increases initially, but then decreases as the evaporation begins to dominate the collision-coalescence effect. The effect of evaporation is evident in Tables 8-10, because total liquid water decreases from cloud base to ground.

2. Radar reflectivity, like precipitation rate, increases with depth below cloud base. The larger drops backscatter a higher amount of radar energy, so even though the total amount of liquid water decreases, the shift of liquid water from the smaller to the larger drops causes the radar reflectivity to increase.

3. The surface temperature is warmer and the relative humidity lower for Case B because the larger drops sweep out the smaller ones, the more efficient evaporators.

Relative humidity profiles for Cases A and B are presented in Figs. 9 and 10 for initial precipitation rates of 25 and 100 mm/hr, respectively. Fig. 9 illustrates that little difference exists between Cases A and B for the lower precipitation rate and strong downdraft velocity. In each case, the profile approaches the dry adiabatic curve because the strong downdraft velocity does not allow enough time for evaporation. Fig. 10 shows that as the number of larger drops increases, the subsaturation increases. Thus the difference of relative humidity between Cases A and B is maximum for large initial precipitation rate and weak downdraft velocity.

The surface drop-size distributions resulting from Case B are presented in Figs. 11 and 12 for initial precipitation rates of 25 and

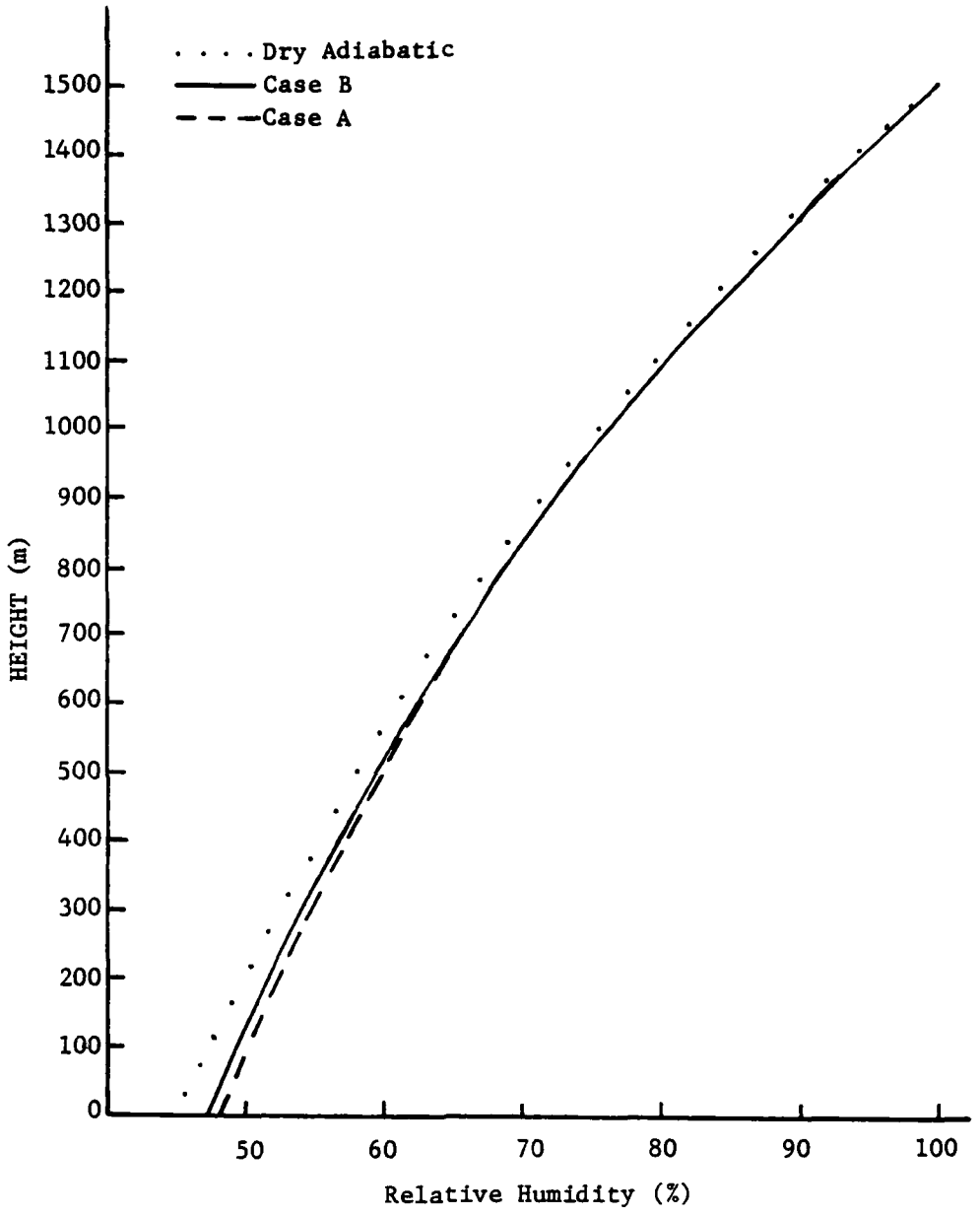

Fig. 9. Relative humidity profiles for Case A and Case B for a constant downdraft of 15 m/sec and initial precipitation rate of 25 mm/hr.

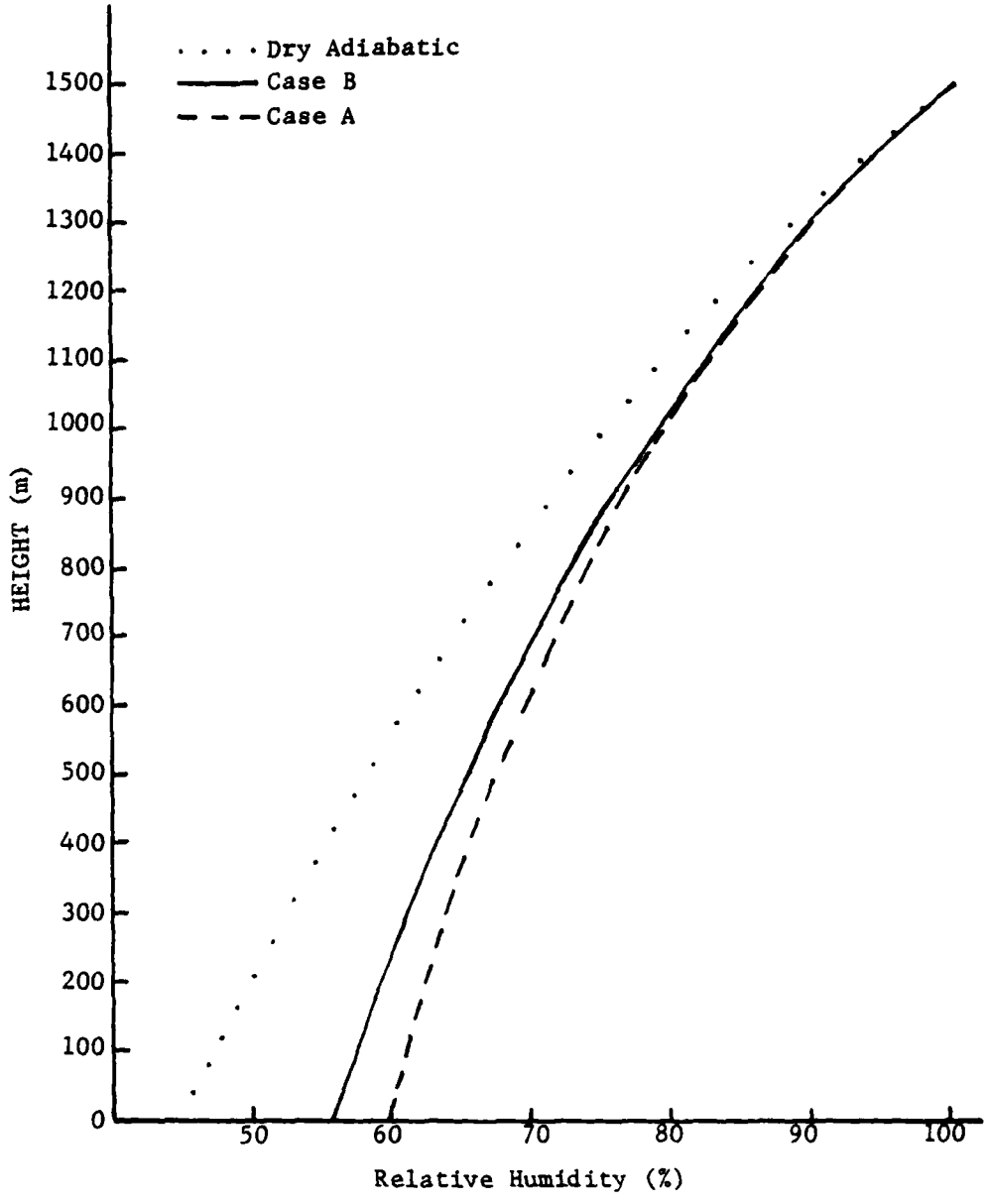

Fig. 10. Same as Fig. 9 except for a constant downdraft of 5 m/sec and initial precipitation rate of 100 mm/hr.

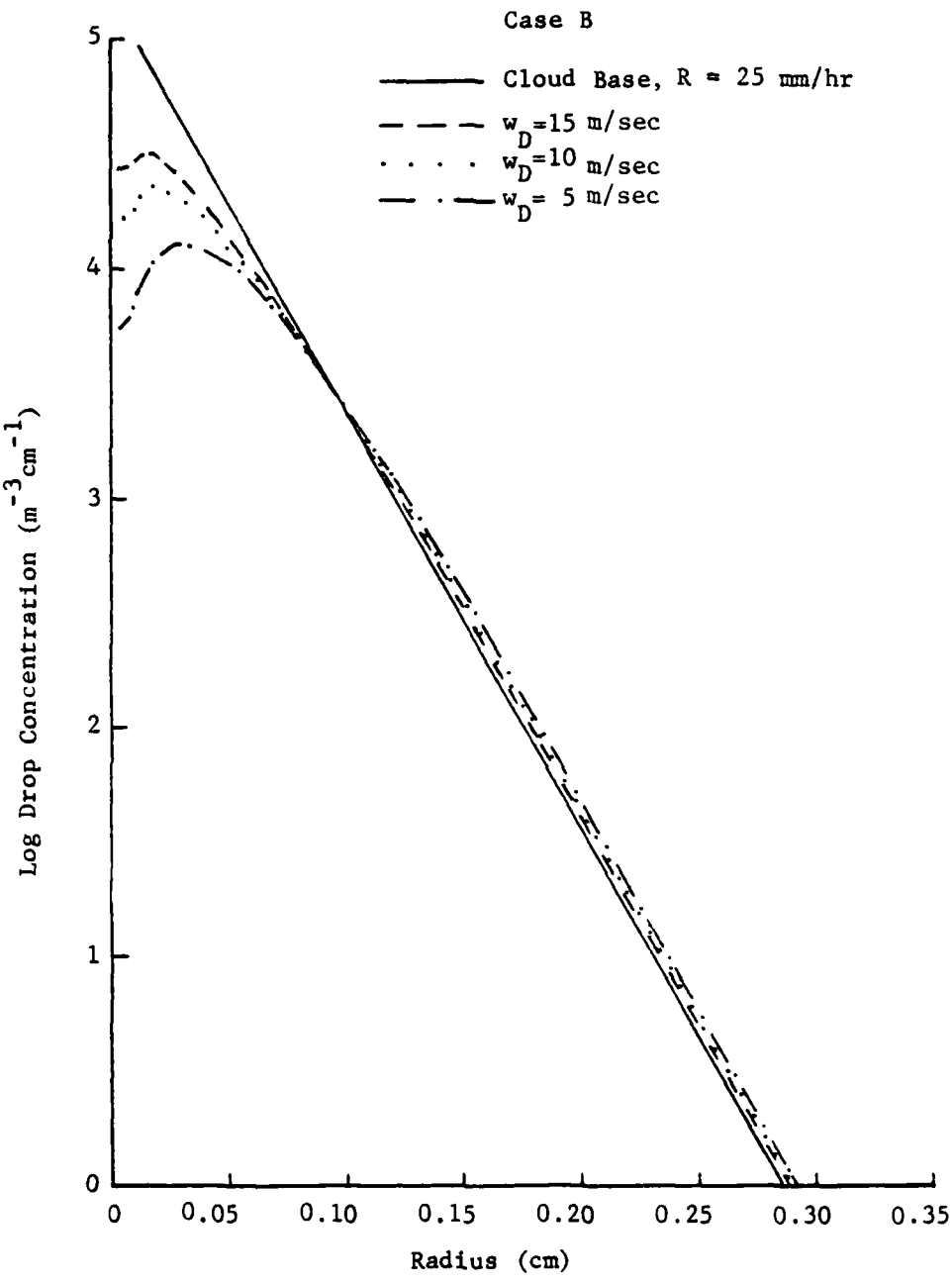

Fig. 11. Same as Fig. 7 except for Case B.

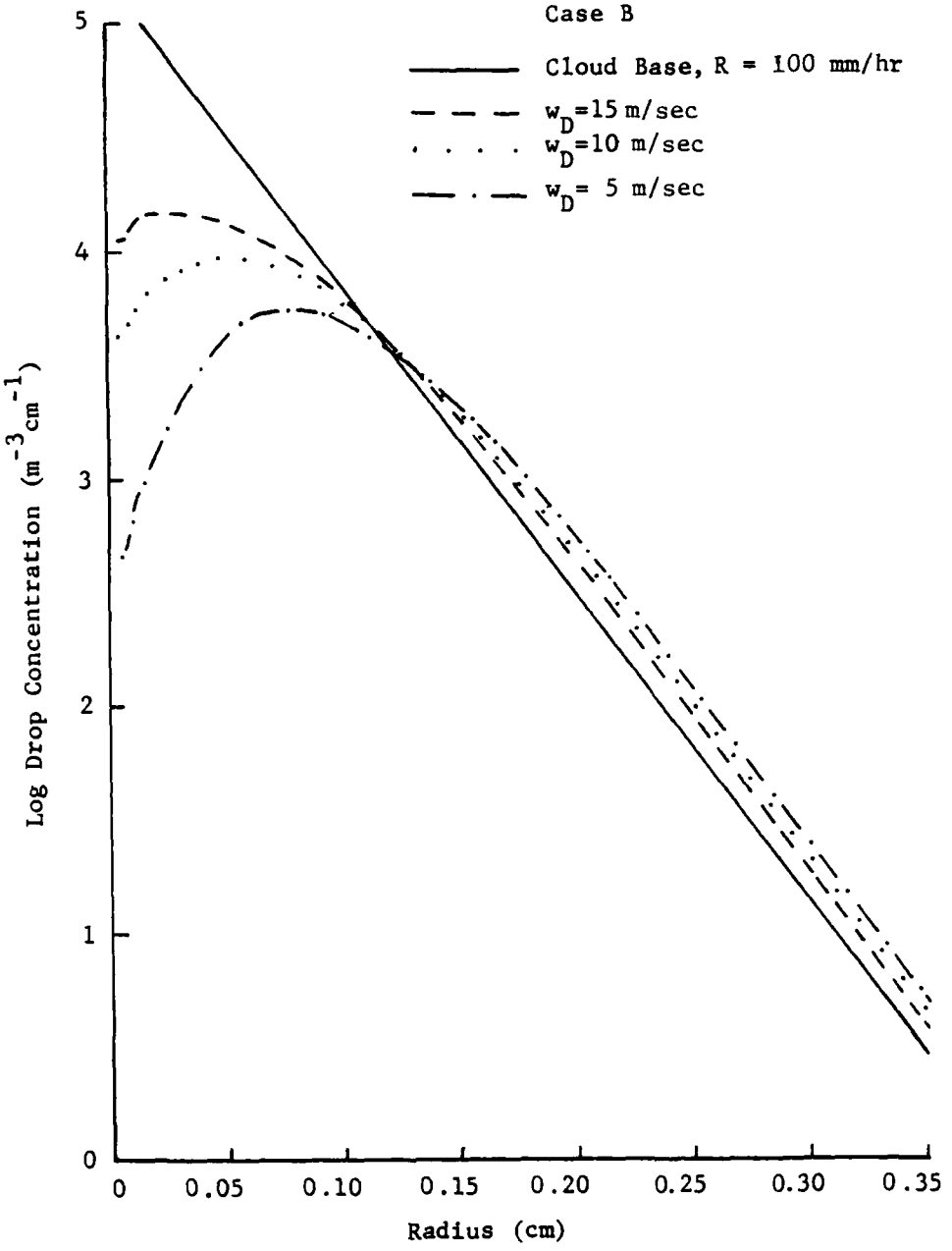

Fig. 12. Same as Fig. 8 except for Case B.

100 mm/hr, respectively. The effect of collision-coalescence in depleting the number of small drops is readily apparent. Fig. 12 illustrates the sharp drop in the number concentration of small drops as the downdraft velocity decreases. This is due to the longer time the large drops have to sweep out the smaller ones.

Figs. 13 and 14 present comparisons of the drop-size distributions at the surface, obtained in Cases A and B. In Fig. 13 which relates to the cloud-base precipitation rate of 25 mm/hr, the number of small drops decreases significantly from Case A to Case B, but this decrease is even sharper in Fig. 14 where the initial concentration of larger drops is higher.

c. Case C: Evaporation, Collision-Coalescence, and Aerodynamic Breakup

The computations in Case C were performed by adding (62) and (63) to Case B. Vertical distributions of thermodynamic and hydrometeoric quantities resulting from these computations are given in Tables 11, 12, and 13.

A comparison of Tables 11-13 with Tables 8-10 points up one fact quite clearly: there is little difference between the two cases for the initial precipitation rate of 25 mm/hr, but the results show marked difference as the initial precipitation rate increases. Relative humidity for 25 mm/hr is lower at the surface for all downdraft velocities in Case C when compared to Case B, but by only 0.1 percent or less. This difference increases to about 0.3 percent for the intensity of 100 mm/hr. The most significant difference in Cases B

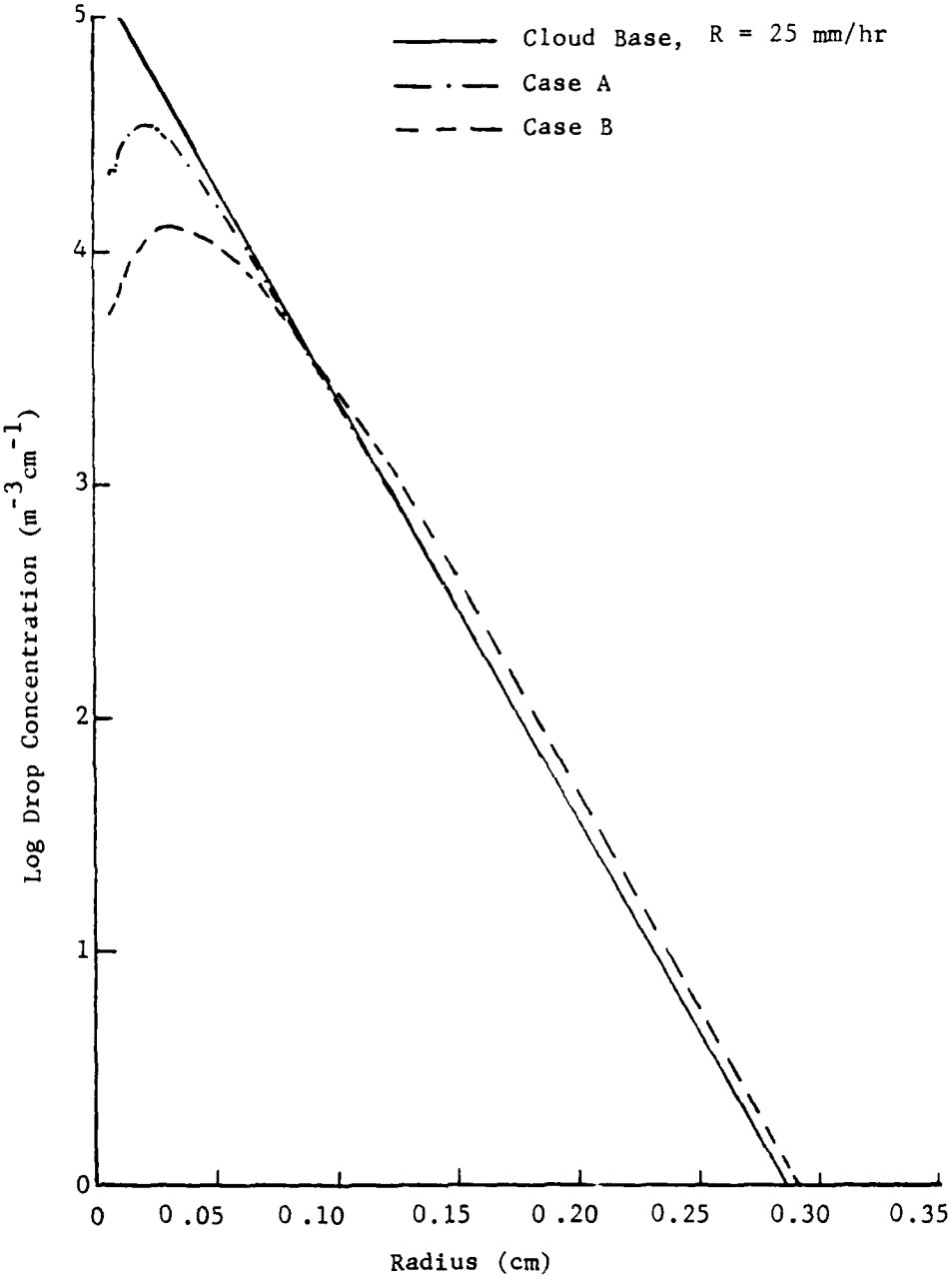

Fig. 13. Drop-size distributions 1500 m below cloud base for Case A and Case B, a constant downdraft of 5 m/sec and an initial precipitation rate of 25 mm/hr.

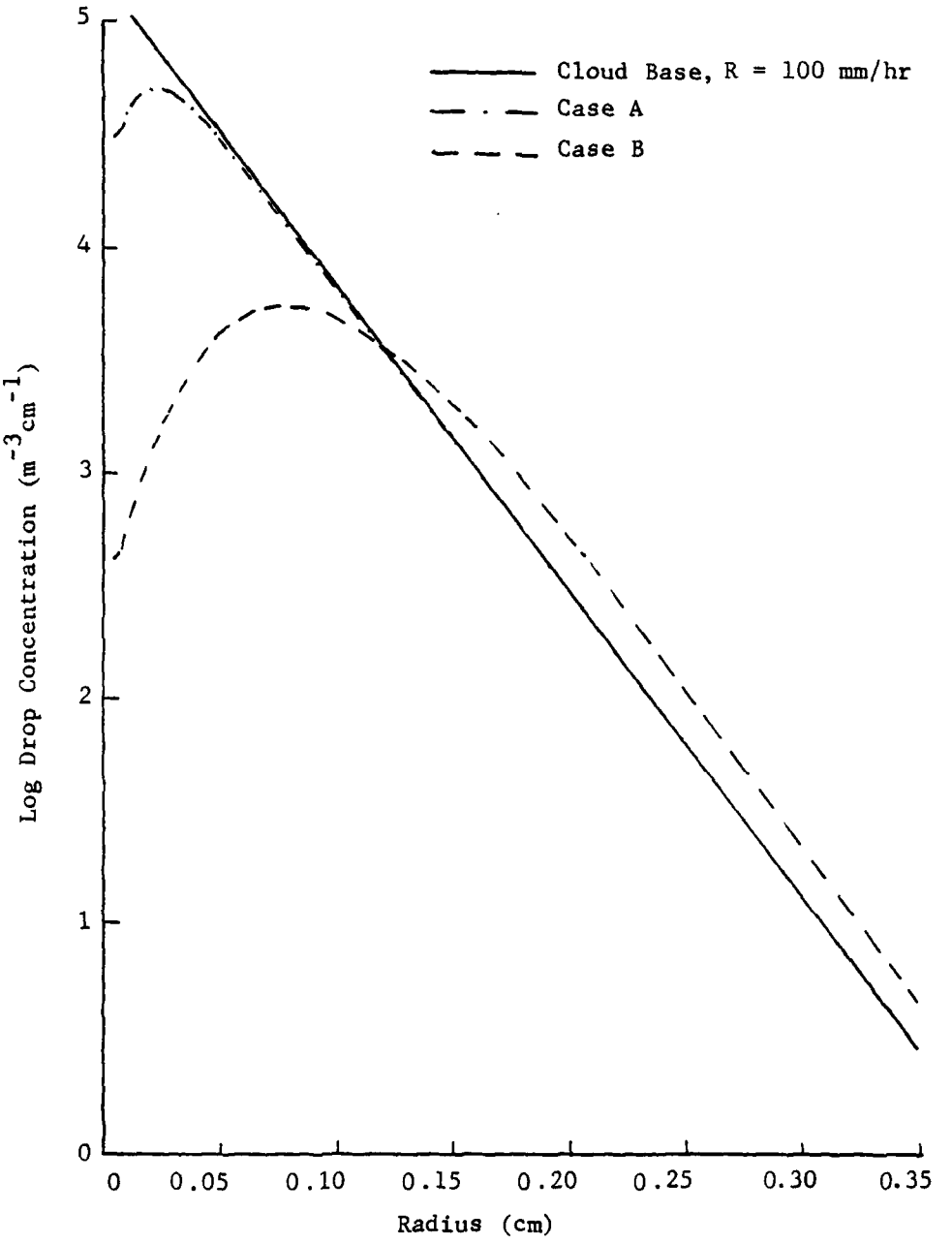

Fig. 14. Same as Fig. 13 except for an initial precipitation rate of 100 mm/hr.

Table 11. Vertical distributions of thermodynamic and hydrometeoric quantities for Case C in a sub-cloud downdraft of 5 m/sec.

z (m)	T_D (K)	T (K)	S (%)	M($\times 10^3$) (kg/m^3)	R (mm/hr)	Z($\times 10^{-5}$) (mm^6/m^3)
			R = 25 mm/hr			
1500	278.0	278.0	100.0	1.24	25.0	0.33
1000	282.9	282.8	77.3	1.22	25.7	0.37
500	287.8	287.3	61.9	1.19	25.9	0.40
0	292.7	291.8	50.8	1.14	25.6	0.43
			R = 50			
1500	278.0	278.0	100.0	2.24	50.0	0.92
1000	282.9	282.7	77.8	2.22	52.9	1.18
500	287.8	287.2	63.2	2.18	54.4	1.39
0	292.7	291.5	52.7	2.12	55.0	1.54
			R = 75 mm/hr			
1500	278.0	278.0	100.0	3.28	75.0	1.77
1000	282.9	282.7	78.2	3.25	81.5	2.58
500	287.8	287.1	64.1	3.21	84.4	3.09
0	292.7	291.2	54.3	3.15	85.0	3.36
			R = 100 mm/hr			
1500	278.0	278.0	100.0	4.03	100.0	2.51
1000	282.9	282.7	78.5	4.00	109.4	3.91
500	287.8	287.0	64.7	3.95	112.7	4.58
0	292.7	291.1	55.4	3.89	112.9	4.83

Table 12. Vertical distributions of thermodynamic and hydrometeoric quantities for Case C in a sub-cloud downdraft of 10 m/sec.

z (m)	T_D (K)	T (K)	S (%)	M($\times 10^3$) (kg/m^3)	R (mm/hr)	Z($\times 10^{-5}$) (mm^6/m^3)
			R = 25 mm/hr			
1500	278.0	278.0	100.0	1.24	25.0	0.33
1000	282.9	282.8	76.7	1.23	25.4	0.36
500	287.8	287.5	60.3	1.19	25.3	0.38
0	292.7	292.2	48.4	1.14	24.9	0.39
			R = 50 mm/hr			
1500	278.0	278.0	100.0	2.24	50.0	0.92
1000	282.9	282.8	77.0	2.22	51.9	1.10
500	287.8	287.4	61.1	2.17	52.8	1.26
0	292.7	292.0	49.6	2.11	53.0	1.37
			R = 75 mm/hr			
1500	278.0	278.0	100.0	3.28	75.0	1.77
1000	282.9	282.8	77.2	3.25	79.8	2.37
500	287.8	287.4	61.6	3.20	82.0	2.81
0	292.7	291.8	50.4	3.14	82.6	3.07
			R = 100 mm/hr			
1500	278.0	278.0	100.0	4.03	100.0	2.51
1000	282.9	282.8	77.3	4.00	107.0	3.58
500	287.8	287.3	62.0	3.94	110.2	4.23
0	292.7	291.8	51.0	3.87	110.6	4.54

Table 13. Vertical distributions of thermodynamic and hydrometeoric quantities for Case C in a sub-cloud downdraft of 15 m/sec.

z (m)	T_D (K)	T (K)	S (%)	M($\times 10^3$) (kg/m^3)	R (mm/hr)	Z($\times 10^{-5}$) (mm^6/m^3)
			R = 25 mm/hr			
1500	278.0	278.0	100.0	1.24	25.0	0.33
1000	282.9	282.9	76.4	1.23	25.3	0.35
500	287.8	287.6	59.8	1.20	25.1	0.36
0	292.7	292.3	47.5	1.15	24.7	0.37
			R = 50 mm/hr			
1500	278.0	278.0	100.0	2.24	50.0	0.92
1000	282.9	282.8	76.7	2.22	51.4	1.06
500	287.8	287.1	61.7	2.18	52.1	1.18
0	292.7	292.2	48.4	2.12	52.1	1.28
			R = 75 mm/hr			
1500	278.0	278.0	100.0	3.28	75.0	1.77
1000	282.9	282.8	76.8	3.26	78.5	2.25
500	287.8	287.5	60.7	3.21	80.5	2.62
0	292.7	292.1	49.0	3.14	82.2	2.87
			R = 100 mm/hr			
1500	278.0	278.0	100.0	4.03	100.0	2.51
1000	282.9	282.8	76.9	4.00	105.6	3.38
500	287.8	287.5	61.0	3.95	108.5	3.97
0	292.7	292.0	49.4	3.88	109.2	4.31

and C subcloud quantities is the radar reflectivity and rainfall rate. Both of these quantities increase due to the aerodynamic breakup of the largest drops into smaller drop categories.

In order to have a better understanding of the dependence of aerodynamic breakup on drop radius, (28) and (29) were investigated in more detail. Table 14 shows how P_k, the probability of drop breakup per unit time, varies with drop radius. It is seen that only the

Table 14. Probability of aerodynamic drop breakup.

Radius (cm)	P_k (sec^{-1})
0.2416	0.001
0.2712	0.003
0.3044	0.009
0.3417	0.033
0.3835	0.135

largest category of drops has a significant probability of aerodynamic breakup. Aerodynamic breakup, consequently, has a greater effect on drop-size distributions having large initial concentrations of large drops which will be the case for Marshall-Palmer distributions at a high precipitation intensity. The fragment probability given by Q(k, k') in (29) determines how many fragment drops fall in each smaller radius category k due to breakup of a large drop of radius k', and shows that the fragment population will be maximum at the drop radius $r_k/7$. Since the mid-point radius in the largest category is r_k, = 0.3835 cm, the fragment maximum will be at a radius of about 0.055 cm. This

fragment maximum will decrease with decreasing $r_{k'}$, so when a drop distribution has a high concentration of large drops, the small radius end of the distribution will benefit most from aerodynamic breakup.

Figs. 15 and 16 show the drop-size distributions resulting from Case C, while a comparison of drop-size distributions for Cases B and C is shown in Figs. 17 and 18. The results in Fig. 17 show little difference between Cases B and C; however, the contribution to the concentration of small drops due to breakup of the largest drops is apparent. The data used to plot Figs. 17 and 18 are given in Tables 15 and 16, respectively. Note, in Table 16, that the drop concentration for the two largest radius categories is smaller for Case C than B. This can be expected from the probabilities in Table 14. Fig. 18 illustrates the dramatic effect of a high concentration of large drops. These results are consistent with the results of Srivastava (1971), who noted that aerodynamic breakup has a tendency to flatten the equilibrium distribution compared to the distributions observed in nature.

Aerodynamic breakup has little effect on drop-size distributions having few large drops. For that reason, this microphysical process is likely to be important in cold rather than warm rain processes. Srivastava (1971) suggested that collisional breakup may help produce better agreement between theory and observation.

d. Case D: Evaporation, Collision-Coalescence, and Collisional Breakup

Case D includes the microphysical processes of evaporation, collision-coalescence with the coalescence efficiency of Whelpdale

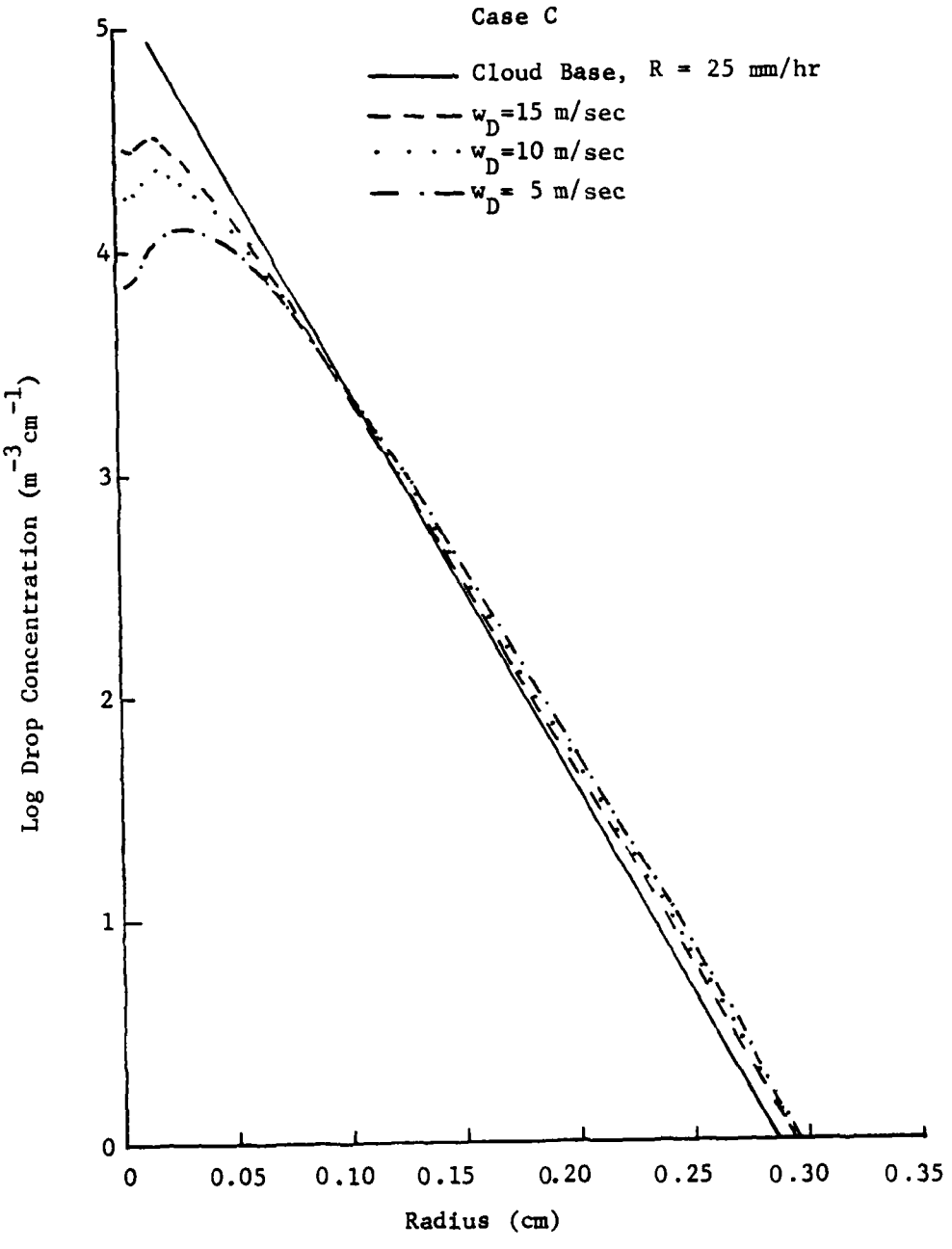

Fig. 15. Same as Fig. 7 except for Case C.

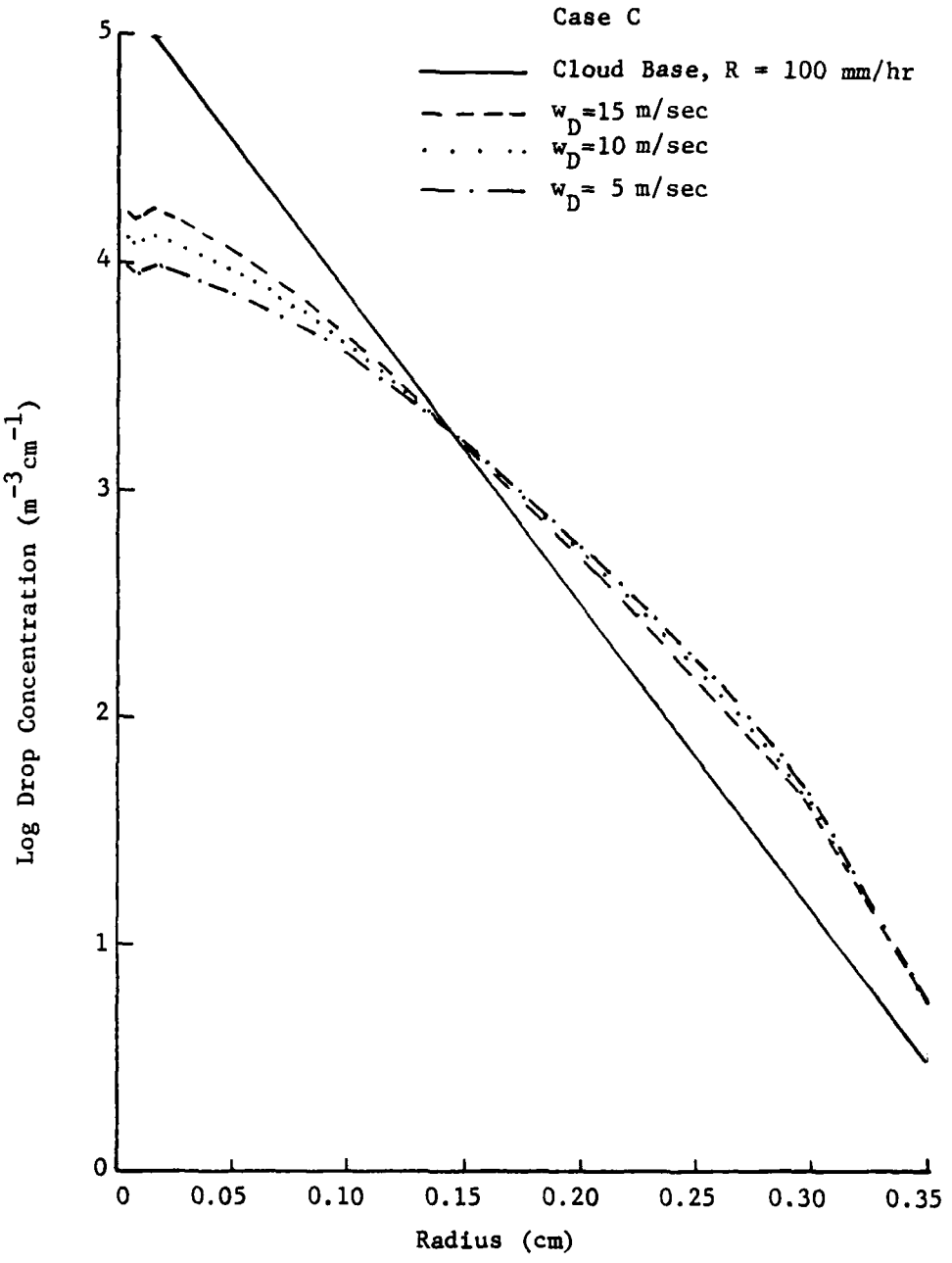

Fig. 16. Same as Fig. 8 except for Case C.

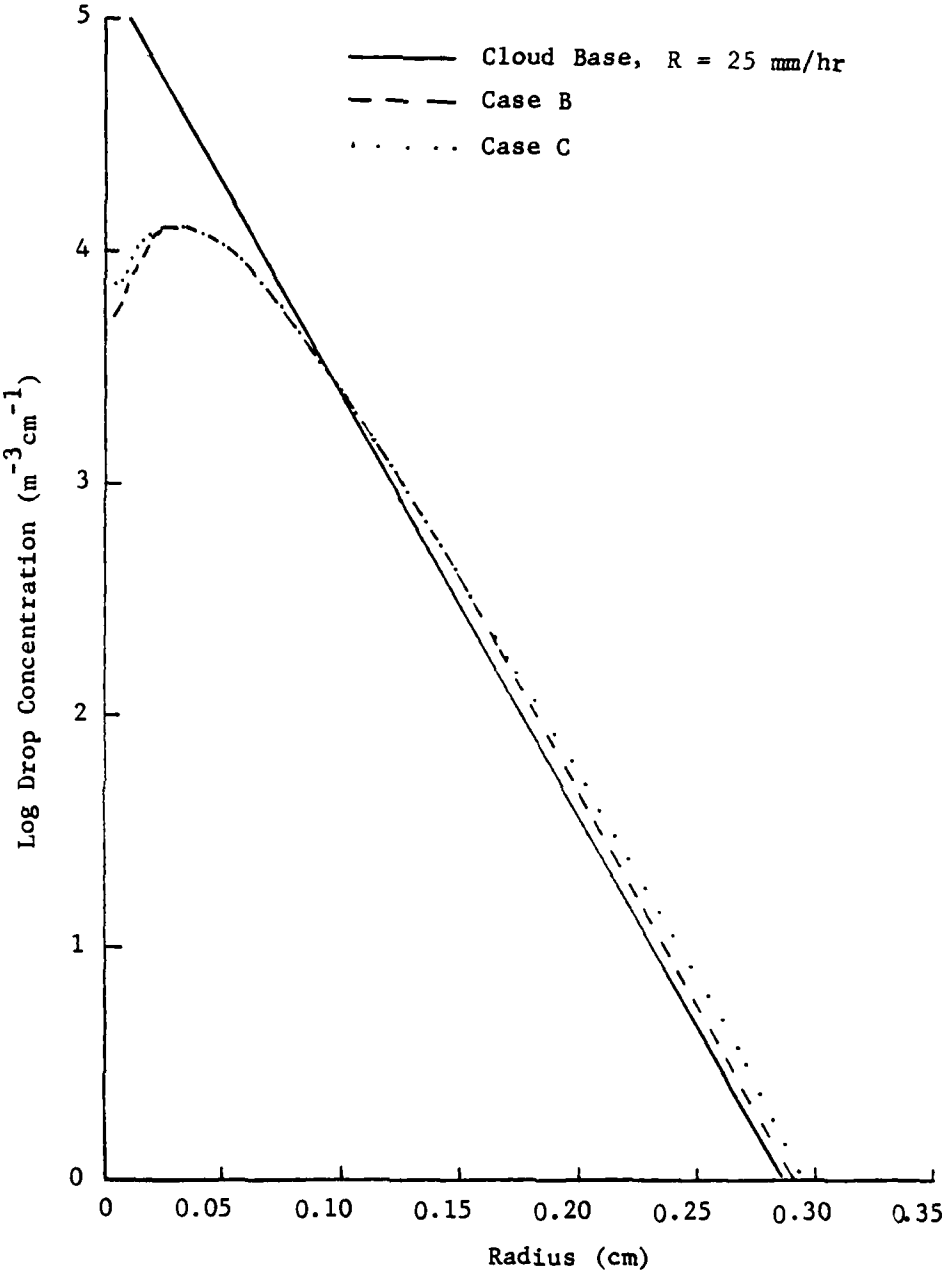

Fig. 17. Drop-size distributions 1500 m below cloud base for Case B and Case C, a constant downdraft of 5 m/sec and an initial precipitation rate of 25 mm/hr.

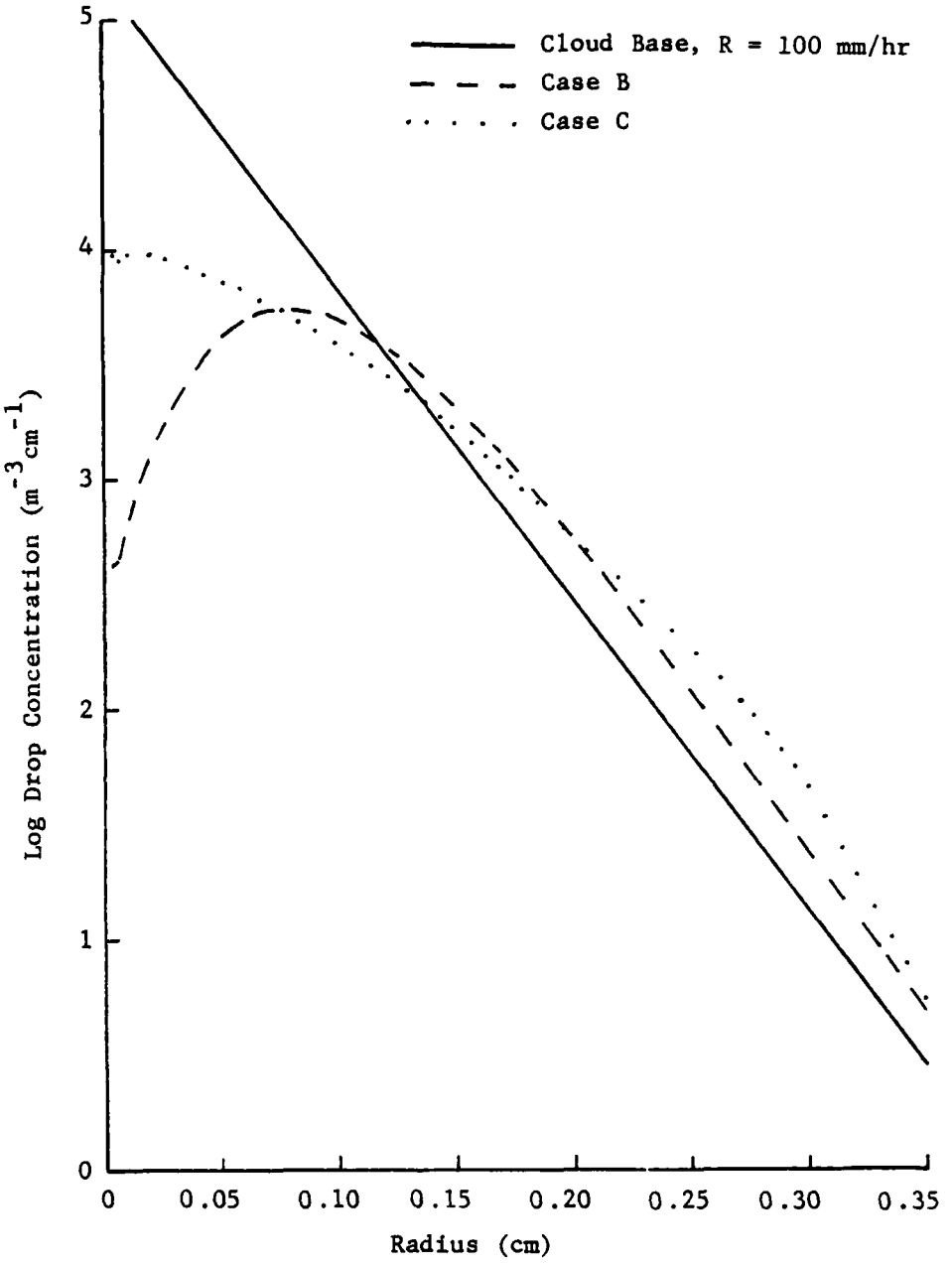

Fig. 18. Same as Fig. 17 except for an initial precipitation rate of 100 mm/hr.

Table 15. Drop-size distributions at cloud base (Marshall-Palmer) and 1500 m below cloud base for Case B and Case C. The constant downdraft is 5 m/sec and the initial precipitation rate is 25 mm/hr.

Radius (cm)	Drop Concentration ($m^{-3}cm^{-1}$)		
	Cloud Base	1500 m Below Cloud Base	
		Case B	Case C
0.0042	1.340×10^{5}	5.739×10^{3}	5.726×10^{3}
0.0048	1.311×10^{5}	5.493×10^{3}	7.100×10^{3}
0.0053	1.280×10^{5}	5.658×10^{3}	7.222×10^{3}
0.0060	1.245×10^{5}	5.697×10^{3}	7.178×10^{3}
0.0067	1.208×10^{5}	5.873×10^{3}	7.299×10^{3}
0.0076	1.167×10^{5}	6.148×10^{3}	7.528×10^{3}
0.0085	1.123×10^{5}	6.526×10^{3}	7.868×10^{3}
0.0095	1.075×10^{5}	7.011×10^{3}	8.317×10^{3}
0.0107	1.024×10^{5}	7.577×10^{3}	8.840×10^{3}
0.0120	9.692×10^{4}	8.233×10^{3}	9.444×10^{3}
0.0135	9.115×10^{4}	8.969×10^{3}	1.012×10^{4}
0.0151	8.508×10^{4}	9.731×10^{3}	1.079×10^{4}
0.0170	7.875×10^{4}	1.020×10^{4}	1.114×10^{4}
0.0190	7.220×10^{4}	1.092×10^{4}	1.173×10^{4}
0.0214	6.550×10^{4}	1.143×10^{4}	1.210×10^{4}
0.0240	5.871×10^{4}	1.190×10^{4}	1.242×10^{4}
0.0269	5.193×10^{4}	1.221×10^{4}	1.258×10^{4}
0.0302	4.525×10^{4}	1.239×10^{4}	1.261×10^{4}
0.0339	3.876×10^{4}	1.235×10^{4}	1.243×10^{4}
0.0381	3.259×10^{4}	1.209×10^{4}	1.205×10^{4}
0.0427	2.682×10^{4}	1.170×10^{4}	1.156×10^{4}
0.0479	2.155×10^{4}	1.103×10^{4}	1.081×10^{4}
0.0538	1.686×10^{4}	1.001×10^{4}	9.750×10^{3}
0.0604	1.280×10^{4}	8.714×10^{3}	8.455×10^{3}
0.0678	9.392×10^{3}	7.249×10^{3}	7.015×10^{3}
0.0761	6.637×10^{3}	5.736×10^{3}	5.546×10^{3}
0.0854	4.495×10^{3}	4.311×10^{3}	4.171×10^{3}
0.0959	2.902×10^{3}	3.038×10^{3}	2.949×10^{3}
0.1076	1.776×10^{3}	1.998×10^{3}	1.951×10^{3}
0.1208	1.024×10^{2}	1.224×10^{2}	1.207×10^{2}
0.1356	5.513×10^{2}	6.893×10^{2}	6.894×10^{2}
0.1522	2.753×10^{2}	3.544×10^{2}	3.622×10^{2}
0.1708	1.263×10^{2}	1.654×10^{2}	1.745×10^{2}
0.1918	5.265×10^{1}	6.930×10^{1}	7.661×10^{1}
0.2152	1.972×10^{1}	2.594×10^{1}	3.059×10^{1}
0.2416	6.549×10^{0}	8.531×10^{0}	1.087×10^{1}
0.2712	1.900×10^{0}	2.465×10^{0}	3.260×10^{0}
0.3044	4.739×10^{-1}	6.103×10^{-1}	6.665×10^{-1}
0.3417	9.970×10^{-2}	1.277×10^{-1}	6.837×10^{-2}
0.3835	1.733×10^{-2}	2.208×10^{-2}	5.384×10^{-3}

Table 16. Drop-size distributions at cloud base (Marshall-Palmer) and 1500 m below cloud base for Case B and Case C. The constant downdraft is 5 m/sec and the initial precipitation rate is 100 mm/hr.

Radius (cm)	Drop Concentration ($m^{-3}cm^{-1}$)		
	Cloud Base	1500 m Below Cloud Base	
		Case B	Case C
0.0042	1.402×10^{5}	3.634×10^{2}	8.313×10^{3}
0.0048	1.380×10^{5}	4.340×10^{2}	9.507×10^{3}
0.0053	1.355×10^{5}	4.539×10^{2}	9.521×10^{3}
0.0060	1.327×10^{5}	4.627×10^{2}	9.246×10^{3}
0.0067	1.297×10^{5}	4.840×10^{2}	9.139×10^{3}
0.0076	1.265×10^{5}	5.155×10^{2}	9.120×10^{3}
0.0085	1.229×10^{5}	5.586×10^{2}	9.179×10^{3}
0.0095	1.190×10^{5}	6.150×10^{2}	9.300×10^{3}
0.0107	1.147×10^{5}	6.844×10^{2}	9.431×10^{3}
0.0120	1.101×10^{5}	7.704×10^{2}	9.582×10^{3}
0.0135	1.052×10^{5}	8.756×10^{2}	9.741×10^{3}
0.0151	9.994×10^{4}	9.995×10^{3}	9.869×10^{3}
0.0170	9.435×10^{4}	1.114×10^{3}	9.704×10^{3}
0 0190	8.844×10^{4}	1.283×10^{3}	9.723×10^{3}
0.0214	8.225×10^{4}	1.460×10^{3}	9.577×10^{3}
0.0240	7.581×10^{4}	1.676×10^{3}	9.409×10^{3}
0.0269	6.918×10^{4}	1.924×10^{3}	9.173×10^{3}
0.0302	6.243×10^{4}	2.223×10^{3}	8.902×10^{3}
0.0339	5.564×10^{4}	2.578×10^{3}	8.600×10^{3}
0.0381	4.889×10^{4}	2.989×10^{3}	8.251×10^{3}
0.0427	4.228×10^{4}	3.520×10^{3}	7.931×10^{3}
0.0479	3.592×10^{4}	4.087×10^{3}	7.571×10^{3}
0.0538	2.992×10^{4}	4.628×10^{3}	7.151×10^{3}
0.0604	2.436×10^{4}	5.094×10^{3}	6.673×10^{3}
0.0678	1.935×10^{4}	5.409×10^{3}	6.125×10^{3}
0.0761	1.494×10^{4}	5.550×10^{3}	5.531×10^{3}
0.0854	1.117×10^{4}	5.548×10^{3}	4.928×10^{3}
0.0959	8.065×10^{3}	5.161×10^{3}	4.237×10^{3}
0.1076	5.594×10^{3}	4.575×10^{3}	3.553×10^{3}
0.1208	3.710×10^{3}	3.800×10^{3}	2.873×10^{3}
0.1356	2.340×10^{3}	2.875×10^{3}	2.201×10^{3}
0.1522	1.395×10^{3}	1.977×10^{3}	1.599×10^{3}
0.1708	7.803×10^{2}	1.234×10^{3}	1.094×10^{3}
0.1918	4.066×10^{2}	6.865×10^{2}	7.007×10^{2}
0.2152	1.956×10^{2}	3.449×10^{2}	4.210×10^{2}
0.2416	8.604×10^{1}	1.518×10^{2}	2.294×10^{2}
0.2712	3.422×10^{1}	6.040×10^{1}	1.104×10^{2}
0.3044	1.216×10^{1}	2.109×10^{1}	3.959×10^{1}
0.3417	3.806×10^{0}	6.514×10^{0}	7.896×10^{0}
0.3835	1.034×10^{0}	1.746×10^{0}	8.490×10^{-1}

and List (1971), and collisional breakup incorporating the experimental fragment size distributions of McTaggart-Cowan and List (1975) as formulated by List and Gillespie (1976).

Vertical distributions of thermodynamic and hydrometeoric quantities resulting from Case D for initial precipitation rates of 25, 50, 75, and 100 mm/hr are given in Tables 17, 18, and 19 for constant downdrafts of 5, 10, and 15 m/sec, respectively.

On comparing the results in Case D as detailed in Tables 17-19 with those in Case B (Tables 8-10) and Case C (Tables 11-13), the following points become clear.

1. The difference in the rainshaft temperature and relative humidity between Cases B and D is greater for a weak downdraft (5 m/sec) than for stronger downdrafts (10 and 15 m/sec). Collisional breakup is a more efficient process than aerodynamic breakup in depleting the large drops and creating small fragments. With weaker downdrafts the small drops have more time to evaporate, thus yielding a higher rainshaft relative humidity and lower rainshaft temperature. With stronger downdrafts the small fragments are not given as much time to evaporate, so the difference between Cases B and D is less pronounced.

2. Both the rainfall rate and the radar reflectivity are greatly reduced for Case D when compared to Cases B and C. This is due to the significant loss, in Case D, of large drops which, with their high terminal velocities, contribute heavily to the overall rainfall rate. These large drops also are efficient scatterers of the radar signal, so their loss results in a significant loss of radar reflectivity.

Table 17. Vertical distributions of thermodynamic and hydrometeoric quantities for Case D in a sub-cloud downdraft of 5 m/sec.

z (m)	T_D (K)	T (K)	S (%)	M($\times 10^3$) (kg/m^3)	R (mm/hr)	Z($\times 10^{-5}$) (mm^6/cm^3)
			R = 25 mm/hr			
1500	278.0	278.0	100.0	1.24	25.0	0.33
1000	282.9	282.8	77.4	1.22	24.1	0.22
500	287.8	287.3	62.4	1.18	23.1	0.19
0	292.7	291.6	51.7	1.11	22.0	0.17
			R = 50 mm/hr			
1500	278.0	278.0	100.0	2.24	50.0	0.92
1000	282.9	282.7	78.1	2.21	46.8	0.45
500	287.8	287.0	64.4	2.15	45.2	0.38
0	292.7	291.1	55.1	2.07	43.7	0.35
			R = 75 mm/hr			
1500	278.0	278.0	100.0	3.28	75.0	1.77
1000	282.9	282.6	78.8	3.25	71.3	0.69
500	287.8	286.8	66.2	3.17	69.3	0.58
0	292.7	290.7	58.1	3.07	67.4	0.55
			R = 100 mm/hr			
1500	278.0	278.0	100.0	4.03	100.0	2.51
1000	282.9	282.6	79.2	3.99	90.3	0.85
500	287.8	286.6	67.4	3.91	88.0	0.73
0	292.7	290.4	60.1	86.0	86.0	0.69

AD-A107 262 AIR FORCE INST OF TECH WRIGHT-PATTERSON AFB OH F/G 4/2
A COMPUTATIONAL STUDY OF THE MODIFICATION OF RAINDROP SIZE DIST--ETC(U)
AUG 81 R G BORCHERS
UNCLASSIFIED AFIT-CI-81-44D NL

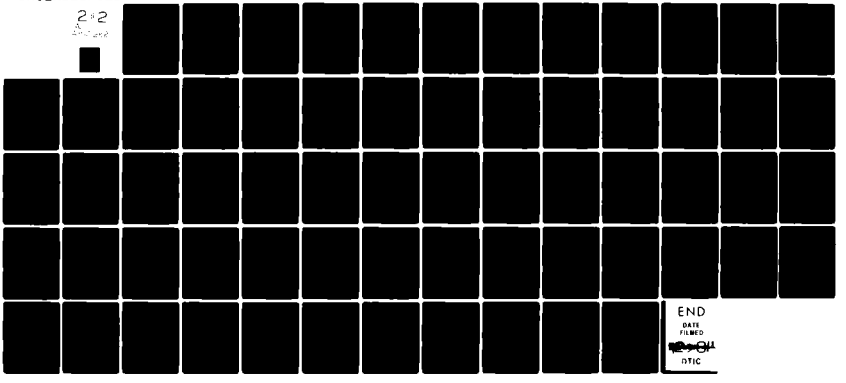

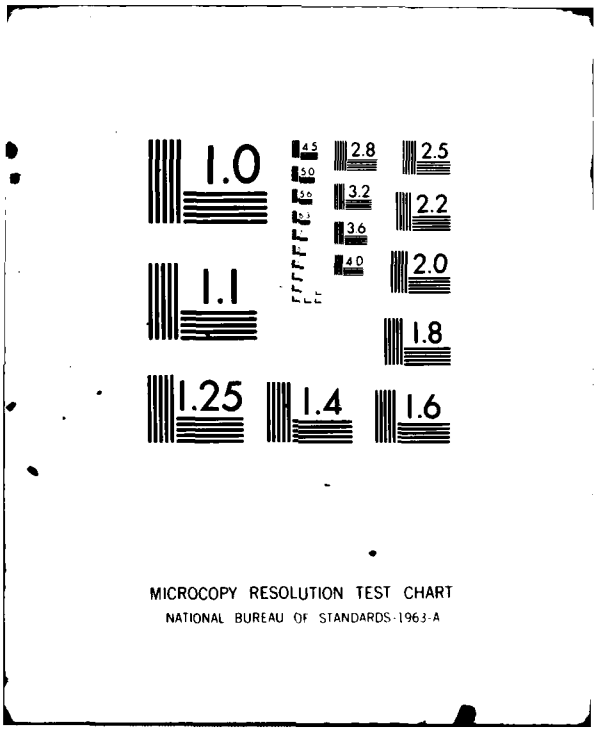
1.0
1.1
1.25
1.4
1.6
1.8
2.0
2.2
2.5
2.8
3.2
3.6
4.0
4.5
5.0
5.6
MICROCOPY RESOLUTION TEST CHART
NATIONAL BUREAU OF STANDARDS-1963-A

Table 18. Vertical distribution of thermodynamic and hydrometeoric quantities for Case D in a sub-cloud downdraft of 10 m/sec.

z (m)	T_D (K)	T (K)	S (%)	M($\times 10^3$) (kg/m^3)	R (mm/hr)	Z($\times 10^{-5}$) (mm^6/m^3)
			R = 25 mm/hr			
1500	278.0	278.0	100.0	1.24	25.0	0.33
1000	282.9	282.8	76.7	1.23	24.1	0.24
500	287.8	287.5	60.5	1.18	23.2	0.20
0	292.7	292.1	48.8	1.12	22.0	0.18
			R = 50 mm/hr			
1500	278.0	278.0	100.0	2.24	50.0	0.92
1000	282.9	282.8	77.1	2.22	47.0	0.49
500	287.8	287.4	61.6	2.16	45.2	0.40
0	292.7	291.8	50.7	2.07	43.4	0.36
			R = 75 mm/hr			
1500	278.0	278.0	100.0	3.28	75.0	1.77
1000	282.9	282.8	77.4	3.25	71.7	0.76
500	287.8	287.2	62.7	3.17	69.1	0.61
0	292.7	291.5	52.4	3.06	66.7	0.55
			R = 100 mm/hr			
1500	278.0	278.0	100.0	4.03	100.0	2.51
1000	282.9	282.7	77.7	3.99	90.1	0.94
500	287.8	287.2	63.4	3.90	87.7	0.76
0	292.7	291.3	53.6	3.78	85.0	0.69

Table 19. Vertical distribution of thermodynamic and hydrometeoric quantities for Case D in a sub-cloud downdraft of 15 m/sec.

z (m)	T_D (K)	T (K)	S (%)	M($\times 10^3$) (kg/m^3)	R (mm/hr)	Z($\times 10^{-5}$) (mm^6/m^3)
			R = 25 mm/hr			
1500	278.0	278.0	100.0	1.24	25.0	0.33
1000	282.9	282.9	76.5	1.23	24.2	0.25
500	287.8	287.6	59.9	1.19	23.4	0.21
0	292.7	292.3	47.8	1.14	22.3	0.19
			R = 50 mm/hr			
1500	278.0	278.0	100.0	2.24	50.0	0.92
1000	282.9	282.8	76.7	2.22	47.4	0.53
500	287.8	287.5	60.6	2.17	45.6	0.43
0	292.7	292.1	49.1	2.09	43.8	0.38
			R = 75 mm/hr			
1500	278.0	278.0	100.0	3.28	75.0	1.77
1000	282.9	282.8	77.0	3.25	72.3	0.82
500	287.8	287.4	61.4	3.18	69.5	0.65
0	292.7	291.9	50.3	3.08	67.0	0.57
			R = 100 mm/hr			
1500	278.0	278.0	100.0	4.03	100.0	2.51
1000	282.9	282.8	77.1	3.99	91.6	1.02
500	287.8	287.3	61.9	3.91	88.2	0.80
0	292.7	291.7	51.1	3.80	85.3	0.71

3. For a given downdraft, the thermodynamic and hydrometeoric quantities in Case D are not very different from those in Cases B and C for small initial precipitation rates (25 and 50 mm/hr); for larger initial precipitation rates (75 and 100 mm/hr), the differences are greater. This is due to the smaller number of larger drops at small R, as indicated in Fig. 8.

The drop-size distributions resulting from Case D for various constant downdraft velocities are given in Figs. 19 and 20 for initial rainfall rates of 25 and 100 mm/hr, respectively. Comparing the large radius ends of these two figures, it is easily seen how drastically the concentration of large drops is reduced by collisional breakup. This is especially true in Fig. 20. The sharp variations that occur near 0.05 cm and 0.14 cm result from the numerical formulation given in Chapter 4, in which the loss term is computed differently in the three segments of the drop-size range. As indicated earlier, these sharp breaks probably do not occur in nature. They were employed to permit comparisons could be made with the results of List and Gillespie (1976) and Gillespie and List (1978/79).

Figs. 21 and 22 compare the drop-size distributions in Cases C and D for precipitation rates of 25 and 100 mm/hr, respectively. Fig. 21 illustrates how collisional breakup depletes the large drops and distributes the fragments into the smaller radius categories. The concentration of small drops in Fig. 21 approaches the same value for both Case C and Case D because evaporation proceeds quickly for these drops, while drops in the radius range from 0.03 cm to 0.12 cm sweep out the drops of radii less than 0.03 cm due to collision-coalescence.

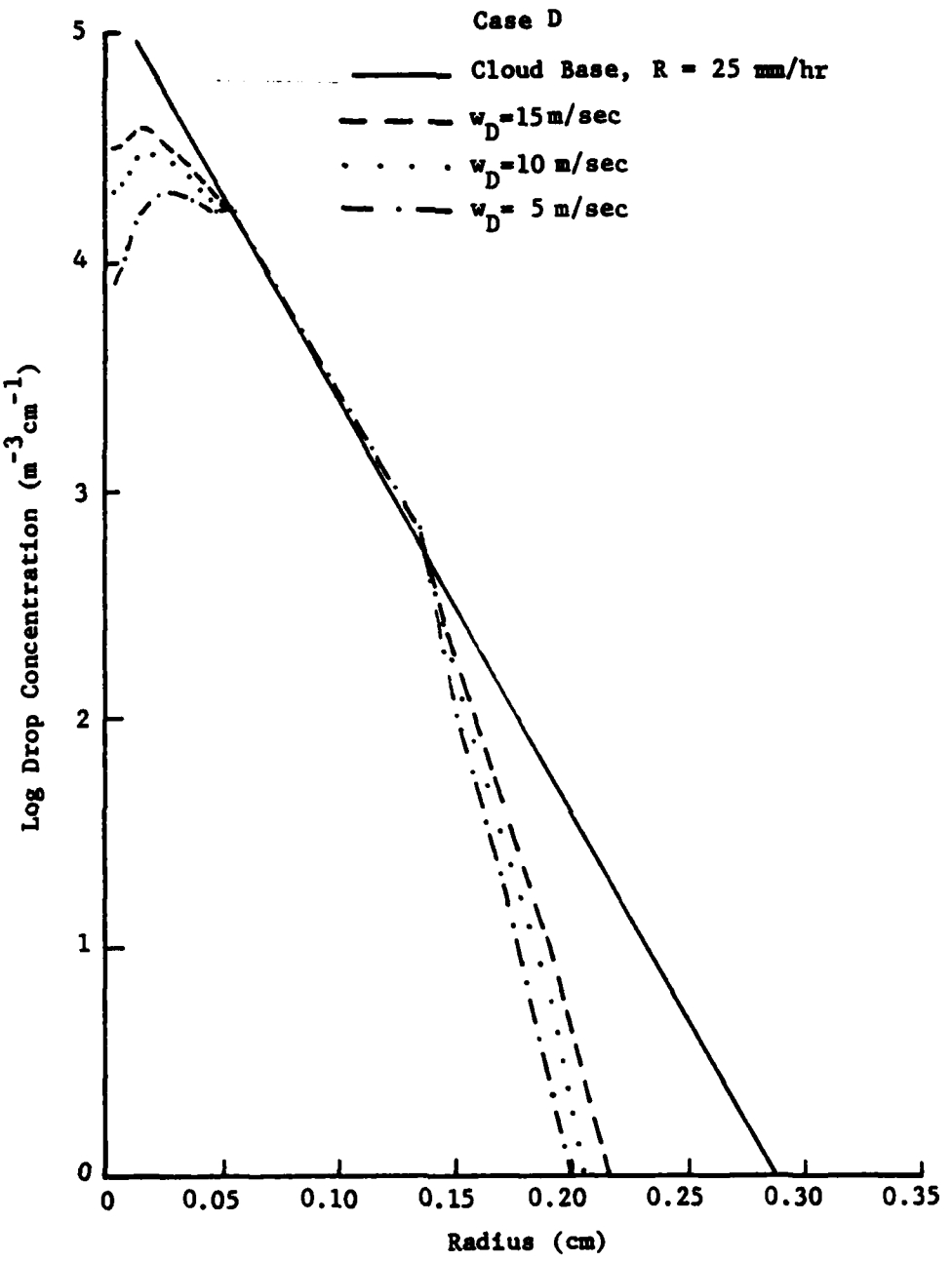

Fig. 19. Same as Fig. 7 except for Case D.

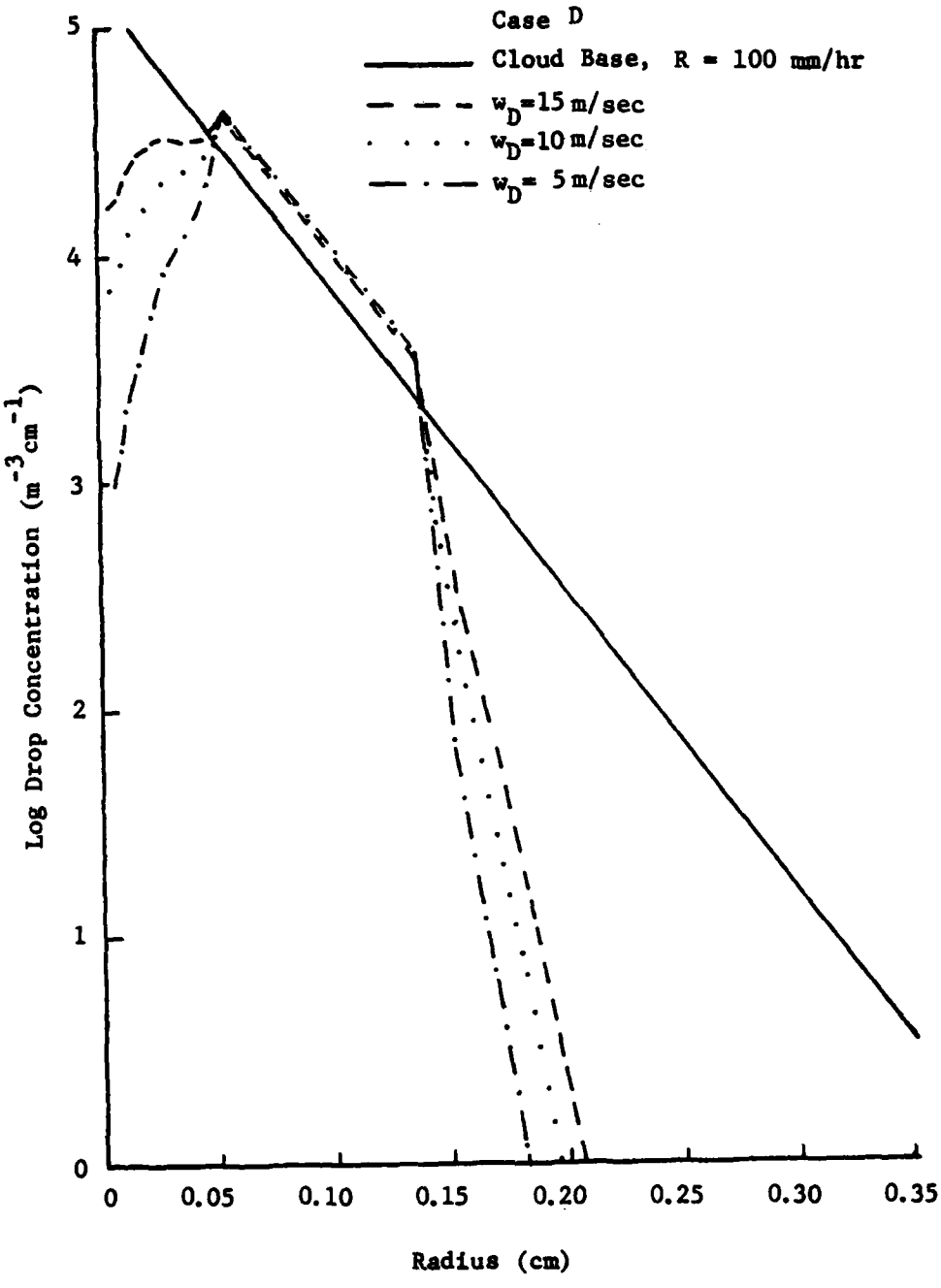

Fig. 20. Same as Fig. 8 except for Case D.

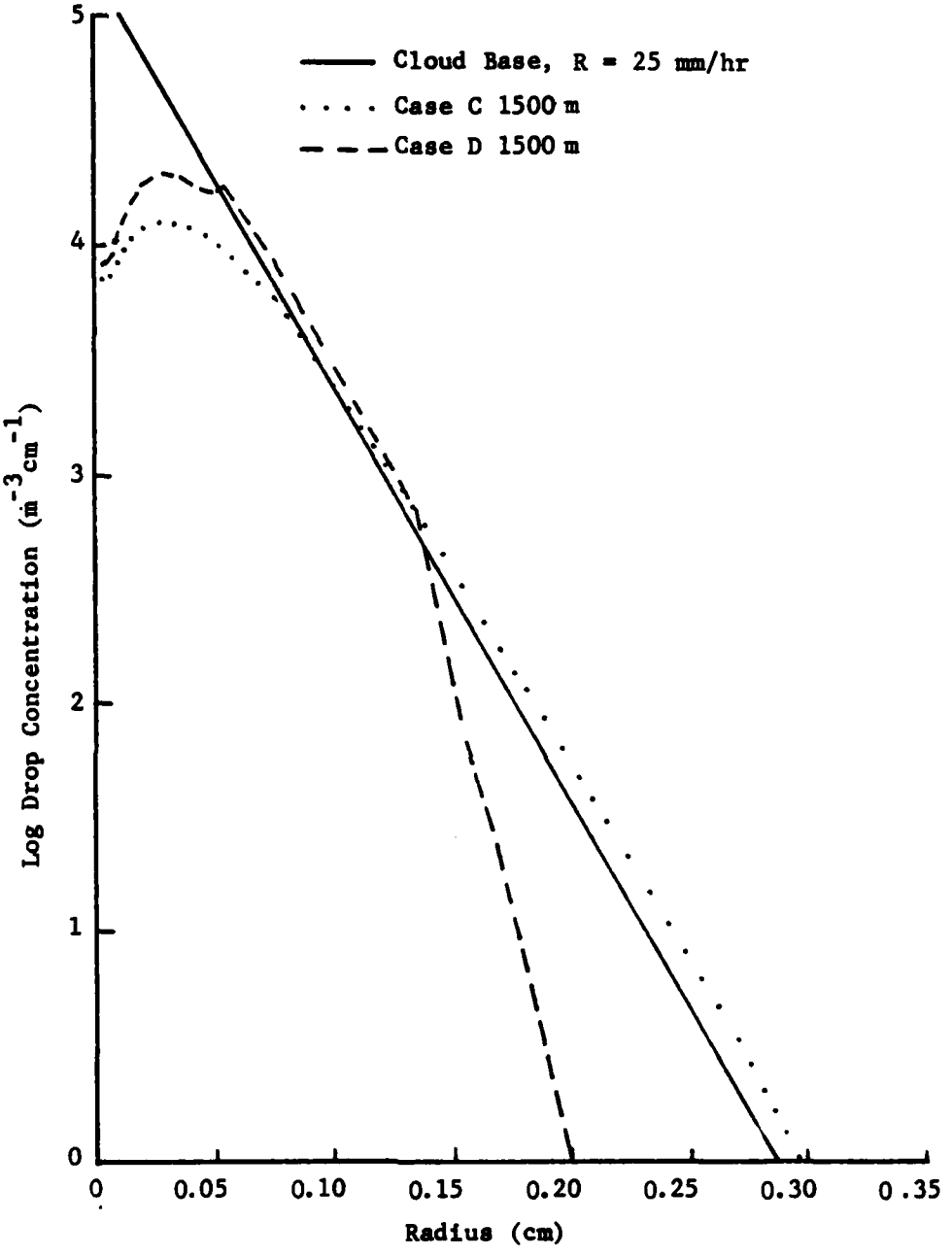

Fig. 21. Drop-size distributions 1500 m below cloud base for Case C and Case D, a constant downdraft of 5 m/sec, and an initial precipitation rate of 25 mm/hr.

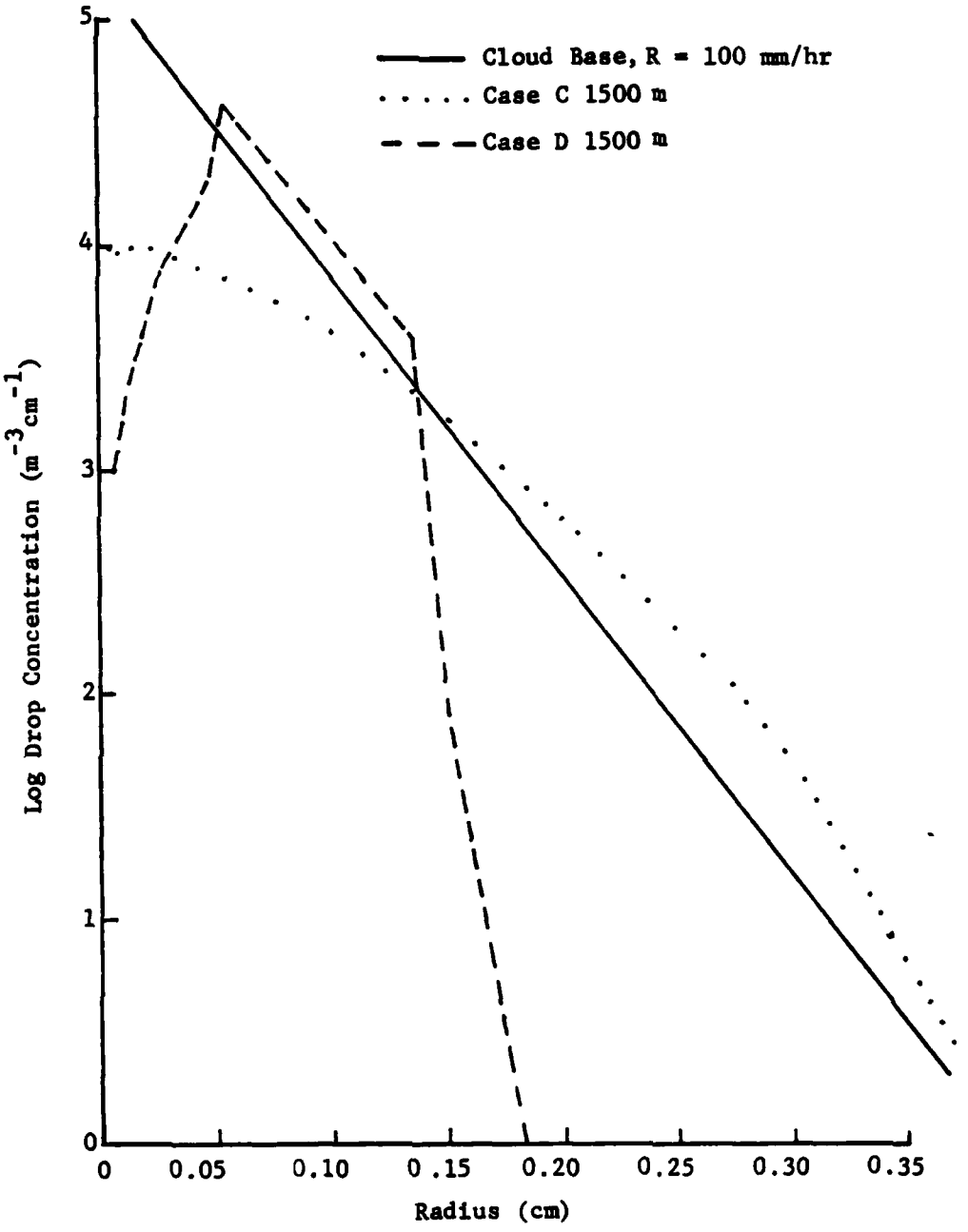

Fig. 22. Same as Fig. 21 except for an initial precipitation rate of 100 mm/hr.

This effect is more dramatic in Fig. 22 where in Case D there are fewer drops both with radii less than 0.05 cm and with radii greater than 0.15 cm than in Case C. These results indicate that rainshafts with weak downdrafts may result in ground base distributions having fewer drops at both the smaller and the larger ends of the distribution when the precipitation rate is higher.

Figs. 23 and 24 depict the evolution of drop-size distributions in Case D for initial precipitation rates of 25 and 100 mm/hr, respectively. Collisional breakup proceeds quickly as noted by the large decrease in the concentration of large drops in the first 500 m below cloud base. The fragments are distributed in all drop categories below a drop radius of 0.15 cm. The effect of evaporation is not as strong for the 500-m distribution as for the 1000- and 1500-m distributions. Downward from the cloud base, the concentration of larger drops can be seen to decrease so that the number of small fragments produced also decreases and the effect of evaporation becomes more apparent. Fig. 24 illustrates the same effect, except more dramatically. Also, Fig. 24 shows the effect of collision-coalescence of the mid-size drops on the smaller drops.

When Figs. 23 and 24 were analyzed, a significant difference was noted between the Case D results and the results reported by List and Gillespie (1976) and Gillespie and List (1978/79). Replotted in Fig. 25 are the results of Gillespie and List (1978/79) on the evolution of the drop-size spectrum through collision-coalescence and collisional breakup for an initial precipitation rate of 25 mm/hr. The shape of the distribution at the ground (Z = 0 m) in Fig. 25 agrees fairly

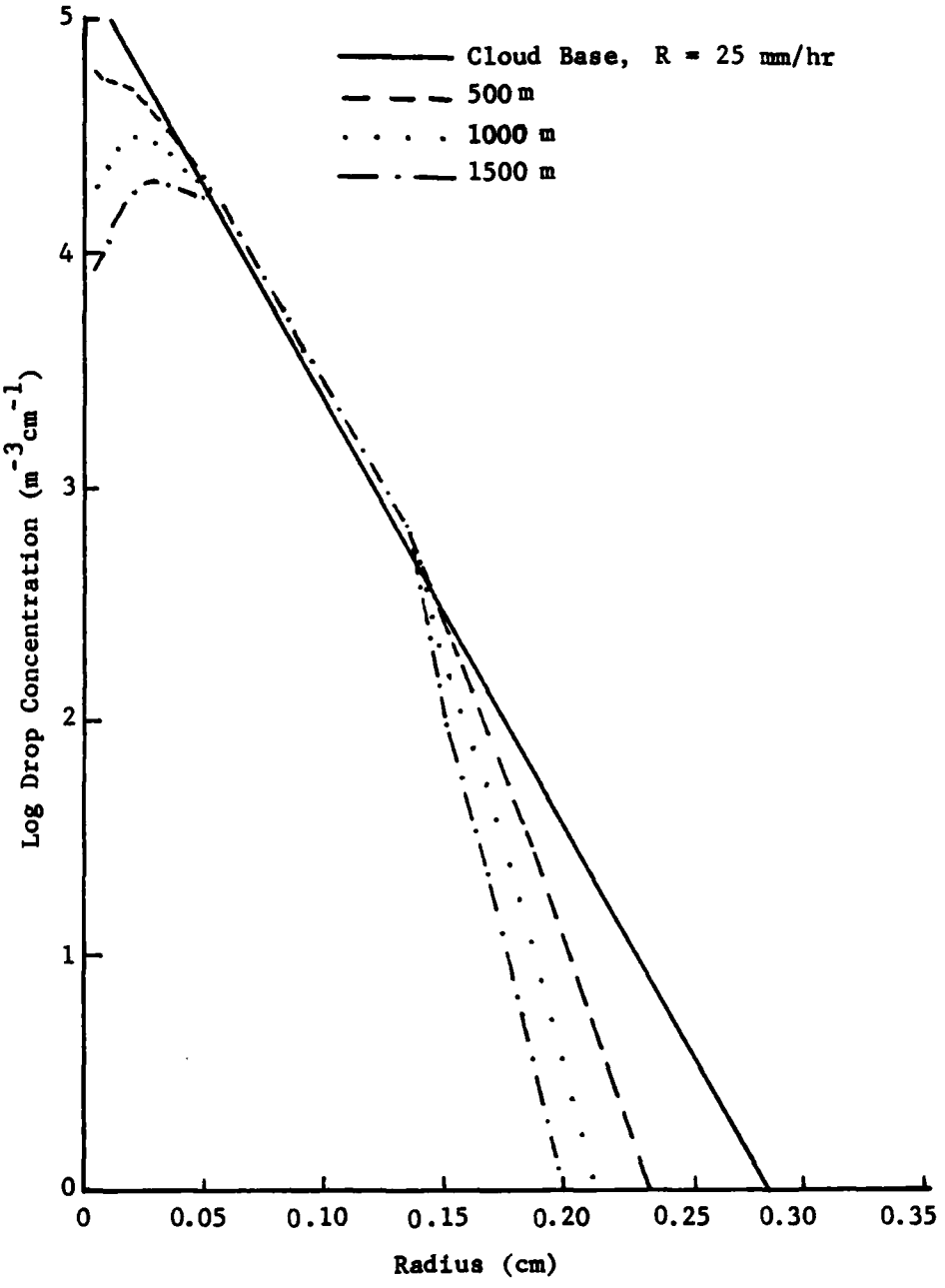

Fig. 23. Evolution of drop-size distribution in Case D for an initial precipitation rate of 25 mm/hr and a constant downdraft of 5 m/sec.

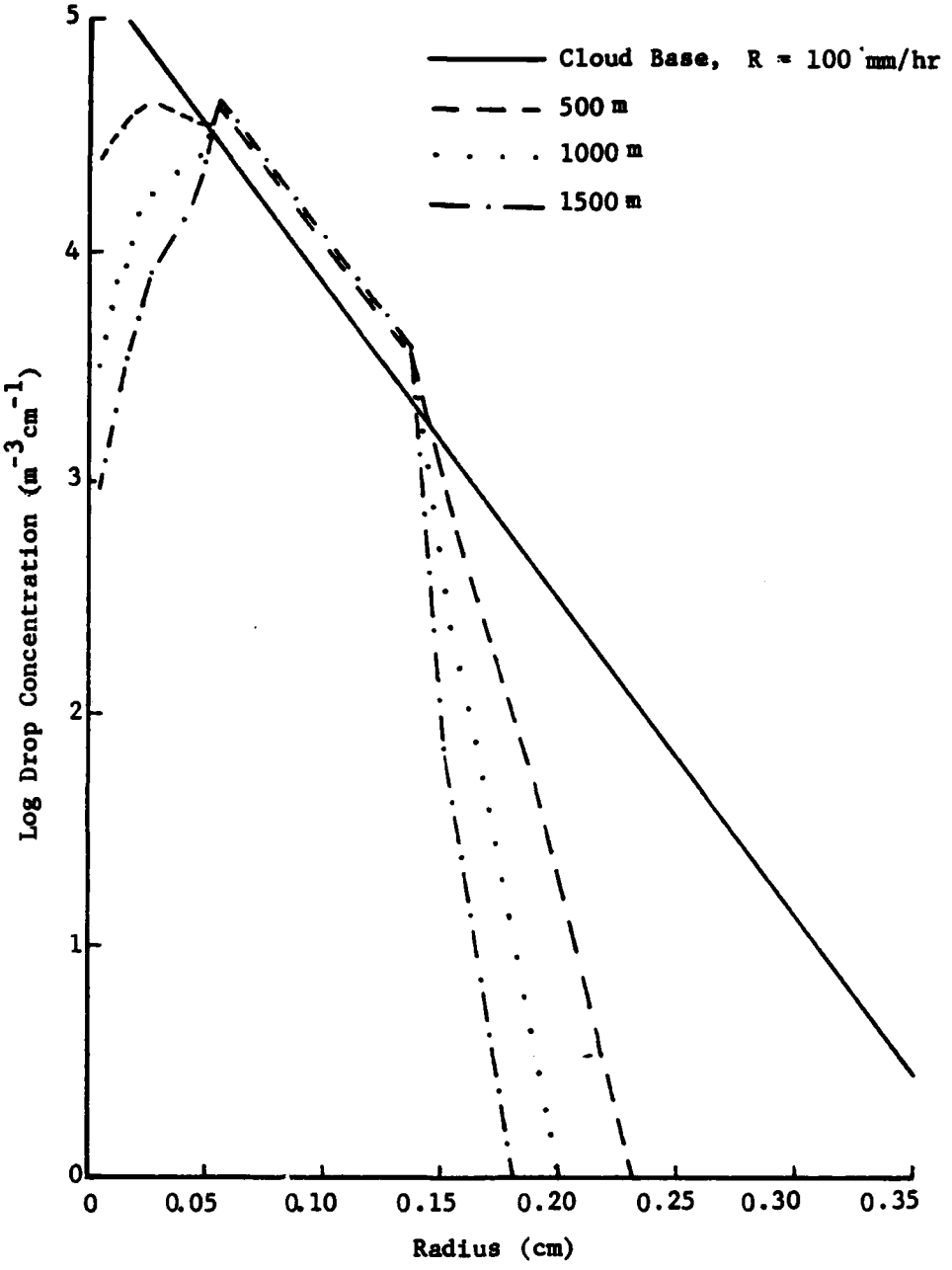

Fig. 24. Same as Fig. 23 except for an initial precipitation rate of 100 mm/hr.

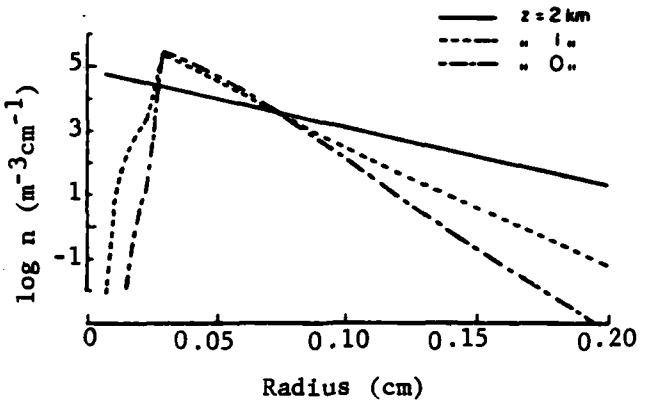

Fig. 25. Evolution with altitude of drop-size distribution through collision-coalescence and collisional breakup from an initial Marshall-Palmer distribution for rainfall rate of 25 mm/hr (after Gillespie and List, 1978/79).

closely with the shape of the 1500-m distribution in Fig. 23, but the drop concentration at the peak of the distribution is higher in Fig. 25 than in Fig. 23. In Fig. 26, in which the results of Gillespie and List are plotted against those of Case D at 1000 m and 1500 m below cloud base, the peaks in the Gillespie and List curves cross the Marshall-Palmer distribution at a drop radius of about 0.075 cm, while in Case D the crossover occurs at about r = 0.14 cm. Gillespie and List did not report results for heavier precipitation rates, although in their earlier work, List and Gillespie (1976) provided the distribution resulting from an initial precipitation rate of 100 mm/hr. The comparison of our results with this case is discussed below.

Fig. 27 is a time evolution through coalescence and collisional breakup of an initial Marshall-Palmer spectrum for a rainfall rate of

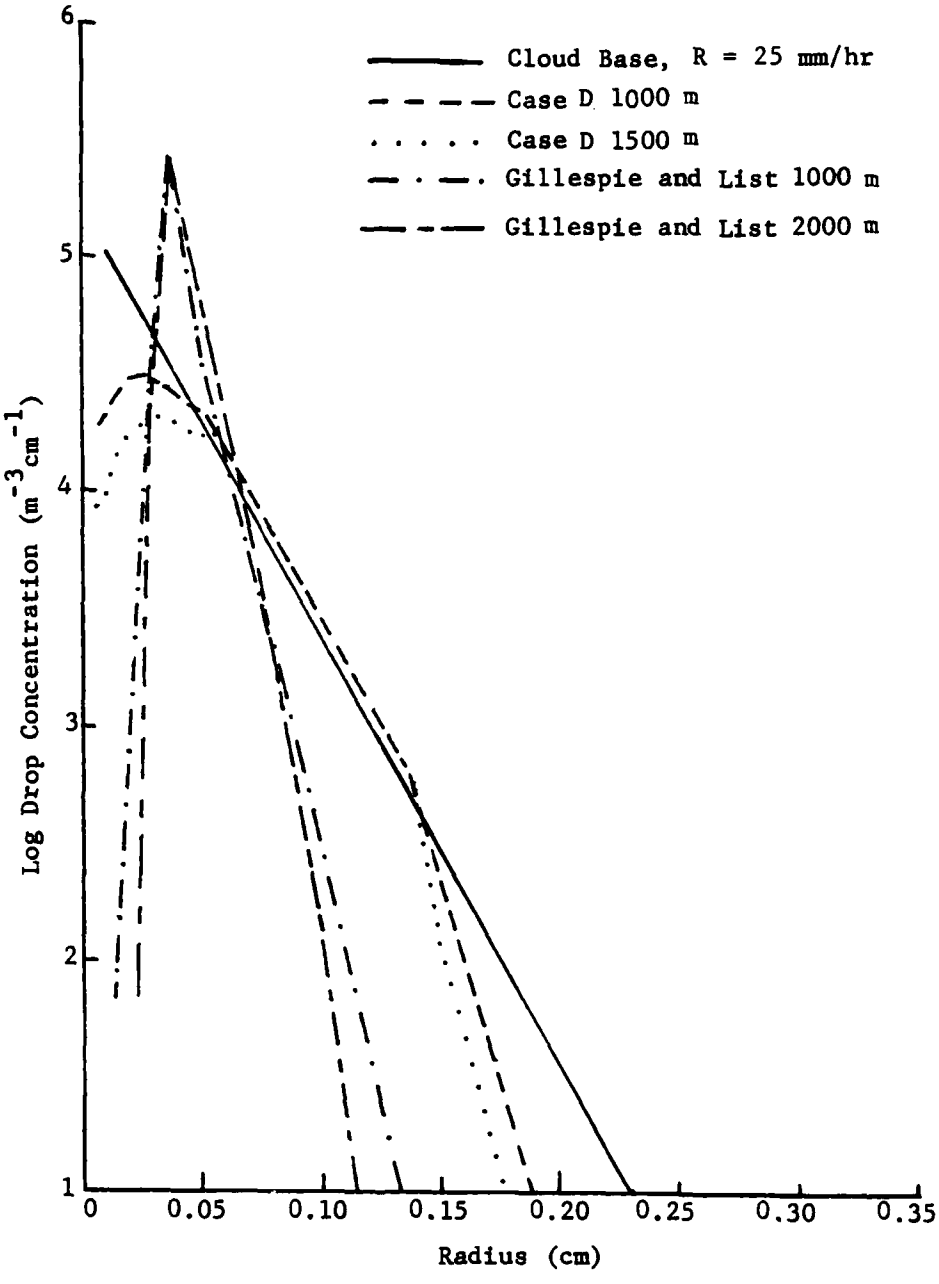

Fig. 26. Drop-size distributions in Case D compared with analogous computation of Gillespie and List (1978/79).

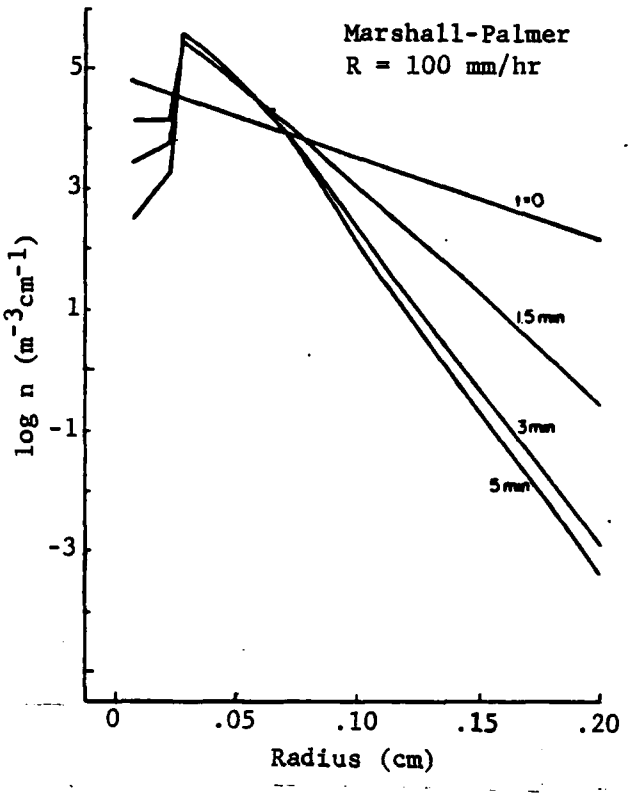

Fig. 27. Time evolution through coalescence and breakup of a raindrop spectrum from an initial Marshall-Palmer distribution for the rainfall rate of 100 mm/hr (after List and Gillespie, 1976).

100 mm/hr as reported by List and Gillespie (1976). The drop-concentration characteristics that appear in this figure are similar to those in Fig. 25, and if compared against Fig. 24, would reveal differences from Case D as seen above for a 25-mm/hr precipitation rate. A possible explanation for the difference is in the formulation of fragment probability resulting from collisional breakup. It appears there is an error in Eq. (17) of List and Gillespie. The Gaussian

distribution fitted to the observed points for large fragments did not have a negative sign in the exponent - an error that this research corrected in (40). At the time the error was noted, it appeared to be restricted to the journal only and not the actual List and Gillespie computer program. In order to determine the effect of this error on the final drop-size distribution if, in fact, List and Gillespie had programmed their (17) as reported in the literature, a test case was run for an initial precipitation rate of 100 mm/hr and a constant downdraft of 5 m/sec. The results of this test are shown in Fig. 28. Since List and Gillespie (1976) did not employ rainshaft downdraft velocity in their research, the case of w_D = 5 m/sec was chosen for comparison, this being the case with the weakest downdraft in our computations. The results in Fig. 28 show that the peak concentration and the crossover points of the Marshall-Palmer distribution agree quite well between the test case (the modified Case D) and List and Gillespie (1976). The only major disagreement in these two figures is the drop radius of the peak concentration. This peak occurs at r = 0.03 cm for List and Gillespie and r = 0.05 cm for the modified Case D. This is probably due to the numerical formulation used by List and Gillespie (1976).

Since there was strong evidence of an error in List and Gillespie (1976), that probably was carried over to Gillespie and List (1978/79), this study continued to the final step of adding aerodynamic breakup to the Case D microphysical processes.

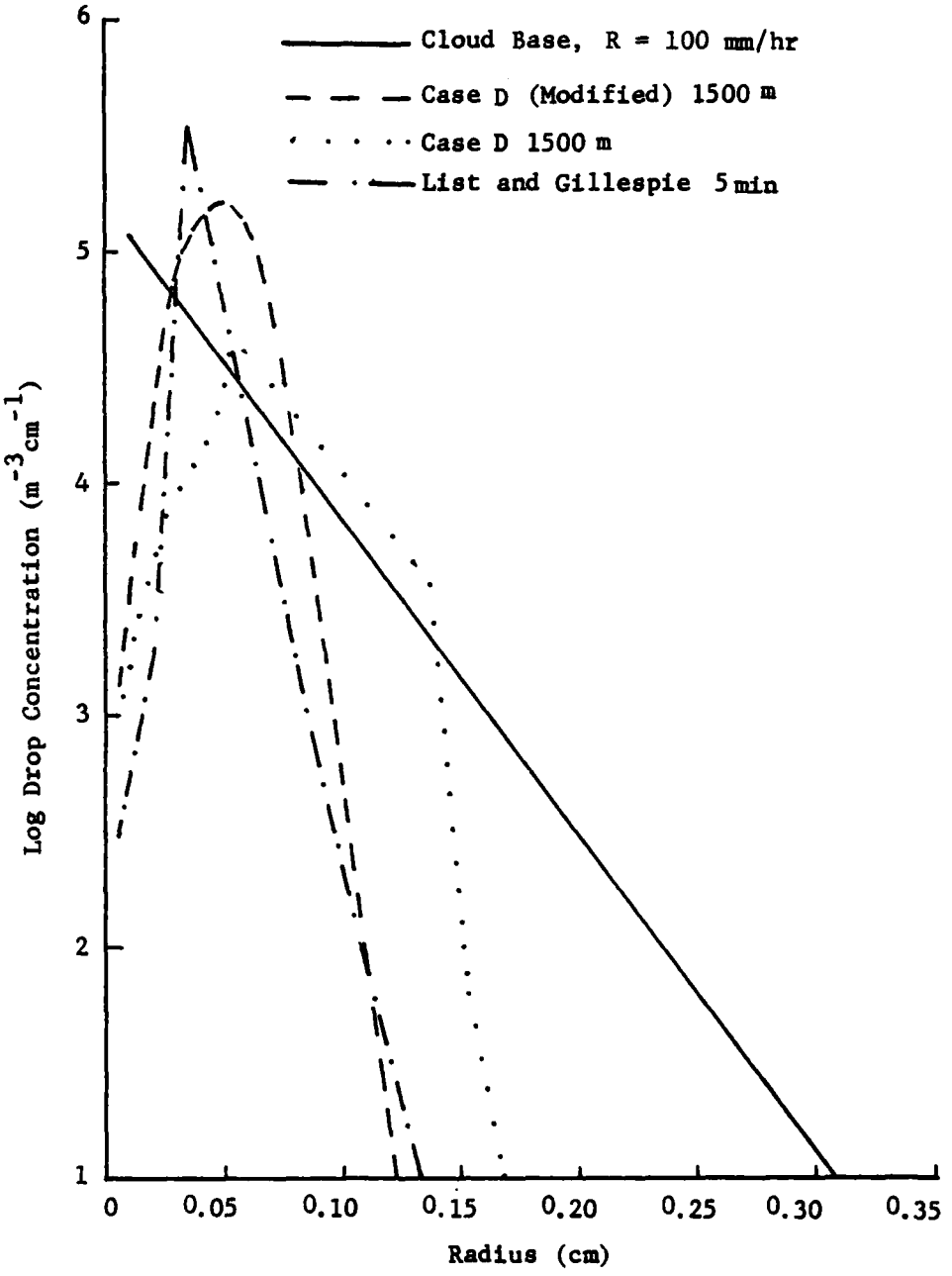

Fig. 28. Comparison of drop-size distributions at 1500 m below cloud base, for Case D computed with incorrect and correct fragment distribution of List and Gillespie (1976). The initial precipitation rate is 100 mm/hr and the subcloud downdraft is 5 m/sec.

e. Case E: Evaporation, Collision-Coalescence, Collisional and Aerodynamic Breakup

Case E includes the Case D microphysical processes and formulations together with aerodynamic breakup formulations of Srivastava (1971) and is the last case considered in this research.

Vertical distributions of thermodynamic and hydrometeoric quantities resulting from Case E for the initial precipitation rates of 25, 50, 75, and 100 mm/hr are given in Tables 20, 21, and 22, respectively, for constant downdrafts of 5, 10, and 15 m/sec. It may be recalled that in the comparison of Cases B and C, the effects of aerodynamic breakup were found to be insignificant for small precipitation rates, but became significant with larger precipitation rates with their higher concentration of large drops. There is virtually no difference between Case D and the Case E even for the larger precipitation rates. Collisional breakup depletes the concentration of large drops to the point where aerodynamic breakup becomes an insignificant process.

Drop-size distributions resulting from Case E are given, respectively, in Figs. 29, 30, 31, and 32 for initial precipitation rates of 25, 50, 75, and 100 mm/hr. A comparison of Figs. 29 and 32 with Figs. 19 and 20 indicates no perceptible difference between the drop-size distributions for Cases D and E, thereby showing, again, the insignificance of aerodynamic breakup compared to collisional breakup. The distributions in Figs. 29-32 maintain a Marshall-Palmer (exponential) slope between the drop radii of 0.05 to 0.14 cm. For a light initial precipitation rate (Fig. 28), the final distributions maintain this

Table 20. Vertical distribution of thermodynamic and hydrometeoric quantities in a subcloud downdraft of 5 m/sec.

z (m)	T_D (K)	T (K)	S (%)	M($\times 10^{-3}$) (kg/m^3)	R (mm/hr)	Z($\times 10^{-5}$) (mm^6/m^3)
			R = 25 mm/hr			
1500	278.0	278.0	100.0	1.24	25.0	0.33
1000	282.9	282.8	77.4	1.22	24.0	0.22
500	287.8	287.3	62.4	1.18	23.1	0.19
0	292.7	291.6	51.8	1.11	22.0	0.17
			R = 50 mm/hr			
1500	278.0	278.0	100.0	2.24	50.0	0.92
1000	282.9	282.7	78.1	2.21	46.7	0.45
500	287.8	287.0	64.4	2.15	45.1	0.38
0	292.7	291.1	55.1	2.07	43.5	0.35
			R = 75 mm/hr			
1500	278.0	278.0	100.0	3.28	75.0	1.77
1000	282.9	282.6	78.8	3.25	71.2	0.68
500	287.8	286.8	66.3	3.17	69.1	0.58
0	292.7	290.7	58.2	3.07	67.2	0.54
			R = 100 mm/hr			
1500	278.0	278.0	100.0	4.03	100.0	2.51
1000	282.9	282.6	79.2	3.99	90.1	0.84
500	287.8	286.6	67.5	3.91	87.8	0.72
0	292.7	290.4	60.2	3.79	85.7	0.69

Table 21. Vertical distributions of thermodynamic and hydrometeoric quantities for Case E in a sub-cloud downdraft of 10 m/sec.

z (m)	T_D (K)	T (K)	S (%)	M($\times 10^3$) (kg/m^3)	R (mm/hr)	Z($\times 10^{-5}$) (mm^6/m^3)
			R = 25 mm/hr			
1500	278.0	278.0	100.0	1.24	25.0	0.33
1000	282.9	282.8	76.7	1.23	24.1	0.24
500	287.8	287.5	60.5	1.18	23.2	0.20
0	292.7	292.1	48.8	1.12	22.0	0.18
			R = 50 mm/hr			
1500	278.0	278.0	100.0	2.24	50.0	0.92
1000	282.9	282.8	77.1	2.22	47.0	0.50
500	287.8	287.4	61.6	2.16	45.2	0.40
0	292.7	291.8	50.7	2.07	43.3	0.36
			R = 75 mm/hr			
1500	278.0	278.0	100.0	3.28	75.0	1.77
1000	282.9	282.8	77.4	3.25	71.7	0.76
500	287.8	287.2	62.7	3.17	69.0	0.61
0	292.7	291.5	52.4	3.06	66.6	0.55
			R = 100 mm/hr			
1500	278.0	278.0	100.0	4.03	100.0	2.51
1000	282.9	282.7	77.7	3.99	90.8	0.94
500	287.8	287.1	63.4	3.90	87.6	0.75
0	292.7	291.3	53.6	3.78	84.8	0.69

Table 22. Vertical distributions of thermodynamic and hydrometeoric quantities for Case E in a sub-cloud downdraft of 15 m/sec.

z (m)	T_D (K)	T (K)	S (%)	M($\times 10^3$) (kg/m^3)	R (mm/hr)	Z($\times 10^{-5}$) (mm^6/m^3)
			R = 25 mm/hr			
1500	278.0	278.0	100.0	1.24	25.0	0.33
1000	282.9	282.9	76.5	1.23	24.2	0.25
500	287.8	287.6	59.9	1.19	23.4	0.21
0	292.7	292.3	47.8	1.14	22.3	0.18
			R = 50 mm/hr			
1500	278.0	278.0	100.0	2.24	50.0	0.92
1000	282.9	282.8	76.7	2.22	47.4	0.53
500	287.8	287.5	60.6	2.17	45.5	0.43
0	292.7	292.1	49.1	2.09	43.6	0.38
			R = 75 mm/hr			
1500	278.0	278.0	100.0	3.28	75.0	1.77
1000	282.9	282.8	77.0	3.25	72.3	0.82
500	287.8	287.4	61.4	3.18	69.4	0.64
0	292.7	291.9	50.3	3.08	66.9	0.57
			R = 100 mm/hr			
1500	278.0	278.0	100.0	4.03	100.0	2.51
1000	282.9	282.8	77.1	3.99	91.6	1.02
500	287.8	287.3	61.9	3.91	88.0	0.80
0	292.7	291.7	51.1	3.80	85.1	0.71

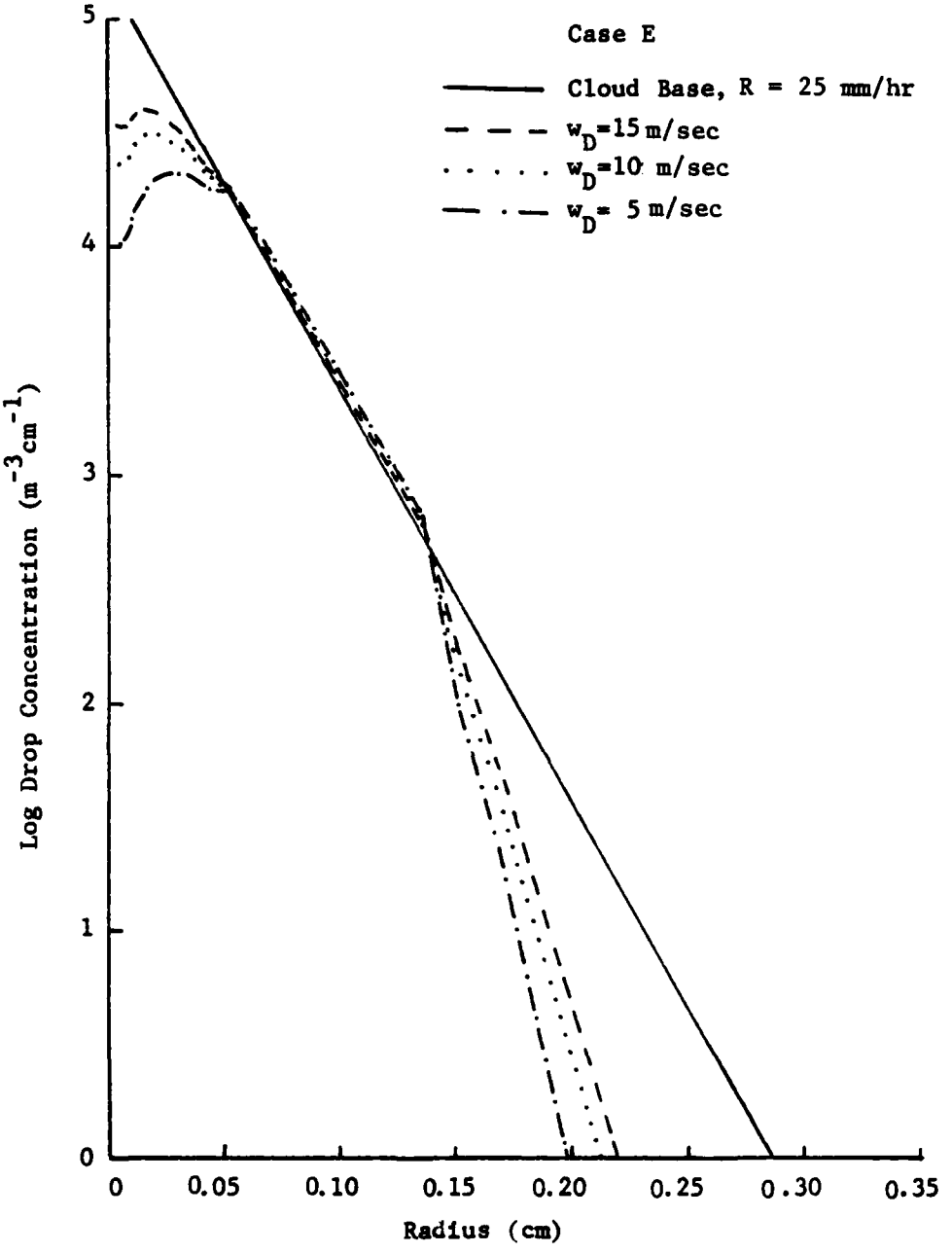

Fig. 29. Same as Fig. 7 except for Case E.

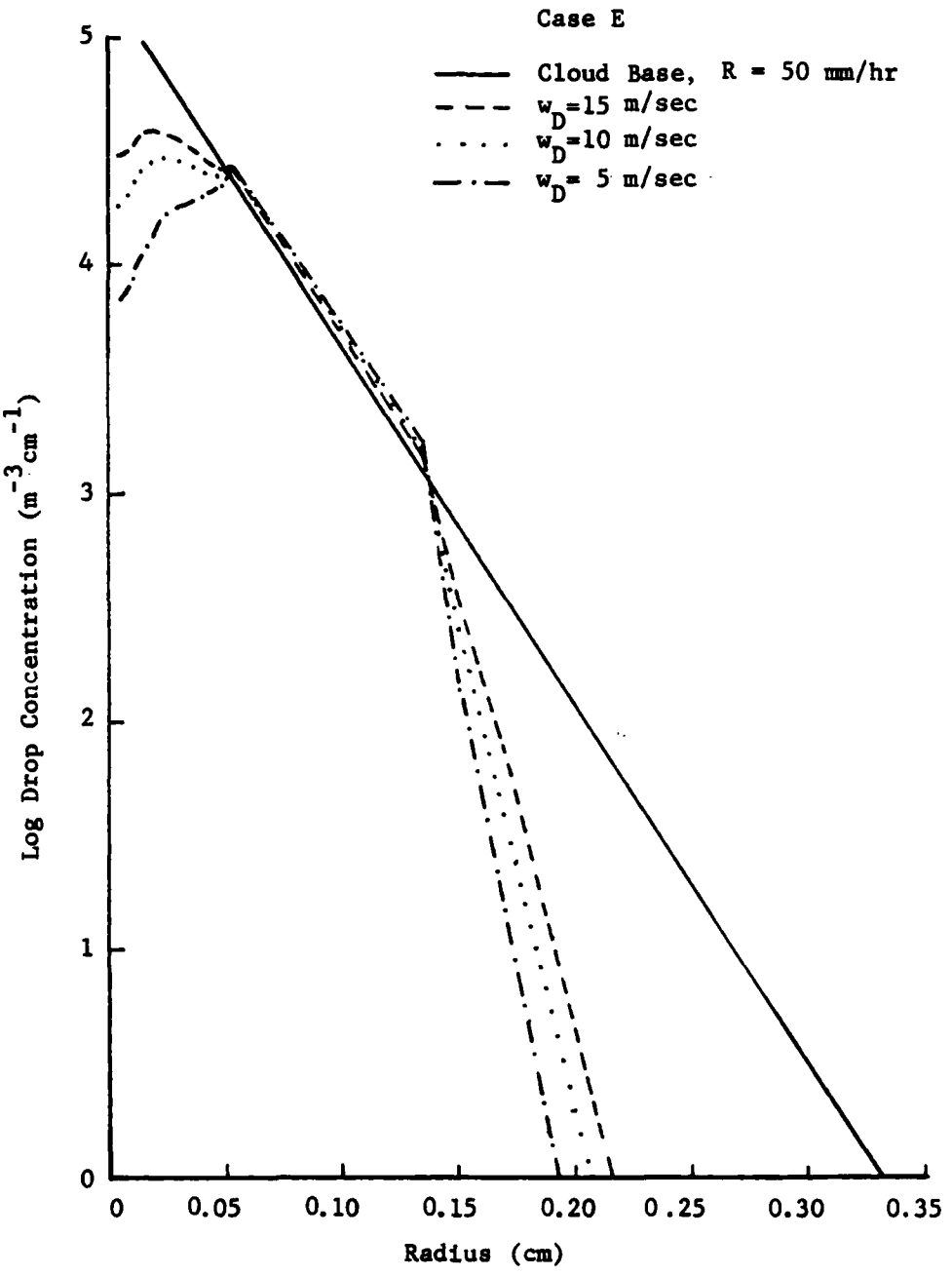

Fig. 30. Same as Fig. 29 except for initial R = 50 mm/hr.

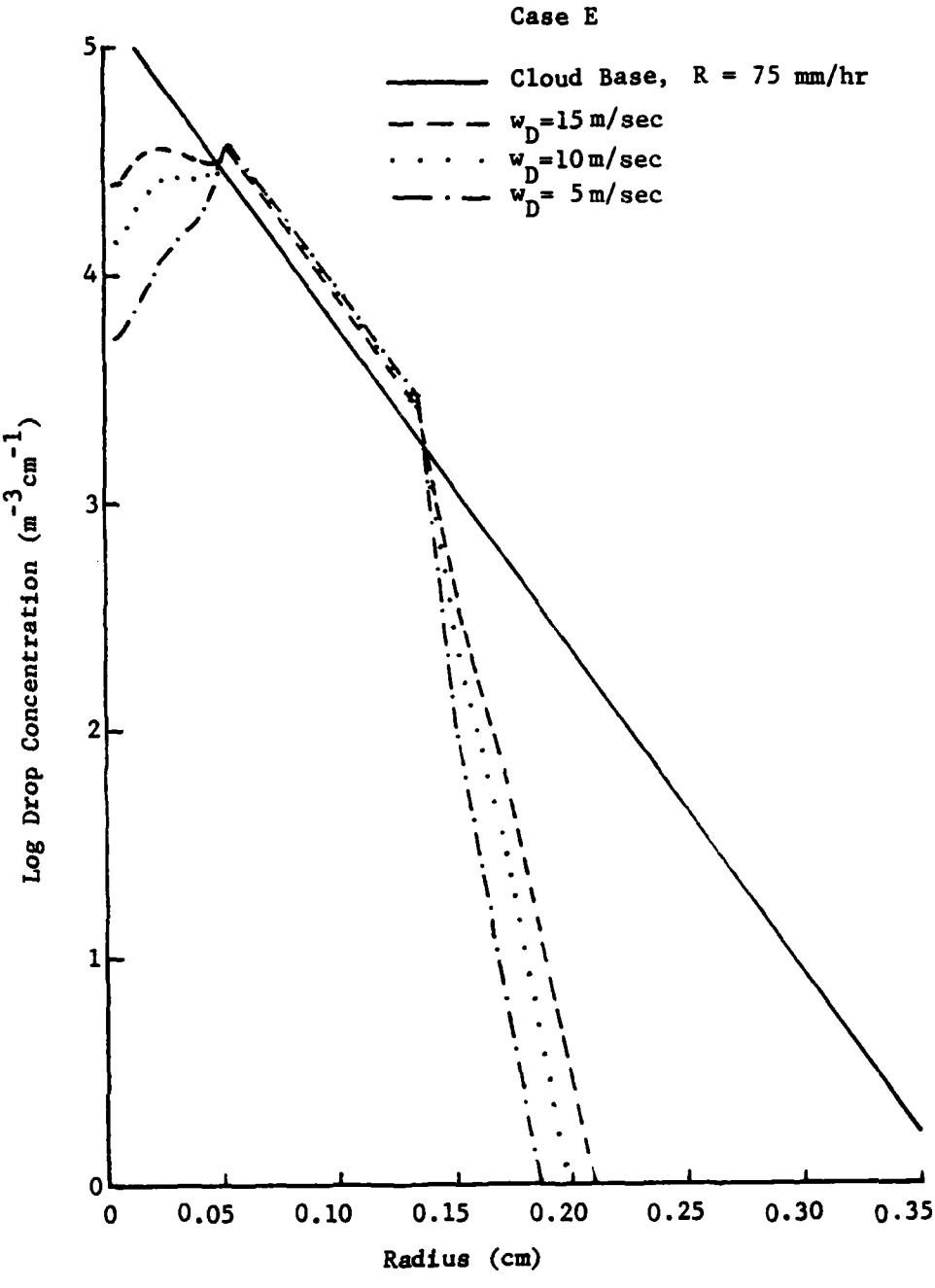

Fig. 31. Same as Fig. 29 except for initial R = 75 mm/hr.

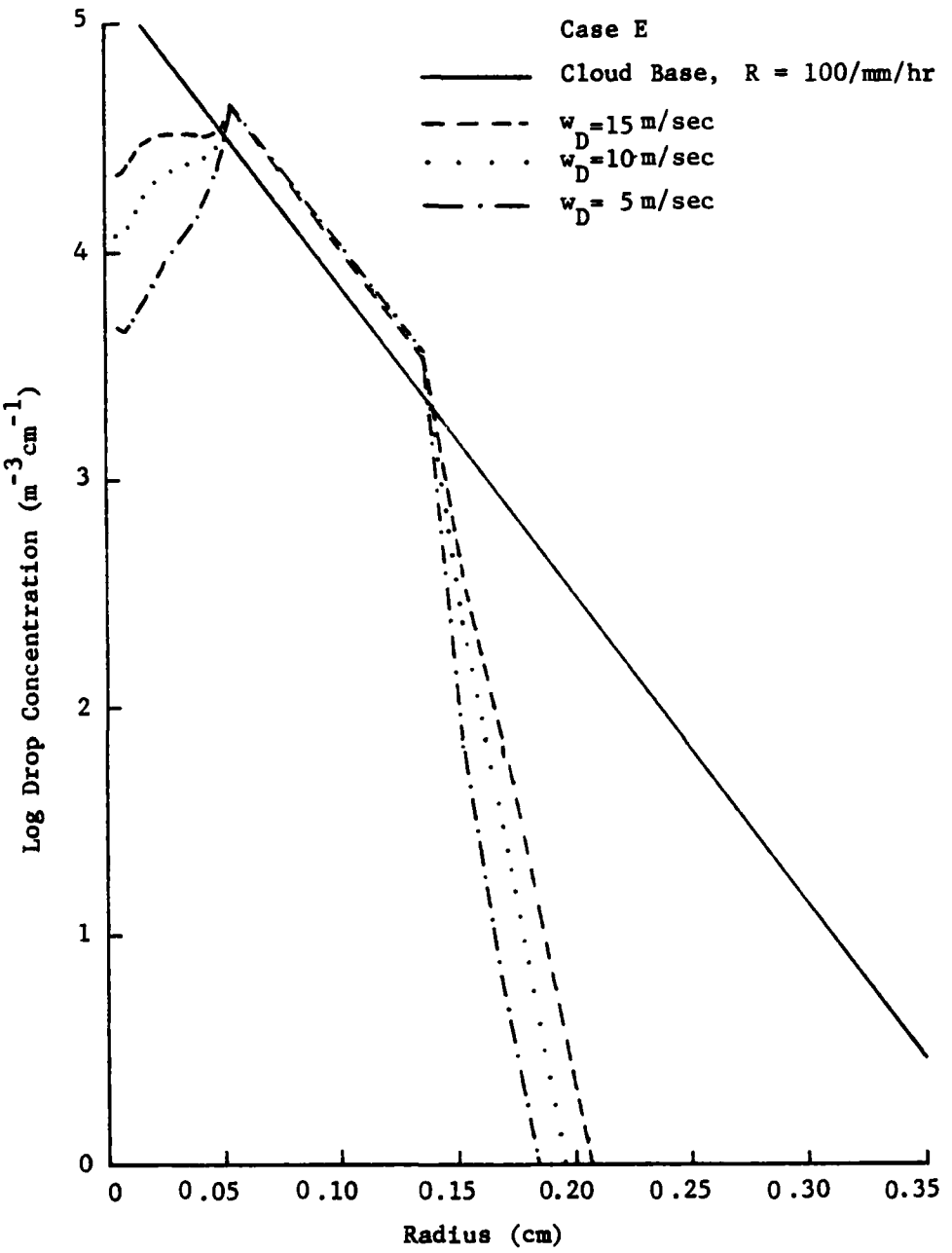

Fig. 32. Same as Fig. 8 except for Case E.

exponential characteristic down to a radius of about 0.02 cm. Young (1975) and Srivastava (1978) achieved similar results when they studied the time-dependent interaction of condensation, coalescence, and collisional and aerodynamic breakup in the initiation of warm rain. Both researchers used the aerodynamic breakup formulated by Srivastava (1971) and the collision-induced breakup of Brazier-Smith et al. (1972) in their studies. Young found that not only did collision breakup dominate over aerodynamic breakup, but the resulting steady-state distribution was exponential and provided fair agreement with average observed drop spectra. Srivastava (1978) appeared to find similar results in his theoretical study.

CHAPTER VI

COMPARISON WITH OBSERVED RAINDROP SPECTRA

We have computed steady-state raindrop-size distributions for several constant downdraft velocities and cloud-base precipitation rates, but how well do these calculated distributions agree with observed spectra? In this chapter we will compare our computed results with measured spectra from both warm rain and also thunderstorm (cold rain) situations.

a. Warm Raindrop Measurements

Austin and Geotis (1979) reported several sets of drop-size measurements made on board a ship during the Global Atmospheric Research Program's (GARP) Atlantic Tropical Experiment (GATE). They used a Joss disdrometer which was manually activated during moderate and heavy showers. The Joss disdrometer has the capability to record drop sizes in the radiusrange 0.02 to about 0.25 cm, but due to noisy conditions aboard ship, most drops < 0.10 cm in radius were suppressed in the measurements. For this reason very large correction factors had to be added to the small drop measurements. For a full explanation of the problems and solutions associated with these measurements, see Austin and Geotis (1979).

Fig. 33 is plot of an Austin-Geotis drop distribution for R = 34.4 mm/hr together with Case E distributions for initial precipitation rates of 25 and 50 mm/hr. The observed distribution has more drops of the small radii and fewer at the large radii than either of

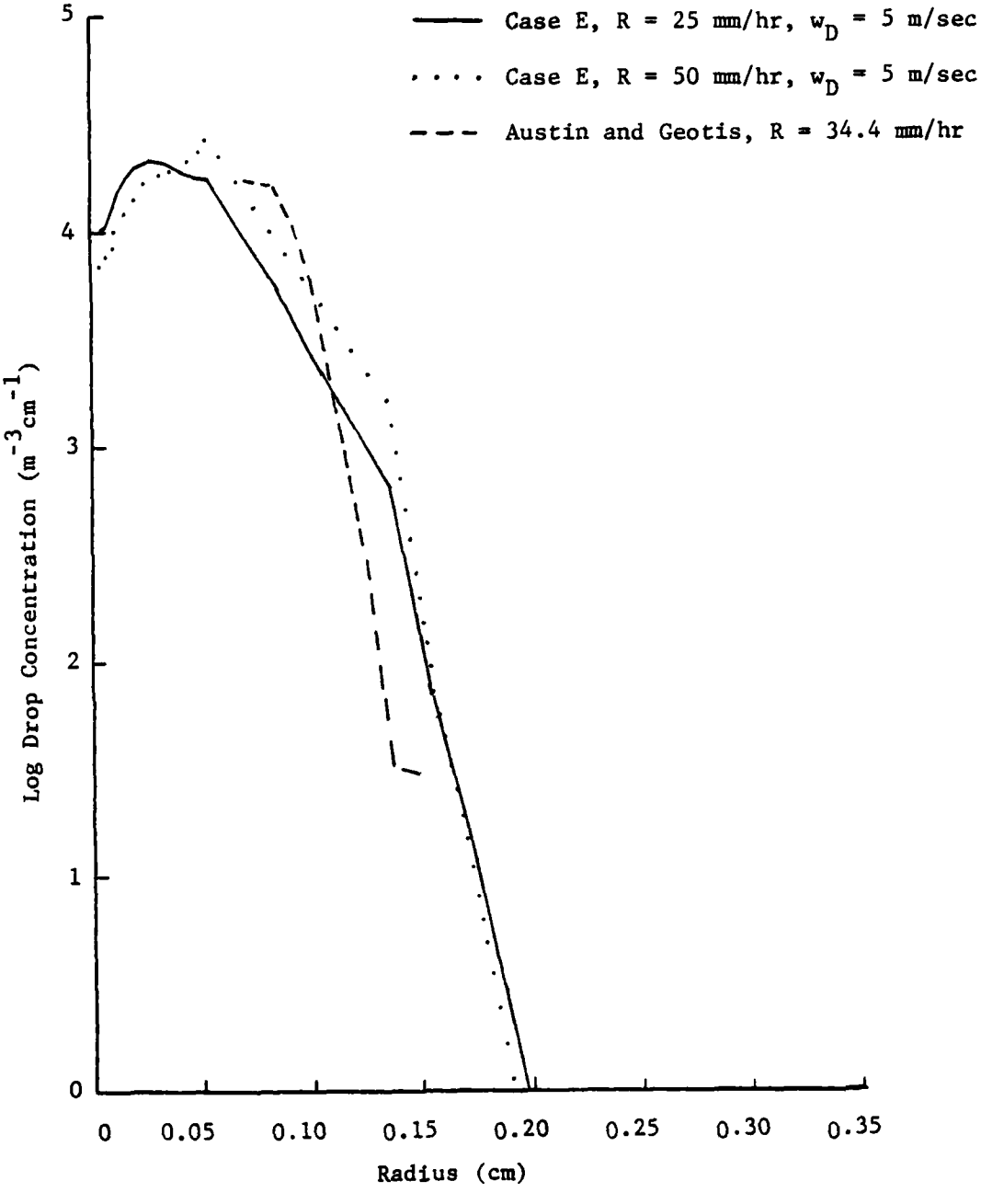

Fig. 33. Comparison of drop-size distributions computed in Case E with those observed by Austin and Geotis (1979) in convective rain. Computed distributions refer to 1500 m below cloud base, and are for initial precipitation rates of 25 and 50 mm/hr and a downdraft velocity of 5 m/sec. Observed distributions are for a precipitation rate of 34.4 mm/hr at the surface.

the computed distributions. In Fig. 34, a comparison of distributions resulting from heavier rain shows that the observed distribution has the same general shape, but overall a higher concentration of drops than the computed spectra. Both Figs. 33 and 34 are for computed distributions resulting from a 5 m/sec constant downdraft. Fig. 35 shows that the Case E spectrum for w_D = 15 m/sec is in closer agreement with Austin and Geotis than the two distributions resulting from weaker downdrafts. This is especially true in the radius range from 0.14 to 0.18 cm. This result should be expected since observations were taken in moderate to heavy rainshafts where the downdraft velocity could be stronger.

In order to insure that their instrument corrections were valid, Austin and Geotis compared their observed spectra with distributions observed in other maritime regions. The spectra from Majuro Atoll in the Marshall Islands, observed by Mueller and Sims (1967), and the Panama drop-size distributions measurements made by Geotis (1968) were selected for comparison. Mueller and Sims used a raindrop camera, while Geotis (1968) used a Joss disdrometer. Fig. 36 is a plot of averaged drop-size distributions measured by Austin and Geotis (1979), Mueller and Sims (1967), and Geotis (1968) together with a computed distribution at 1500 m below cloud base for Case E and an initial precipitation rate of 25 mm/hr. The computed distribution has a higher drop concentration across the entire radius spectrum than any of the averaged observed distributions. This trend is less noticeable with higher precipitation rates as shown in Fig. 37. Here, the calculated drop concentration agrees much better with average observed

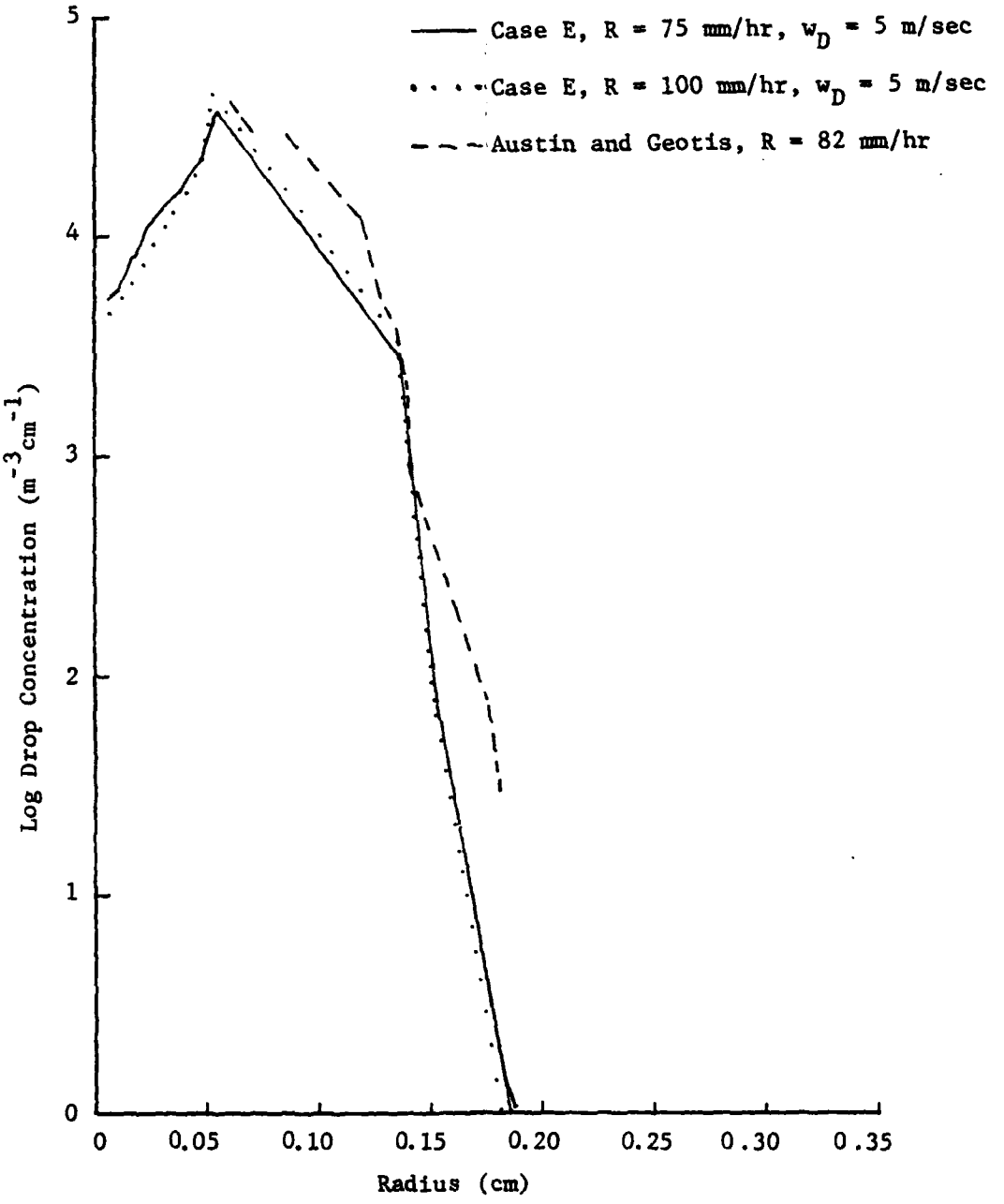

Fig. 34. Same as Fig. 33 except that computed distributions are for precipitation rates of 75 and 100 mm/hr and observed distributions are for a precipitation rate of 82 mm/hr.

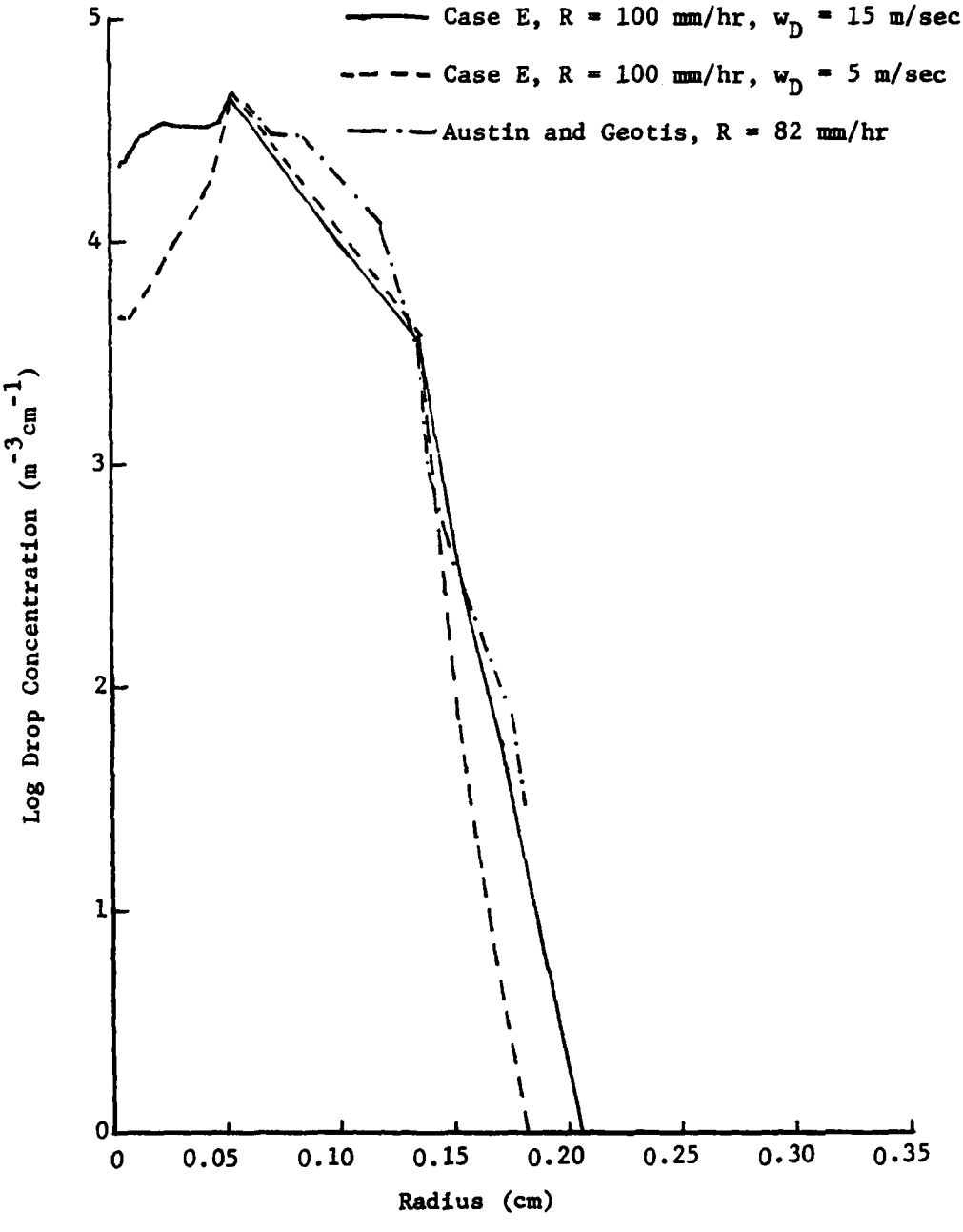

Fig. 35. Computed drop-size distributions in Case E, 1500 m below cloud base, for constant downdrafts of 5 and 15 m/sec, and a precipitation rate of 100 mm/hr. Also plotted is the drop-size distribution for Austin and Geotis (1979) for R = 83 mm/hr.

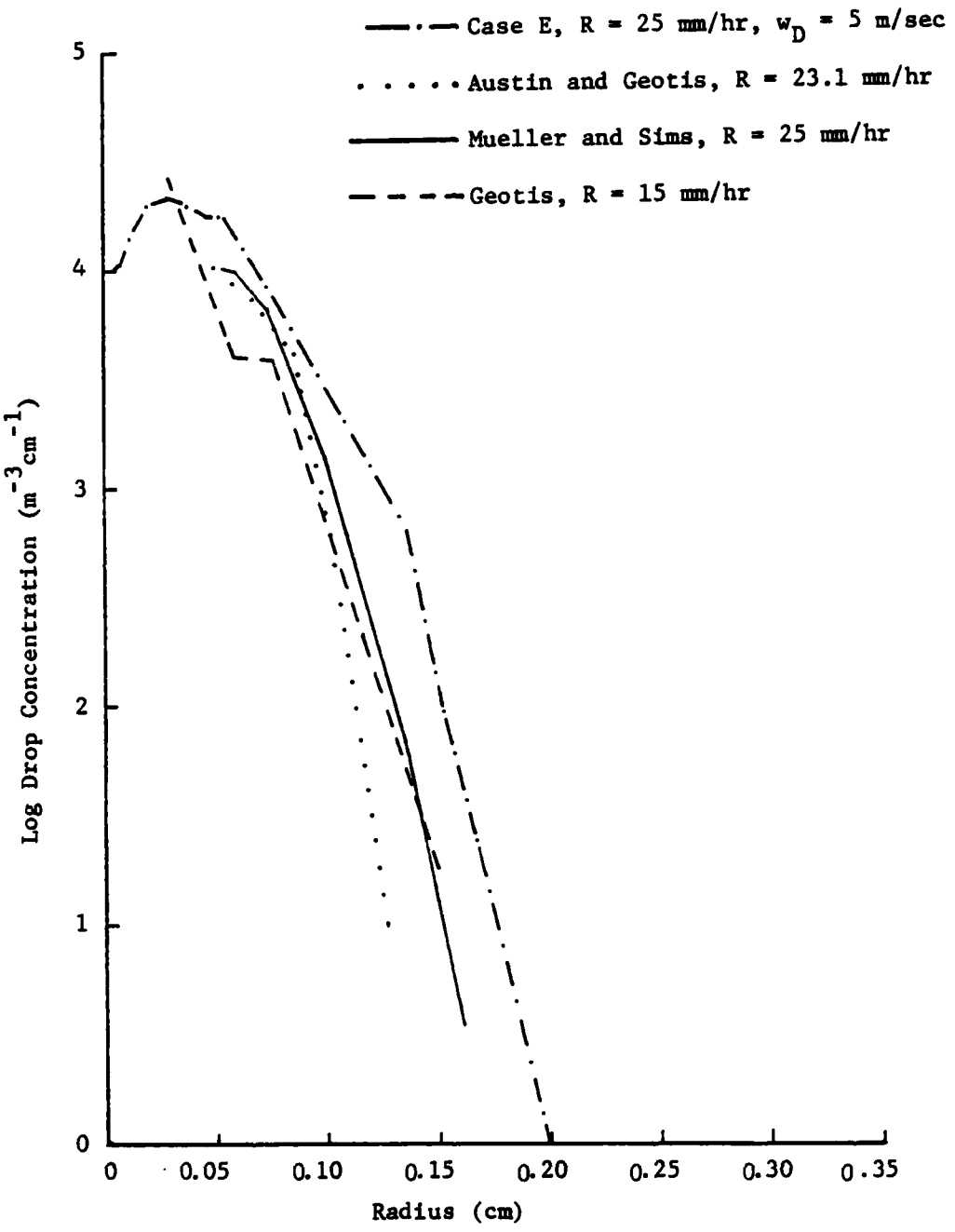

Fig. 36. Averaged observed drop-size distributions from Mueller and Sims (1967), Geotis (1968), and Austin and Geotis (1979) together with a computed distribution for Case E. The initial precipitation rate is 25 mm/hr.

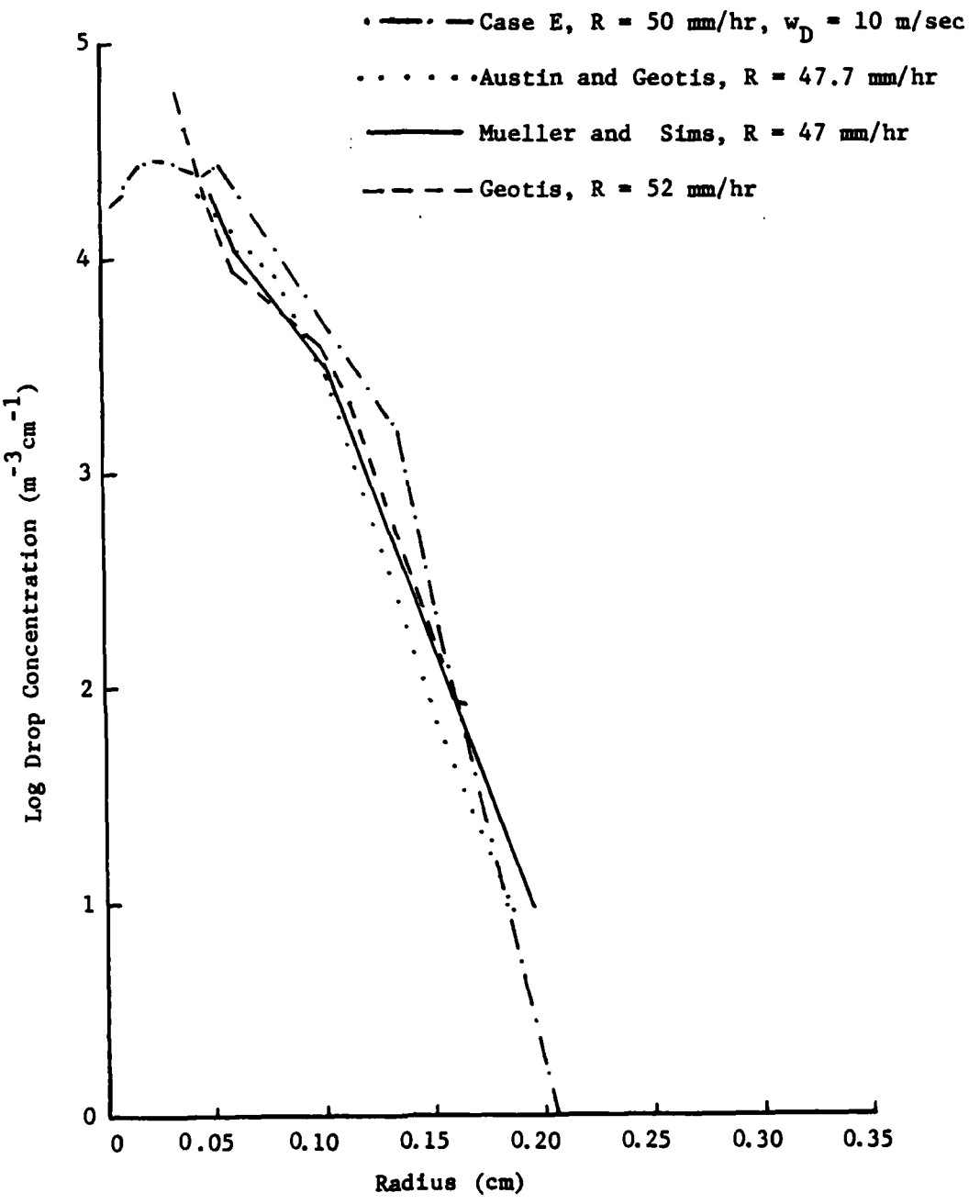

Fig. 37. Averaged observed drop-size distributions from Mueller and Sims (1967), Geotis (1968), and Austin and Geotis (1979) together with a computed distribution for Case E. The initial precipitation rate is 50 mm/hr.

spectra. Note in both Figs. 36 and 37 that the Geotis (1968) distributions have a much higher drop concentration for small radius drops. This is in the minimum radius range of drop resolution for the Joss disdrometer and, based on acoustical problems in this radius range, should probably not be highly regarded. Two things are clear, however, from Figs. 33 through 37. First, the computed distributions for R = 25 mm/hr have drop concentrations considerably higher than observed spectra for the same precipitation rate, while Figs. 34, 35, and 37 indicate that for higher precipitation rates this trend becomes less evident. Second, all distributions are very steep, with numerous drops in the range 0.05 cm $\leq$ r $\leq$ 0.10 cm and relatively few drops with r > 0.15 cm. This last conclusion is important since it shows that, in warm rain, collisional drop breakup is the driving mechanism in shaping the final drop-size distribution.

b. Thunderstorm Raindrop Measurements

Thunderstorm raindrop-size distributions were measured by Dingle and Hardy (1962) using a photoelectric raindrop spectrometer. They took several measurements from storms in the fall of 1959 in the Ann Arbor, Michigan, area that would strongly indicate frozen hydrometeors in the rainshaft. Fig. 38 depicts an averaged Dingle and Hardy distribution (average of seven 1-min distributions) for R = 24.2 mm/hr plotted against the distributions in Case E for R = 25 mm/hr and w_D = 5 and 15 m/sec. As in the warm rain comparison (Fig. 33), the observed distribution has a lower concentration of large drops when compared to the calculated distribution, although this difference is

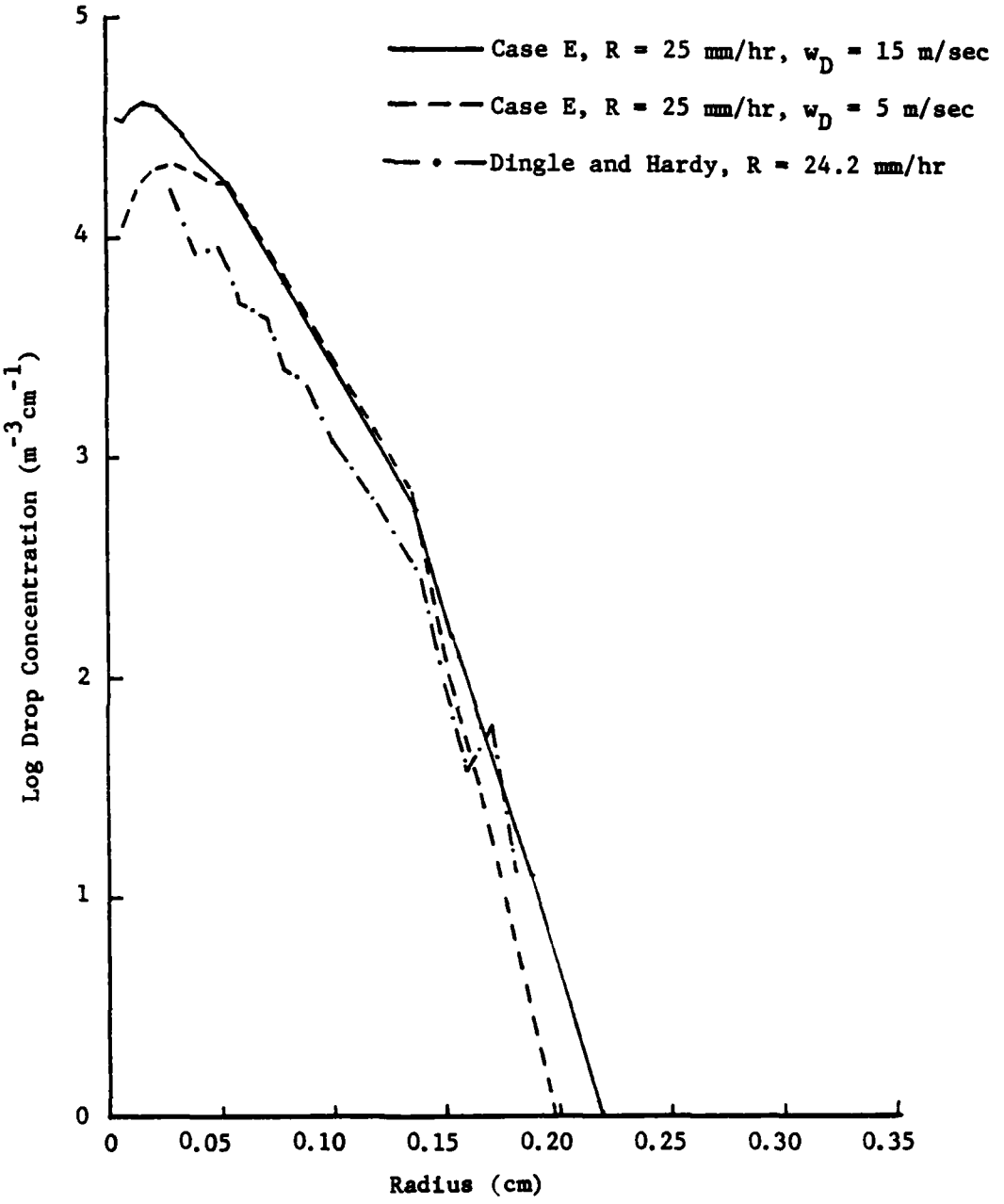

Fig. 38. Drop-size distributions computed in Case E for an initial precipitation rate of 25 mm/hr compared with an averaged drop-size distribution observed by Dingle and Hardy (1962) in thunderstorm rain of 24.2 mm/hr intensity.

less in Fig. 38 than in Fig. 33. The difference between observed and calculated drop concentrations increases in Fig. 38 toward smaller drop-sizes. Note the increase in drop concentration (Fig. 38) which occurs at about r = 0.17 cm. As indicated earlier, the Dingle and Hardy distributions are averages which means this has to be a persistent phenomenon. A similar trend is apparent in Fig. 33 at about r = 0.15 cm. The comparison of Figs. 33 and 38 illustrates a greater effect of drop breakup on warm rain than on thunderstorm rain. Fig. 39 shows a comparison of averaged Dingle and Hardy distributions (average of three 1-min distributions) for R = 65.5 mm/hr plotted against Case E results for R = 75 mm/hr. The trend in Fig. 39 is the same as in Fig. 38 in that the observed drop concentrations are lower than Case E values until about r = 0.18 cm, where the slope of the observed distribution changes drastically. Having no detail is available on the drop-size resolution of the equipment or on any problems associated with the measurements of Dingle and Hardy it will not be proper to speculate on the possible cause of this drop concentration increase.

In summary, in the radius range from 0.03 to about 0.19 cm, the calculated drop-size distributions appear to agree with the observed average distributions in shape, but disagree in drop concentration in the small drop-size portions of the spectra.

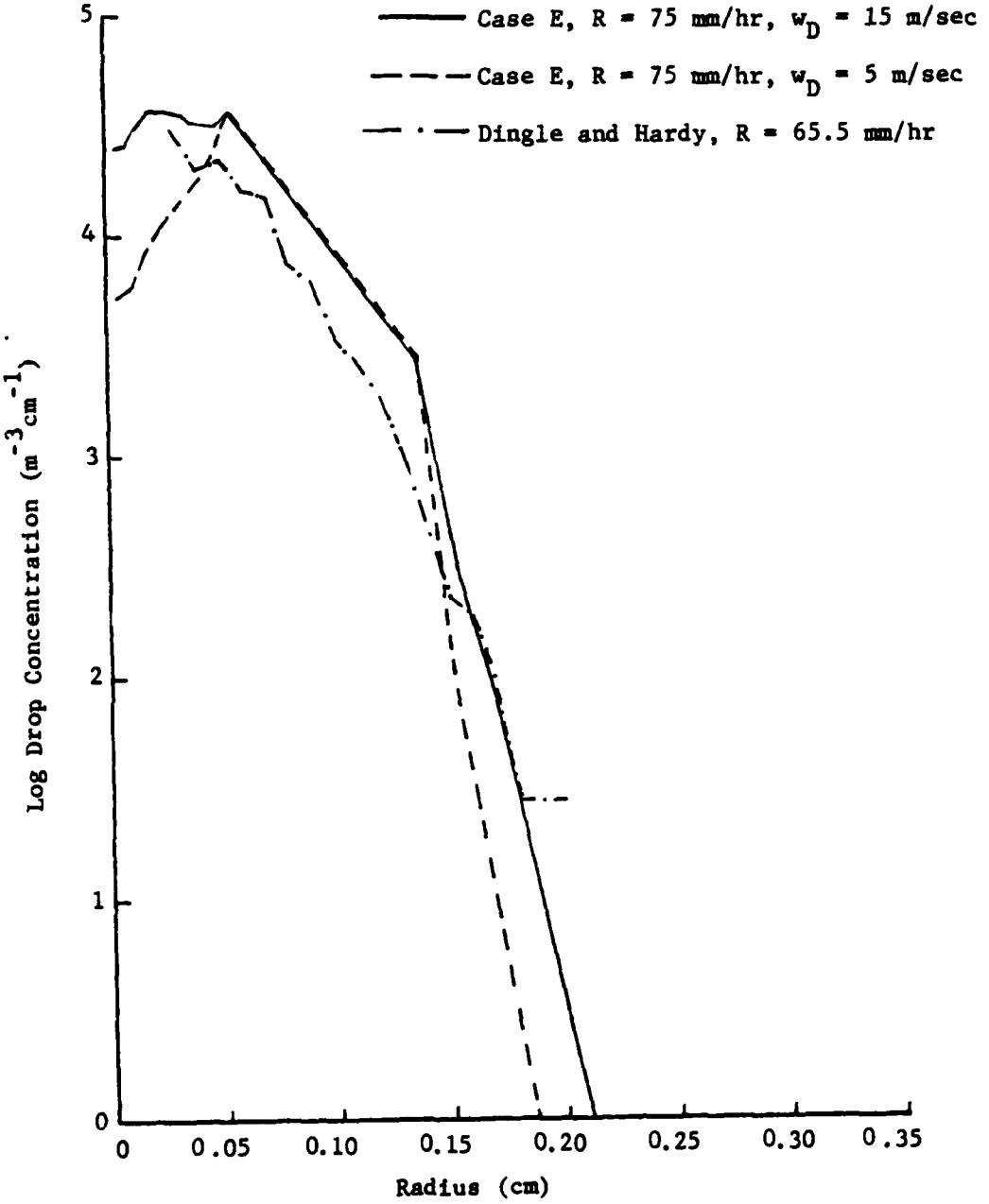

Fig. 39. Same as Fig. 38 except that the computed distribution is for an intensity of 75 mm/hr and the observed distribution is for a precipitation rate of 65.5 mm/hr.

CHAPTER VII

SUMMARY AND CONCLUSIONS

By assuming steady state and adiabatic (nonentraining) conditions in a constant downdraft below a cloud with raindrops at the cloud base following a Marshall-Palmer distribution, we have computed the temperature, relative humidity, and drop-size distribution in the downdraft as it progresses downward. Modification in the drop-size distribution has been considered as resulting from the microphysical processes of evaporation, collision-coalescence, and collisional and aerodynamic breakup. The drops resolved in the computation cover the range from 0.004 cm to 0.4 cm in radius; the drops with radii less than 0.004 cm are collectively treated as "cloud droplets." Drops with radii greater than 0.4 cm are assumed to break up spontaneously and instantly. We also have compared our calculated drop-size distributions with several measured on the ground and on ships.

Evaporation by itself (Case A) affects primarily drops with radii less than 0.015 cm. The evaporation time constants for these smaller drops are so short that they do not survive a height interval $\Delta z = 25$ m once the relative humidity decreases to a value of about 60%. The concentration of the small drops is replenished by the evaporation of larger drops, but since the evaporation rate is less for larger drops, fewer drops enter and leave the small radius categories. Thus our final drop-size distribution peak at radii from 0.015 to 0.020 cm depending on the strength of the constant downdraft. The

peak drop concentration shifts to smaller radius categories for stronger downdrafts since the faster moving drops have less time to evaporate. The rainshaft relative humidity is minimum and temperature maximum for small precipitation rates and strong downdrafts. The minimum relative humidity computed was 47.8% at 1500 m below cloud base for R = 25 mm/hr and w_D = 15 m/sec. Evaporation does not affect rainfall rate and radar reflectivity to a great extent, the magnitude of the decrease was less than 10% in the most severe case.

In Case B, when collision-coalescence is considered together with evaporation, several interesting changes occur. The precipitation rate increases dramatically as the large drops with their higher terminal velocities sweep out the small drops, while the radar reflectivity, which depends on the concentration of larger drops increases significantly. The maximum increases occur with high initial rainfall rates, which, according to the Marshall-Palmer distribution, provide higher initial concentrations of large drops, and with weak downdrafts permitting the larger drops a longer time to sweep out the smaller drops. Rainshaft relative humidity is lower and the temperature higher for Case B than Case A because the larger drops which are poor evaporators deplete the more efficiently evaporating small drops. For high initial rainfall rates, the concentration of drops with radii less than 0.075 cm is severely depleted by collision-coalescence.

In Case C, when aerodynamic breakup is added to evaporation and collision-coalescence, one notes little difference from Case B for small initial rainfall rates. The effect of aerodynamic breakup

becomes more apparent for higher initial precipitation rates because of the higher concentration of large drops. Subcloud relative humidity is lower and temperature higher for Case C when compared to Case B, although this effect is minor for small initial rainfall rates. The probability of aerodynamic breakup becomes very small (<0.01/sec) for drops of radii less than 0.3 cm. As shown earlier in Chapter VI, the fragment population resulting from aerodynamic breakup has a maximum in our spectrum at a drop radius of 0.055 cm. For large initial precipitation rates, the drop-size distribution in Case C has a much larger concentration of small drops than in Case B because of the breakup of the largest drops.

Case D combines collisional breakup with the processes of evaporation and collision-coalescence; aerodynamic breakup is not included in this case. Collisional breakup is a much more efficient process for depleting large drops than is aerodynamic breakup. As a result, the subcloud relative humidity is higher and temperature lower in Case D than in Case C for weak downdrafts. For strong downdrafts, this effect is not as great because the higher concentration of small drops is given less time to evaporate. Radar reflectivity as well as rainfall rate in the subcloud layers is drastically reduced in Case D due to rapid breakup of the large radius drops. Drop-size distributions in this case exhibit a rapid decrease in drop concentration beginning with drops of radius 0.15 cm such that very few drops with radii greater than 0.20 cm exist in the final distribution.

In Case E, when aerodynamic breakup is added to the Case D processes, virtually no change is noted. This is due to the rapid depletion of drops with large radii by collisional breakup. Aerodynamic breakup is probably a more important microphysical process in cold rain resulting from strong convective storms and just beneath the melting level where large drops resulting from the melting of ice pellets and hail can become unstable and break up.

The computed drop-size distributions obtained in Case E compare favorably with maritime spectra measured by Austin and Geotis (1979), Mueller and Sims (1967), and Geotis (1968). The general shape of the computed distributions, although quite similar to measured warm rain spectra, generally shows a higher concentration of drops with radii greater than 0.10 cm than observed with small precipitation. However, for higher precipitation rates the computed distributions provide an excellent fit to observed spectra in the radius range 0.05 - 0.20 cm, which was the range of the measuring disdrometers. Case E drop-size distributions also were compared with the measured cold rain distributions of Dingle and Hardy (1962). Computed distributions displayed higher concentrations of small drops in the radius range of 0.05 - 0.15 cm than in measured cold rain spectra. Although the measurement of drop concentration was limited at the large radius end ($r > 0.20$ cm), indications are that the observed concentration of drops with radii greater than 0.20 cm would be higher than the computed distributions.

In conclusion, the study reported herein throws considerable light on the role of the microphysical processes in determining the thermodynamic and microphysical characteristics of the warm rain accompanied by a convective downdraft. The results are encouraging because of the qualitative agreement of the drop-size distributions observed in nature with those computed. However, there should be no doubt that this agreement is somewhat fortuitous, in view of the extreme simplicity of the model vis-a-vis the possibility that the details of the basic model (such as the Marshall-Palmer drop-size distribution at the cloud base, assumed at a height of 1500 m above the ground) are different from the conditions under which the measured drop-size distributions had been obtained. Obviously further research is required, with an improved model incorporating realistic initial and environmental conditions.

CHAPTER VIII

RECOMMENDATIONS

In developing this study, several simplifying assumptions were made, many of which were invoked so we could compae our results with those of previous studies incorporating the same assumptions. In addition, our goal was to explore the role of the fundamental processes rather than reproduce results in natural situations. For closer comparison with observations, the present computations need several improvements as indicated below.

1. Smoother coalescence efficiencies utilizing the latest experimental results should help eliminate the sharp breaks which occur at radii of 0.05 cm and 0.15 cm. Also the collection kernel should incorporate more realistic collision efficiencies than geometric sweepout.

2. In this study, it was assumed that breakup was constant below the radius of 0.025 cm, since the McTaggart-Cowan and List (1975) experiments had a lower-size limitation of r = 0.025 cm. The results of Brazier-Smith et al. (1972) included drop interactions down to drop radii of about 0.015 cm. Incorporating the experimental data of Brazier-Smith et al. into those of McTaggart-Cowan and List (1975) could make the resulting drop-size distributions more representative at the smaller drop radii.

3. Variable subcloud density and raindrop terminal velocity in future computations should improve the realism of the computed drop-size spectra. The error in assuming these two quantities constant is

not too large for a shallow subcloud region, however.

4. The assumptions of a constant subcloud downdraft and of steady-state are unrealistic. The former can be changed easily for better realism. The latter would require extensive changes in computational procedure. Introduction of the effects of turbulence would be almost prohibitively difficult.

5. Cloud base drop-size distributions other than Marshall-Palmer should be investigated. Specifically, cloud base spectra measured during GATE and reported in the literature should be used as the initial distribution. This will enable one to see how well the resulting steady state distributions agree with those measured at the surface during that experiment.

REFERENCES

Austin, P., and S. Geotis, 1979: Raindrop sizes and related parameters for GATE. J. Appl. Meteor., 18, 569-575.

Beard, K. V., 1976: Terminal velocity and shape of cloud and precipitation drops aloft. J. Atmos. Sci., 33, 851-863.

Battan, L. J., 1973: Radar Observations of the Atmosphere. The University of Chicago Press, 161 pp.

Berry, E. X., 1967: Cloud droplet growth by collection. J. Atmos. Sci., 24, 688-701.

Bradley, S. G., and C. D. Stow, 1977: The effect of raindrop interactions on observed drop-size distributions. J. Appl. Meteor., 16, 1206-1213.

_____, and _____, 1979: On the production of satellite droplets during collisions between water drops falling in still air. J. Atmos. Sci., 36, 495-500.

Brazier-Smith, P. R., S. G. Jennings, and J. Latham, 1972: The interaction of falling drops: coalescence. Proc. Roy. Soc. London, A326, 393-408.

_____, _____, and _____, 1973a: Raindrop interactions and rainfall rates within clouds. Quart. J. Roy. Meteor. Soc. 99, 704-722.

_____, _____, and _____, 1973b: The influence of evaporation and drop-interactions on a rainshaft. Quart. J. Roy. Meteor. Soc., 99, 704-722.

Byers, H. R., 1965: Elements of Cloud Physics. The University of Chicago Press, 191 pp.

Byers, H. R., and R. R. Braham, Jr. 1949: The Thunderstorm. U. S. Government Printing Office, 287 pp.

Caplan, P. M., 1969: On thunderstorm downdraft. Preprints Sixth Conf. Severe Local Storms. Chicago, Amer. Meteor. Soc., 68-70.

Das, P., 1962: Influence of windshear on the growth of hail. J. Atoms. Sci., 19, 407-414.

_____, 1969: The thermodynamic equation in cumulus dynamics. J. Atmos. Sci., 26, 399-407.

_____, and M. C. Subbarao, 1968: The unsaturated downdraft. Proc. Intern. Conf. Cloud Physics, Toronto, 592-596.

_____, and _____, 1972: The unsaturated downdraft. Indian J. Meteor. Geoghys. 23, 135-144.

Dingle, A. N. and K. R. Hardy, 1962: The description of rain by means of sequential rain drop size distributions. Quart. J. Roy. Meteor. Soc., 88, 301-314.

Findeisen, W., 1939: Zur Frage der Regetropfenbildung in reiner Wasserwolken. Met. Zeitschrift, 56, 365-371.

Geotis, S., 1968: Characteristics of rain in Panama in November, 1968. Final Report, Contract DAAG 25-69-C-0287 for Frankford Arsenal, Philadelphia, Pa.

Gillespie, J. R. and R. List, 1976: Evolution of raindrop size distributions in steady-state rainshafts. Preprints of Papers, Intern. Cloud Physics Conf., Boulder, Amer. Meteor. Soc., 472-477.

_____, and _____, 1978/1979: Effects of collision-induced

breakup on drop-size distributions in steady-state rainshaft. Pageoph, 117, 599-626.

Gunn, R., and G. D. Kinzer, 1949: The terminal velocity of fall for water droplets in stagnant air. J. Meteor., 6, 243-248.

Hardy, K. R., 1963: The development of raindrop-size distributions and implications related to the physics of precipitation. J. Atmos. Sci., 20, 299-312.

Hitschfeld, W., 1955: Size distribution generated by a random process. Artificial Stimulation of Rain, New York, Pergamon Press, 224-228.

Houghton, H. G., 1968: On precipitation mechanisms and their artificial modification. J. Appl. Meteor., 7, 851-859.

Jorgensen, D. J., 1974: The microphysical effects of stochastic coalescence on an initially-steady, one-dimensional, adiabatic cloud. M. S. Thesis, Texas A&M University, College Station, Texas, Available from University Microfilms, Inc., Ann Arbor, Michigan.

Kamburova, P. L., and F. H. Ludlam, 1966: Rainfall evaporation in thunderstorm downdrafts. Quart. J. Roy. Meteor. Soc., 92, 510-518.

Kintigh, E. L. and P. Das, 1970: Modification of drop-size distribution in an unsaturated downdraft. Preprints of Papers, Conf. Cloud Physics, Fort Collins, Amer. Meteor. Soc., 125-126.

Kinzer, G. D., and R. Gunn, 1951: The evaporation, temperature and thermal relaxation time of freely falling waterdrops. J. Meteor., 8, 71-83.

Komabayasi, T., T. Gonda, and K. Isono, 1964: Lifetime of waterdrops before breaking and size distribution of fragment droplets. J. Meteor. Soc. Japan, 42, 330-340.

Langmuir, L., 1948: The production of chain reaction in cumulus clouds at temperatures above freezing. J. Meteor., 5, 175-192.

Laws, J. O., and D. A. Parsons, 1943: The relation of raindrop size to intensity. Trans. Amer. Geophys. Union, 24, Part II, 452-460.

List, R. J., 1949: Smithsonian Meteorological Table, 6th ed., The Smithsonian Institution, 527 pp.

List, R., and J. R. Gillespie, 1976: Evolution of raindrop spectra with collision-induced breakup. J. Atmos. Sci., 33, 2007-2013.

_____, C. F. MacNeil, and J. D. McTaggart-Cowan, 1970: Laboratory collisions of raindrops. J. Geophys. Res., 75, 7573-7580.

Marshall, J. S., and W. M. K. Palmer, 1948: The distribution of raindrops with size. J. Meteor., 5, 165-166.

Mason, B. J., and R. Ramanadham, 1954: Modification of the size distribution of falling raindrops by coalescence. Quart. J. Roy. Meteor. Soc., 80, 388-394.

McTaggart-Cowan, J. D., and R. List, 1975: Collision and breakup of water drops at terminal velocity. J. Atmos. Sci., 32, 1401-1411.

Mueller, E., and A. Sims, 1967: Raindrop distributions at Majuro Atoll, Marshall Islands. Tech. Rep. ECOM-0271-RRI, University of Illinois, Urbana, 93 pp. NTIS AD-650913.

Murray, F. W., 1967: On the computation of saturation vapor pressure. J. Appl. Meteor., 6, 203-204.

Ogura, Y., and T. Takahashi, 1973: The development of warm rain in a cumulus model. J. Atmos. Sci., 30, 262-277.

Rigby, E. D., J. S. Marshall, and W. Hitschfeld, 1954: The development of the size distribution of raindrops during their fall. J. Meteor., 11, 363-372.

Shumann, T., 1938: The theory of hailstone formation. Quart. J. Roy. Meteor. Soc., 64, 3-21

Sivaraman, K. R., and M. V. Sivaramakrishnan, 1962: Modification of the size distribution of raindrops with distance fallen. Indian J. Meteor. Geophys., 13, Spec. No., 17-20.

Srivastava, R. C., 1967: On the role of coalescence between drops in shaping their size distribution. J. Atmos. Sci, 24, 287-292.

_____, 1971: Size distribution of raindrops generated by their breakup and coalescence. J. Atmos. Sci., 28, 410-415.

_____, 1978: Parameterization of raindrops size distributions. J. Atmos. Sci., 35, 108-117.

Takahashi, T., 1977: A study of Hawaiian warm rainshowers based on aircraft observations. J. Atmos. Sci., 34, 1773-1790.

Telford, J., 1955: A new aspect of coalescence theory. J. Meteor., 12, 436-444.

Watts, R. G., 1971: Relaxation time and steady evaporation rate of freely falling raindrops. J. Atmos. Sci., 28, 219-225.

Whelpdale, D. M. and R. List, 1971: The coalescence process in raindrop growth. J. Geophys. Res., 76, 2836-2856.

Young, K. C., 1975: The evolution of drop spectra due to condensation, coalescence and breakup. J. Atmos. Sci., 32, 965-973.

APPENDIX A

LIST OF SYMBOLS

a	Empirical constant (= 62.3)
A	Liquid water content in precipitation (kg m^{-3})
b	Empirical constant (=7)
C_p	Specific heat of air at constant pressure
d_i	Raindrop diameter (cm) in the i-th category
D	Diffusivity of water vapor in air (m^2 sec^{-1})
$\overline{D}$	Power law constant in equation (39)
DLOGR	Logarithmic difference in radii between any two adjacent size classes
e_a	Vapor pressure (Pa)
e_s	Saturation vapor pressure (Pa)
E(i,1)	Collection efficiency for a drop of radius i colliding with a drop of radius 1
$E_1(i,1)$	Collision efficiency for drops of radius i and 1
$E_2(i,1)$	Coalescence efficiency for drops of radius i and 1
$\overline{f}$	Total number of small fragments
F	Dimensionless factor which is a function of Reynolds Number
g	Acceleration due to gravity (9.8 m/sec^2)
i	Size category of drops
j	Integer subscript indicating height ($j\Delta z$)
$\hat{k}$	Unit vector in the z direction
k	Size category of drops
K_h	Thermal conductivity of air

k_o	Adjustable scale factor that fixes the data points at integer values of k
kc	The class index of drops which coalesce with drops between class kh and class k to form drops of class k+1
kh	The class index of drops whose mass is half that of class k
L_v	Latent heat of vaporization
M_i	Mass of a single drop in radius class i
n	Number of drops per cubic meter in radius class i (m^{-3})
n_r	Number of drops of radius r per cubic meter per unit radius class interval ($m^{-3}cm^{-1}$)
N'	Total number of drops per kilogram of air (kg^{-1})
N	Number of drops per kilogram of air (kg^{-1})
N_r	Number of drops of radius r per kilogram of air per unit radius interval r
P	Atmospheric pressure (Pa)
$P_i(L,s)$	Probability of a drop of radius r_i to be formed by the collisional breakup of a large (L) and a small (s) drop per unit time (sec^{-1})
P_i	Probability of a drop of radius r_i breaking up due to instability per unit time (sec^{-1})
Q_r	Source and sink term in the continuity equation for drop concentration
$Q(r_\ell, r_i)$	Probability by which a breaking drop of radius r_ℓ yields a drop of radius r_i per unit time (sec^{-1})
r	Drop radius (cm)
r_i	The drop radius in the i-th category (cm)
R_d	Precipitation rate (mm/hr)
Rd	Specific gas constant for dry air
Re	Reynolds number

Rv	Specific gas constant for water vapor
s	Equivalent thickness of the transition shell outside the raindrop
S	Relative humidity (percent)
t	Time (sec)
T	Environmental temperature (K)
$\overline{T}$	Mean temperature in a 25-m layer (K)
T_D	Dry adiabatic Temperature (K)
V	Velocity of air (m/sec)
V_r	Velocity of a liquid drop of radius r relative to the air (m/sec)
V_T	Terminal speed of drops (m/sec)
w_D	Steady-state downdraft speed (m/sec)
$W_i(L,s)$	Rate of formation of drops of radius r_i by collisional breakup of drops with radii r_L and r_s
z	Height above ground (m)
Z	Radar reflectivity (mm^6/m^3)
Δr_i	Radius interval of the i-th category (cm)
α	Difference between drop class k and drop class kc
γ	r_{k+1}/r_k
γd	Dry adiabatic lapse rate (9.81×10^{-3} k/m)
δ_ℓ	Density of liquid water (kg/m^3)
Δz	Thickness of a layer (25 m)
θ	Potential temperature (K)
Λ	Exponent in Marshall-Palmer Equation (40)
μ	Kinematic viscosity
ρa	Saturated vapor density at raindrop surface (kg/m^3)

ρ_b	Environmental vapor density (kg/m^3)
ρ_d	Density of dry air (kg/m^3)
ρ_ℓ	Liquid water content in air (kg/m^3)
ξ	Water vapor mixing ratio
$\sigma(z)$	Defined as $-\frac{1}{\rho_d}\frac{d\rho_d}{dz}$
ϕ	Specific entropy ($jkg^{-1}K^{-1}$)
$\Phi(r_i, r_\ell)$	Collection kernel for drops of radius r_i colliding with drops of radius r_ℓ (m^3/sec)

APPENDIX B

ANALYSIS OF THE ERROR DUE TO THE ASSUMPTION OF CONSTANT DENSITY AND CONSTANT TERMINAL SPEED

Density

The advection term of (12) is

$$\frac{dN_r}{dz}\,EV = \frac{-1}{\rho\, w_D}\,\frac{d}{dz}\,(\rho\, N_r V_T) \quad . \tag{B.1}$$

Assuming V_T to be constant in the subcloud layer and setting $\sigma(z) = -\frac{1}{\rho}$ one can show that

$$\frac{d}{dz}\,(\ln N_r) = -\frac{\sigma(z) V_T}{w_D + V_T}\,, \tag{B.2}$$

which is solved numerically as

$$N_{k,j+1} = N_{k,j}\,\exp\left[\frac{V_T}{w_D + V_{T,i}}\,\sigma(z)\Delta z\right] \quad . \tag{B.3}$$

If ρ is assumed constant over Δz, $\sigma(z) \to 0$, and $N_{k,j+1} = M_{k,j}$. In order to estimate the error in this assumption, (B.3) is solved for large raindrops ($r = 0.33$ cm) by using

$$V_T = 9.2 \text{ m/sec}, \quad \Delta z = 1500 \text{ m}, \quad \sigma(z) = 10^{-4}\text{m}^{-1}, \text{ and } \quad w_D = 5 \text{ m/sec}.$$

The result is $N_{k,j+1} = 0.903\, N_{k,j}$. Assuming ρ to be a constant over $\Delta z = 1500$ m results in a 9.7% error in $N_{k,j+1}$.

Terminal Velocity

Using (B.1) and assuming ρ constant in the subcloud layer we have

$$N_{k,j+1} = N_{k,j} \exp \frac{\Delta z}{w_D + V_T} \frac{dV_T}{dz} \quad . \qquad (B.4)$$

The summer atmosphere results of Beard (1976) give the change in terminal velocity with height, $\frac{dV_T}{dz}$, as approximately 0.0005 sec^{-1} for drops of 0.3 cm radius. With Δz = 1500 m, w_D = 5 m/sec and V_T = 9.2 m/sec, (B.4) is solved as $N_{k,j+1} = 0.947\ N_{k,j}$. The error incurred by assuming a constant V_T in the subcloud layers is about 5.3%.

APPENDIX C

EXTENSION OF KINZER AND GUNN'S MASS EVAPORATION RESULTS

The rate of mass evaporation from liquid water drops in motion relative to their environment has been explored both theoretically and experimentally by Kinzer and Gunn (1951). Their experimental results are expressed as

$$-\frac{DM}{Dt} = [4\pi r(1 + \frac{F}{s}r)]\ [D(\rho_a - \rho_b)] \qquad (C.1)$$

and the two factors on the right-hand side are shown in Table C 1. In (C.1), s is the equivalent thickness of the transition shell outside the drop, F is a dimensionless factor which is a function of Reynolds number Re, D is the diffusivity of water vapor in air, ρ_a the saturated vapor density at the surface of the drop, and ρ_b is the vapor density of the environment.

This research deals with raindrops of radii ranging from 0.004 cm to 0.40 cm, which requires an extension of the Kinzer and Gunn data. Byers (1965) showed that the mass evaporation rate for drops in motion could be written,

$$-\frac{DM}{Dt} = [4\pi r(1 + 0.22\ F\ Re^{1/2})]\ \frac{S-1}{a'+b'} \quad , \qquad (C.2)$$

where $a' = L^2/KR_vT^2$, $b' = R_vT/e_sD$, and $(1 + 0.22\ F\ Re^{1/2})$ is the ventilation factor. Eq. (C.2) was used to expand the evaporation data since (C.1) required a knowledge of the equivalent thickness of the

transition shell outside the drop, which was not available.

Table C.1. Evaporation of freely falling water drops (after Kinzer and Gunn, 1951).

Table C.1A

$4\pi r(1 + \frac{F_r}{s})$*

Radius (cm)	Temperature (C) 0	10	20	30	40
0.005	0.086	0.082	0.079	0.076	0.073
0.010	0.29	0.29	0.29	0.28	0.28
0.015	0.49	0.48	0.48	0.47	0.47
0.020	0.73	0.72	0.71	0.70	0.69
0.025	1.01	0.99	0.97	0.96	0.94
0.030	1.31	1.29	1.27	1.25	1.24
0.035	1.66	1.63	1.61	1.58	1.55
0.040	2.03	2.00	1.97	1.94	1.91
0.045	2.5	2.4	2.4	2.3	2.3
0.050	2.9	2.8	2.8	2.7	2.7
0.06	3.9	3.8	3.7	3.6	3.6
0.07	4.9	4.8	4.7	4.6	4.5
0.08	6.0	5.9	5.8	5.7	5.6
0.09	7.3	7.2	7.0	6.9	6.8
0.10	8.8	8.5	8.3	8.1	8.0
0.11	10.5	10.1	9.9	9.6	9.4
0.12	12.4	12.0	11.7	11.3	11.0
0.13	14.7	14.2	13.8	13.3	12.8
0.14	17.2	16.6	16.0	15.4	14.9
0.15	20.1	19.3	18.5	17.8	17.2
0.16	23	22	21	21	20
0.17	27	26	25	24	23
0.18	31	30	28	27	26
0.19	35	34	32	31	29
0.20	39	38	36	35	33
0.21	43	42	40	39	37

Table C.1B

$D(\rho_a - \rho_b)$*

S (%)	Temperature (C) 0	10	20	30	40
10	0.61	0.98	1.47	2.06	2.68
20	0.54	0.87	1.29	1.79	2.36
30	0.48	0.76	1.12	1.55	2.05
40	0.41	0.65	0.95	1.32	1.75
50	0.34	0.54	0.78	1.09	1.45
60	0.27	0.43	0.63	0.86	1.15
70	0.20	0.32	0.46	0.64	0.85
80	0.14	0.21	0.31	0.42	0.56
90	0.07	0.11	0.16	0.21	0.28
100	0	0	0	0	0

*See p. 133 for explanation.

a. Method of Computation

The first step was to create Table C.2 for the same radii range as in Table C 1. This was done by first calculating Table C.2B in terms of the second bracketed factor in (C.2) with temperature-dependent values of latent heat of vaporization, thermal conductivity, saturation vapor pressure, and diffusivity taken from the Smithsonian Meteorological Tables (List, 1949).

Next, Table C.2A, for the radii range 0.005 to 0.21 cm, was computed by using the following process:

1. Ten mass evaporation tables, one for each relative humidity, were constructed by multiplying the values in Table C.1A by those in Table C.1B for the same temperature; values in the table represented $(-\,dM/dt)_{C-1}$, that is, the mass evaporation rate represented by Table C.1.

2. Ten tables similar to Table C.2A, one for each relative humidity value, were calculated using

$$4\pi r(1 + 0.22\ F\ Re^{1/2}) = \left(-\frac{dM}{dt}\right)_{C-1} / \left(\frac{S-1}{a'+b'}\right) \qquad (C.3)$$

3. An arithmetic average of the ten tables constructed in step (2) is shown in Table C. 2A for drop radii 0.005 to 0.21 cm.

Table C.2A was extended to radius values below 0.005 cm by assuming F = 1, which is consistent with the values given by Kinzer and Gunn (1951). The Reynolds number data required for these calculations were taken from List (1949). Table C. 2A was extended from 0.21- to 0.40-cm radius in two steps as follows.

Table C.2. Computed evaporation of freely falling water drops.

Table C.2A

$4\pi r\ (1+0{,}22\ FRe^{1}/2)$

Radius (cm)	Temperature (C) 0	10	20	30	40
0.004	0.050	0.038	0.029	0.023	0.017
0.005	0.055	0.042	0.028	0.024	0.019
0.010	0.19	0.15	0.10	0.09	0.07
0.015	0.31	0.24	0.17	0.15	0.12
0.020	0.47	0.37	0.25	0.22	0.18
0.025	0.65	0.50	0.35	0.30	0.24
0.030	0.84	0.66	0.45	0.39	0.32
0.035	1.06	0.83	0.58	0.49	0.39
0.040	1.30	1.02	0.70	0.61	0.49
0.045	1.6	1.22	0.86	0.72	0.59
0.050	1.9	1.4	1.0	0.84	0.69
0.06	2.5	1.9	1.3	1.12	0.92
0.07	3.1	2.4	1.7	1.4	1.14
0.08	3.8	3.0	2.1	1.8	1.4
0.09	4.7	3.7	2.5	2.2	1.7
0.10	5.6	4.3	3.0	2.5	2.0
0.11	6.7	5.1	3.5	3.0	2.4
0.12	7.9	6.1	4.2	3.5	2.8
0.13	9.5	7.2	4.5	4.2	3.3
0.14	11	8.4	5.7	4.8	3.8
0.15	13	10	7.0	5.6	4.4
0.16	15	11	8.0	6.6	5.1
0.17	17	13	9.0	7.5	5.9
0.18	20	15	10	8.4	6.6
0.19	22	17	11	9.7	7.4
0.20	25	19	13	11	8.4
0.22	33	25	19	15	11
0.24	38	29	22	17	13
0.26	43	33	25	20	15
0.28	51	39	30	23	18
0.30	56	43	33	25	19
0.32	62	47	36	28	21
0.34	68	52	40	31	23
0.36	74	57	43	34	26
0.38	80	61	47	36	28
0.40	86	66	50	39	30

Table C.2B

$\frac{S-1}{a'+b'}$

S (%)	Temperature (C) 0	10	20	30	40
10	0.95	1.91	3.59	6.28	10.20
20	0.85	1.70	3.19	5.58	9.08
30	0.74	1.49	2.79	4.89	7.94
40	0.63	1.27	2.39	4.19	6.81
50	0.53	1.06	2.00	3.49	5.67
60	0.42	0.85	1.60	2.79	4.54
70	0.32	0.64	1.20	2.09	3.40
80	0.21	0.43	0.80	1.40	2.27
90	0.11	0.21	0.40	0.70	1.13
100	0	0	0	0	0

Step 1. Reynolds number data from List (1949) along with F factor data from Kinzer and Gunn (1951) were inserted in the expression $4\pi r(1 + 0.22\ F\ Re^{1/2})$ to extend Table C 2A for the radius interval from 0.21 cm to 0.29 cm.

Step 2. From radii between 0.29 and 0.40 cm, Re was calculated by using μ, the temperature dependent kinematic viscosity, and the terminal velocity values given in Table 1. The F factor values were linearly extrapolated from the data given in Kinzer and Gunn (1951). Entries in Table C.2A were then computed with the same expression as given in Step 1.

b. Discussion

Kinzer and Gunn (1951) point out that because of the wide range of sizes in which water drops are found in nature, the physics of their evaporation may be different over different size ranges. They suggest that for the discussion of evaporation, the drops should be treated in three following categories:

1. Those drops that lie in the Stokes Law region ($r < 0.004$ cm);
2. Those drops in the radius range 0.004 to 0.20 cm that have sufficient speed to ventilate adequately the transition layer of vapor and temperature.
3. Those drops with a radius larger than 0.20 cm that fall so fast as to be deformed and whose description requires special mathematical analysis.

Kinzer and Gunn (1951) worked with drops in the second category, and this research extended their results without taking drop deforma-

tion into account. Watts (1971) calculated mass evaporation rates by using heat and mass transfer analysis. He suggests using the long radius of the deformed drop rather than the spherical radius in (C. 1). This suggestion was not incorporated in this study because the data seemed incomplete. In addition, it was intended to compare the results obtained in this study with those of other workers who used the original Kinzer and Gunn evaporation data. It may be noted, however, that in the cases treated in this work, collisional breakup severely limited the number of drops with radii greater than 0.2 cm.

APPENDIX D

INVESTIGATION OF EVAPORATION DATA

a. Background

The unexpected feature, namely, a bimodality in the drop concentration at the lower end of the drop-size range, noted in Chapter 5a, is examined in greater detail. Eq. (53) is the forward differencing formulation used to calculate drop concentration change due to evaporation. For all initial rainfall rates and constant downdraft velocities, the final drop-size distributions were similar to Fig. D.1. The bimodal feature in these distributions, that obviously is due to evaporation, is not documented in the literature.

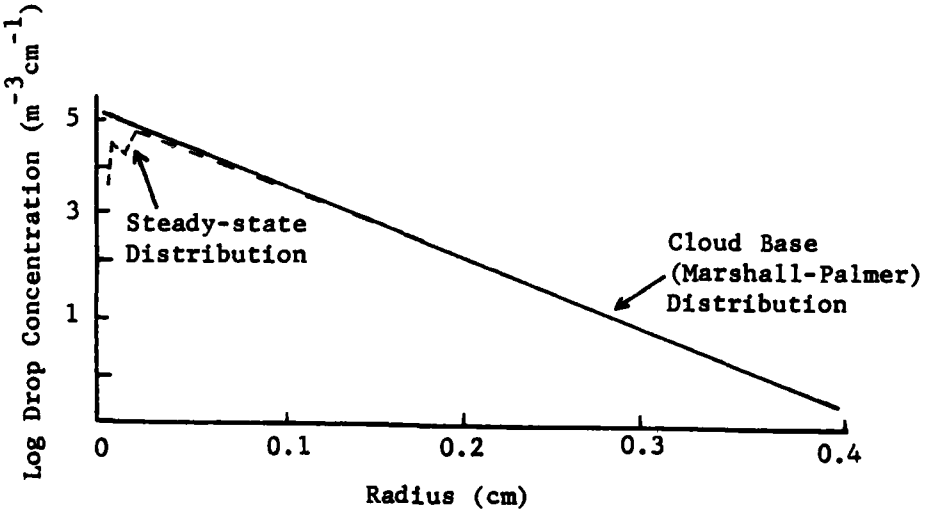

Fig. D.1. Bimodal type distribution resulting from the evaporation process.

In order to isolate the cause of this trend, individual tests were performed by repeating computations in which

1. The number of drop-size categories was decreased from 40 to 20;
2. Δz was increased from 25 to 50 m;
3. backward as well as forward differencing were employed in the numerical calculations;
4. computation was performed with double precision;
5. the convergence criteria were made more stringent in the iterative scheme for obtaining the new temperature at each level;
6. various downdraft velocities (1, 5, 10, and 15 m/sec) were tried; and
7. various initial precipitation rates (25, 50, 75, 100 mm/hr) were used.

The bimodal charactertistic appeared in the final drop concentration for each of these computations. The final drop concentrations exhibited a decrease in the radius range 0.0053-0.0067 cm and increased again to a maximum in the 0.0187-0.0191-cm interval. The results of using w_D = 1 m/sec showed a flattening of the curve, while the bimodality was sharpened by stronger downdrafts. When the downdraft was held constant and the initial precipitation rate allowed to vary, the bimodality was sharpened by larger values of R. When the number of radius categories was decreased to 20, the decrease in final drop concentration occurred in the radius range from 0.0088 to 0.0139 cm

with a peak in the 0.0173 to 0.0277-cm radius range. No difference was noted in the tests in 2, 3, 4, and 5 above.

Following the above tests, the sensitivity of the Kinzer and Gunn (1951) evaporation data was investigated. This was done by smoothing the mass evaporation data by using (C. 2) as reported by Byers (1965). The value of a' and b' were calculated from values of the various parameters at the mean temperature of the rainshaft rather than the temperature-dependent values used initially. This treatment is similar to that used by Brazier-Smith et al. (1973). Their evaporation results, based on an initial Marshall-Palmer distribution, did not show the bimodal characteristic.

b. Method of Computation

The following values were treated as constant in the subcloud region:

$T = 285$

$L_v = 2.47 \times 10^6 j/kg$

$k_h = 0.582\ jm^{-1}sec^{-1}k^{-1}$

$D = 2.44 \times 10^{-5}\ m^2/sec$

$e_s = 14.49 \times 10^2\ n/m^2$

$\mu = 1.445 \times 10^{-5}\ m^2/sec$

Table 117.B in the Smithsonian Meteorological Tables was then reconstructed by using S-1(a' + b'_ with a' + b' = 4.003×10^7/sec-m, and S equal to the saturation values in Table 117.B.

In order to reconstruct Table 117.A, F was assumed equal to

unity, and a constant value of μ was used. Terminal velocity was plotted as a smooth function of drop radius from the results of Gunn and Kinzer (1949).

After Tables 117.A and 117.B were completed, they were read into the evaporation program. The results did not exhibit the bimodal trend depicted in Fig. D.1, but rather demonstrated a single peak at the radius of 0.0179 cm for w_D = 10 m/sec, and at 0.0250 cm for w_D = 5 m/sec.

c. Discussion

The above results indicate that the bimodality in Fig. D.1 is inherently caused by the evaporation data of Kinzer and Gunn (1951). The smooth evaporation results are consistent with the evaporation results of Brazier-Smith *et al*. (1973).

VITA

The author was born on 20 October 1942 in Barron, Wisconsin, to Mr. and Mrs. George W. Borchers. He moved with his family to their curre.. home near Denver, Iowa, in 1950. He attended a one-room country school through the eighth grade and was graduated from Denver Community High School in May 1960.

He holds the B.S. in meteorology from Texas A&M University (1970). He earned a master's degree in aeronomy and planetary atmosphere from the University of Michigan (1973). The author has completed course work at the College of William and Mary, University of Virginia, University of the Philippines, and The Citadel.

The author enlisted in the U.S. Air Force following high school and has been on continuous active duty since that time. United States Air Force commissioning followed his undergraduate education. He is a career meteorologist in the Air Weather Service and has served in positions ranging from surface weather observer to staff meteorologist to a numbered Air Force. He is currently serving as Assistant Chief of the Special Projects Division, Headquarters Air Weather Service, Scott Air Force Base, Illinois.

He is married to the former Claudia Lynn Hamilton and they have two children, a daughter, Kelly, and a son, Scott. His permanent mailing address is that of his parents at Route 1, Denver, Iowa 50622.

The typists for this dissertation were Mrs. Janie Leighman and Mrs. Linda Smith.


DATE
FILMED
12-84